

# Impacts of Holocene Peat Deposits on Nearshore Biogeochemical Processes and Trace Gas Production

Monographische Dissertation  
zur  
Erlangung des akademischen Grades  
doctor rerum naturalium (Dr. rer. nat.)  
der Mathematisch-Naturwissenschaftlichen Fakultät  
der Universität Rostock

vorgelegt von  
**Matthias Kreuzburg**  
Geboren am 03. November 1985 in Heidelberg  
Rostock den 24. Mai 2019



**Thou canst not stir a flower, without troubling of a star.**

*Francis Thompson, The Mistress of Vision*

## Table of contents

Table of contents .....	II
Eigenständigkeitserklärung.....	VI
Abstract .....	VII
Zusammenfassung .....	VIII
Curriculum Vitae .....	IX
Publications .....	X
Articles in peer-reviewed journals.....	X
Conferences, workshops and presentations .....	X
Research stays abroad .....	XII
Grant.....	XII
Acknowledgement .....	XIII
List of abbreviations, symbols and variables .....	XIV
List of Figures .....	XVI
List of Tables .....	XVIII
Motivation .....	XIX
1. Introduction.....	1
1.1. Climate relevant trace gases in coastal zones .....	1
1.1.1. Methane .....	1
1.1.2. Nitrous oxide .....	2
1.2. Geology and physical processes in coastal regions.....	3
1.3. Hydrological processes across the terrestrial marine interface .....	5
1.3.1. Coastal interactions with peatlands .....	6
1.4. Study site .....	7
1.4.1. Onshore area .....	7
1.4.2. Waterline and offshore area .....	9
1.4.3. Warnow-river .....	9
2. Methods .....	10
2.1. Geochemical field surveys.....	10
2.1.1. Offshore water sampling.....	10
2.1.1.1. Water column characteristics .....	10
2.1.1.2. Mini chamber lander system .....	11
2.1.2. Shoreline field campaigns.....	12
2.1.3. Investigations of the Warnow-river system .....	12
2.1.4. Analytical methods used for samples from the field campaigns .....	12

2.1.4.1.	Gas Chromatography.....	12
2.1.4.2.	Nutrients .....	14
2.2.	Geophysical surveys .....	15
2.2.1.	Geophysical data.....	15
2.2.2.	Ground-truthing .....	16
2.2.3.	Grain size distribution .....	16
2.2.4.	Geochemical sediment analysis and <sup>14</sup> C age-determination .....	17
2.3.	Column experiment study .....	17
2.3.1.	Column experiment and instrumentation .....	18
2.3.2.	Ground and seawater flow regimes .....	20
2.3.3.	Analytical methods .....	22
2.3.3.1.	Gas fluxes among the air-water interface.....	22
2.3.3.2.	Porewater geochemical analysis .....	23
2.3.3.3.	Monitoring of dissolved oxygen .....	24
2.3.3.4.	Solid phase geochemistry .....	25
2.3.3.5.	Quantification of methanogens and sulfate reducers.....	25
3.	Results .....	27
3.1.	Trace gas investigation within the study site .....	27
3.1.1.	Offshore concentrations of CH <sub>4</sub> and N <sub>2</sub> O .....	27
3.1.2.	Trace gas concentrations along the waterline .....	30
3.1.3.	Flux measurements from chamber lander incubations.....	31
3.1.4.	Impacts of the Warnow-river on trace gas distribution .....	32
3.2.	Geological surveys .....	34
3.2.1.	Onshore .....	34
3.2.2.	Bathymetry .....	35
3.2.3.	Seafloor composition .....	36
3.2.4.	Sediment cores .....	38
3.2.5.	Subsurface structure .....	40
3.3.	Column experiment .....	42
3.3.1.	Aqueous phase geochemistry .....	42
3.3.1.1.	Salinity .....	42
3.3.2.	Porewater chemistry.....	44
3.3.3.	CO <sub>2</sub> and CH <sub>4</sub> fluxes .....	45
3.3.4.	Abundances of methanogenic archaea and sulfate reducing bacteria .....	46
3.3.5.	Solid phase geochemistry.....	46

4. Discussion .....	48
4.1. Hydrodynamics and trace gas distribution .....	48
4.1.1. Baltic Sea water .....	48
4.1.2. Warnow-river water .....	50
4.1.3. Submarine groundwater discharge .....	51
4.2. Coastal development and geomorphology .....	52
4.2.1. Peatland formation and sea level rise .....	54
4.2.2. Submerged peat deposits in marine sediments .....	56
4.3. Experimental investigation of the interaction of submerged peat with advective groundwater and seawater flow .....	58
4.3.1. Advective flow and solute transport .....	58
4.3.2. Solid phase geochemistry .....	59
4.3.3. Carbon mineralization processes .....	60
4.3.3.1. Mobilization and transformation of DOC .....	60
4.3.3.2. Formation, transport and emission of gases .....	63
5. Summary & Conclusions .....	65
6. Outlook .....	68
7. References .....	69

Die vorliegende Arbeit entstand in dem Zeitraum von Januar 2016 bis Mai 2019 am Leibniz Institut für Ostseeforschung Warnemünde und der Universität Rostock.

This thesis was produced in the period from January 2016 to May 2019 at the Leibniz Institute for Baltic Sea Research Warnemünde and the University of Rostock.

Gutachter / Referees

Prof. Dr. Gregor Rehder | Leibniz Institut für Ostseeforschung

Prof. Dr. Maren Voss | Leibniz Institut für Ostseeforschung

Prof. Dr. Helge Niemann | NIOZ Royal Netherlands Institute for Sea Research

Einreichungsdatum / date of submission: 24th of May 2019

Verteidigungsdatum / date of defense: 22nd of October 2019

## Eigenständigkeitserklärung

Doktorandinnen/Doktoranden-Erklärung gemäß § 4 Absatz 1 Buchstaben g und h der Promotionsordnung der Mathematisch-Naturwissenschaftlichen Fakultät der Universität Rostock

Name: **Matthias Kreuzburg, geb. 03.11.1985**

Ich habe eine Dissertation zum Thema:

### **Impacts of Holocene Peat Deposits on**

### **Nearshore Biogeochemical Processes and Trace Gas Production**

an der Mathematisch-Naturwissenschaftlichen Fakultät der Universität Rostock angefertigt. Dabei wurde ich von Herrn **Prof. Gregor Rehder** betreut.

Ich gebe folgende Erklärung ab:

1. Die Gelegenheit zum vorliegenden Promotionsvorhaben ist mir nicht kommerziell vermittelt worden. Insbesondere habe ich keine Organisation eingeschaltet, die gegen Entgelt Betreuerinnen/Betreuer für die Anfertigung von Dissertationen sucht oder die mir obliegenden Pflichten hinsichtlich der Prüfungsleistungen für mich ganz oder teilweise erledigt.
2. Ich versichere hiermit an Eides statt, dass ich die vorliegende Arbeit selbstständig angefertigt und ohne fremde Hilfe verfasst habe. Dazu habe ich keine außer den von mir angegebenen Hilfsmitteln und Quellen verwendet und die den benutzten Werken inhaltlich und wörtlich entnommenen Stellen habe ich als solche kenntlich gemacht.

Rostock den 24.05.2019



## Abstract

While the majority of coastal sediments consist of sandy and permeable material, in some areas marine ingressions caused the submergence of terrestrial carbon-rich soils in the form of peatlands. These processes have implications for the nearshore marine carbon balance as peat represents a potential source of carbon-containing solutes and gases. This PhD-study combines both: geophysical and geochemical analysis of field data with hydrological processes and their effects on biogeochemical mineralization processes. Onshore- and offshore sediment cores and geo-acoustic surveys reveal that Holocene peat deposits with high organic contents ( $C_{org}$  37–53 %) continue more than 90 m (areal extent: 0.16–0.2 km<sup>2</sup>) in front of the adjoining coastal peatland and nature reserve “Heiligensee und Hütelmoor”. The study site was subject to the interdisciplinary research project Baltic TRANSCOAST, investigating the exchange processes across the land-sea interface. The results of the carbon ages point to a much earlier onset of the peatland formation ( $^{14}C$ -dated to 6725 ± 87 cal yr BP) than previously reported. The C-isotopic signature of the lowermost offshore peat suggests a purely terrestrial origin ( $\delta^{13}C$  –28.9 ‰) while no fractionation processes or contamination with marine organic carbon could be detected. The outer boundary of the peat deposits roughly coincides with the offshore limit of a dynamic coast-parallel longshore bar. In the northern coastal area, temperature, salinity and bottom water CH<sub>4</sub> anomalies coincided with shallower outcropping peat deposits. The different influences of peat-containing, and non-peat containing coastal sands on the carbon balance in shallow water were therefore simulated under controlled conditions in an experimental study. The column experiments using naturally layered sediments were performed in order to better constrain the coupled flow and biogeochemical processes governing carbon transformations in submerged peat under coastal fresh groundwater discharge and recirculation of brackish water. The columns, containing sediments with and without peat layers (organic carbon,  $C_{org}$ , content 39 ± 14 wt %), were alternately supplied with oxygen-rich brackish water from the top (salinity ~18) and oxygen-poor, low-saline groundwater from the bottom (salinity ~1.6). The discharge of low-saline groundwater through the peat layers was accompanied by increasing concentrations of dissolved organic carbon (DOC), having the same C-isotopic composition as the solid phase. The release and ascent of DOC-enriched porewater additionally resulted in the production of dissolved inorganic carbon (DIC) and emission of carbon dioxide (CO<sub>2</sub>), which implies organic matter mineralization likely to be associated with oxygen respiration, sulfate (SO<sub>4</sub><sup>2-</sup>) reduction and methane (CH<sub>4</sub>) formation. In contrast, oxygenated brackish water intrusion lowered DOC and DIC porewater concentrations and led to a significant decrease of CH<sub>4</sub> and CO<sub>2</sub> emissions. This PhD-study illustrates the strong dependency of carbon cycling in shallow coastal areas containing submerged peat deposits on the flow and mixing dynamics within the freshwater-seawater transition zone.

## Zusammenfassung

Zwar bestehen die Küsten größtenteils aus durchlässigen, sandigen Sedimenten, doch verursachte der Rückgang der Küsten in einigen Gebieten eine seeseitige Überflutung und Erosion von kohlenstoffreichen, terrestrischen Moorsedimenten. Dies hat Auswirkungen auf die marine Kohlenstoffbilanz in der Küstenregion, da Torf eine potenzielle Quelle für gelösten Kohlenstoff darstellt. Im Rahmen dieser Doktorarbeit wurden geophysikalische und geochemische Felddaten mit hydrologischen Prozessen und deren Auswirkungen auf biogeochemische Mineralisierungsprozesse kombiniert. Vor der Küste des untersuchten Gebietes wurde die submarine Ausdehnung Holozäner, organikreicher Torfvorkommen ( $C_{org}$  37–53 %) mit Hilfe von land- und seeseitigen Sedimentkernen und geophysikalischen Methoden nachgewiesen. Das Untersuchungsgebiet ist Teil des interdisziplinären Forschungsprojektes Baltic TRANSCOAST, das Austauschprozesse über die Land- und Seegrenze untersucht. Diese Holozänen Torfe erstrecken sich mehr als 90 m (flächenhafte Ausdehnung: 0,16–0,2 km<sup>2</sup>) in die Ostsee. Die Alter der Kohlenstoffe (<sup>14</sup>C-Alter) deuten auf einen früheren Beginn der Moorbildung hin (6725 ±87 cal yr BP) als bisher angenommen. Die Isotopensignaturen des untersten Torfes deutet auf einen rein terrestrischen Ursprung hin ( $\delta^{13}C$  -28.9 ‰), wobei keine Fraktionierungsprozesse oder Verunreinigungen mit marinem organischem Kohlenstoff festgestellt wurden. Die Grenze der Torflagerstätten stimmt in etwa mit der seeseitigen Grenze eines dynamischen, küstenparallelen Sandrückens überein. In der nördlichen Küstenregion decken sich Anomalien (Temperatur, Salzgehalt, CH<sub>4</sub>) im Bodenwasser mit dem Auftauchen der Torfe. Die unterschiedlichen Wechselwirkungen von torfhaltigem Küstensand auf den Kohlenstoffhaushalt im Flachwasser wurden in einem Säulenexperiment unter kontrollierten Bedingungen untersucht. Mit natürlich geschichteten Sedimenten konnte die Kopplung zwischen Flüssen und biogeochemischen Prozessen, welche die Kohlenstoffumwandlung in Torfen unter küstennahen submarinen Grundwasserabflüssen steuern, zeigen. Die Säulen enthielten Sedimente mit und ohne Torfschichten (organischer Kohlenstoff,  $C_{org}$ , Gehalt 39 ±14 Gew.-%), die abwechselnd mit sauerstoffreichem Brackwasser von oben (Salzgehalt ~18) und sauerstoff-, und salzarmem Grundwasser von unten (Salzgehalt ~1,6) versorgt wurden. Die Einleitung von salzarmem Grundwasser durch die Torfschichten ging mit steigenden Konzentrationen an gelöstem organischem Kohlenstoff (DOC) einher, die im salzarmen Porenwasser übereinstimmende Isotopenverhältnisse wie die Festphase aufweisen. Die Freisetzung und der Aufstieg von DOC-angereichertem Porenwasser wurde von der Produktion von gelöstem anorganischem Kohlenstoff (DIC) und der Emission von Kohlendioxid (CO<sub>2</sub>) begleitet, was eine Mineralisierung der organischen Substanz impliziert (z.B. Sauerstoffatmung, Sulfatreduktion (SO<sub>4</sub><sup>2-</sup>) und Methanbildung (CH<sub>4</sub>)). Im Gegensatz dazu führte das Eindringen von sauerstoffhaltigem Brackwasser zu niedrigeren DOC- und DIC-Porenwasserkonzentrationen und deutlich niedrigeren CH<sub>4</sub>- und CO<sub>2</sub>-Emissionen. Diese Doktorarbeit veranschaulicht die starke Abhängigkeit des Kohlenstoffkreislaufs in flachen Küstengebieten mit submarinen Torfablagerungen von der Strömungs- und Mischdynamik innerhalb der Grundwasser-Brackwasser-Übergangszone.

## Curriculum Vitae

NAME: Matthias Kreuzburg  
E-MAIL: Matthias.Kreuzburg@io-Warnemünde.de  
PHONE: Tel.: + 49 381 5197- 3459  
NATIONALITY: German  
FOREIGN LANGUAGES: English/French

### EDUCATION

**2019**

Oct **PhD defense**

May Submission of my PhD Thesis in Chemistry

**2017** **Stay Abroad** in Waterloo, Canada

**2016** **PhD Student** at Graduate School **BALTIC TRANSCOAST**, Marine Chemistry, Working group – Supervision: Prof. Rehder, IOW

2015 Employed as scientific assistant at the Institute of Geosciences, Coastal and Continental Shelf Research, CAU-Kiel

2015 **Master of Marine Geosciences** (M.Sc.), CAU-Kiel

2015 Master Thesis “**Submarine Groundwater Discharge Into Coastal Areas Of The Northern Eckernförde Bay**”, at the Institute of Geosciences, Coastal and Continental Shelf Research, CAU-Kiel

2011 Bachelor Thesis: “Modification Of Resolving Forms In The Elbe Estuary By Means Of Hydraulicacoustic Measurements”, at the Institute of Geoscience, Coastal and Continental Shelf Research, CAU-Kiel

2011 Certified Scientific Diver, Scientific Dive-Center, Kiel

2007 Starting Bachelor of Geosciences, CAU-Kiel

2006 Emergency Medical Assistant at the ASB-Mannheim

2005 Civilian service, Deutsches Rotes Kreuz, Rescue service

2005 General Qualification for University Entrance

## Publications

### Articles in peer-reviewed journals

**Kreuzburg, M.**, Ibenthal, M., Janssen, M., Rehder, G., Voss, M., Naumann, M. and Feldens, P. (2018) **Sub-marine Continuation of Peat Deposits From a Coastal Peatland in the Southern Baltic Sea and its Holocene Development.** Front. Earth Sci. 6:103. doi: 10.3389/feart.2018.00103

Jurasinski, G., Janssen, M., Voss, M., Böttcher, M.E., Brede, M., Burchard, H., Forster, S., Gosch, L., Gräwe, U., Gründling-Pfaff, S., Haider, F., Ibenthal, M., Karow, N., Karsten, U., **Kreuzburg, M.**, Lange, X., Leinweber, P., Massmann, G., Ptak, T., Rezanezhad, F., Rehder, G., Romoth, K., Schade, H., Schubert, H., Schulz-Vogt, H., Sokolova, I., Strehse, R., Unger, V., Westphal, J., Lennartz, B. 2018: **Understanding the Coastal Ecocline: Assessing Sea-Land-Interactions at Non-tidal, Low-lying Coasts through Interdisciplinary Research.** Front. Mar. Sci., Vol 5, Article 342, page 1-22, doi:10.3389/fmars.2018.00342

Gosch, L., Townsend, H., **Kreuzburg, M.**, Janssen, M., Rezanezhad, F., Lennartz, B. **Sulfate mobility in fen peat and its impact on the release of solutes.** Front. Environ. Sci. - Biogeochemical Dynamics <https://doi.org/10.3389/fenvs.2019.00189>

### *Submitted articles*

**Kreuzburg, M.**, Rezanezhad, F., Milojevic, T., Voss, M., Gosch, L., Liebner, S., Van Cappellen, P., Rehder, G. (submitted in April 2019) **Influence of coastal submerged peat deposits on methane production controlled by submarine groundwater discharge: A column experiment study.** Limnol. Oceanogr.

### Conferences, workshops and presentations

**Kreuzburg, M.**, Rezanezhad, F., Voss, M., Feldens, P., Rehder, G.: Influence of submerged peat deposits on methane production in coastal regions by submarine groundwater discharge - controlled carbon release. EGU, 7-12<sup>th</sup> April 2019, Vienna (Talk).

**Kreuzburg, M.**, Westphal, J., M., Voss, M., Jurasinski, G., Rehder, G. 2018. Influences of submarine groundwater discharge on carbon exchange from coastal sediments impacted by submerged peat: A column experiment study. Peat Under Water Workshop, 5<sup>th</sup>–6<sup>th</sup> September 2018 Salem/Malchin, Germany (Poster).

Janssen, M., Ibenthal, M., Böttcher, M.E., Westphal, J., Erkul, E., Koebsch, F., Jurasinski, G., **Kreuzburg, M.**, Voss, M., Sültenfuß, J., Lennartz, B. 2018. Towards understanding complex flow and transport patterns in a coastal peatland- Baltic Sea continuum. TERENO, 8–12 October Berlin (Talk).

**Kreuzburg, M.**, Westphal, J., M., Voss, M., Jurasinski, G., Rehder, G. 2018. Potential relationship between runoff from a coastal peat land on methane and

nitrous oxide fluxes in shallow waters of the Baltic Sea. Ocean Sciences Meeting, 11–16 February 2018, Portland, Oregon, USA (Talk).

Westphal, J., Fernández Fernández, L.E., Rach, B., Schmiedinger, I., **Kreuzburg, M.**, Koebisch, F., and Böttcher, M.E. 2018. Sulfur Isotope Biogeochemistry of Sediments and Soils from a temperate Coastal-Wetland Transition Zone, Southern Baltic Sea. Ocean Sciences Meeting, 11–16 February 2018, Portland, Oregon, USA (Poster).

Fernández, L., Westphal, J., Schmiedinger, I., **Kreuzburg, M.**, Bahlo, R., Koebisch, F., Böttcher, M.E. 2017, European Geosciences Union (EGU2017-14335). Sulfur isotope biogeochemistry of soils from an episodically flooded coastal wetland, southern Baltic Sea (Poster).

Fernández-Fernández, L.E., Westphal, J., Schmiedinger, I., **Kreuzburg, M.**, Bahlo, R., Koebisch, F., Böttcher, M.E. 2017. Sulfur isotope biogeochemistry of soils from an episodically flooded coastal wetland, southern Baltic Sea: Implications for proxy formation. GeoBremen2017 (GeoB17). Bremen, Germany, 24.09.2017 - 29.09.2017 (Poster).

Fernández-Fernández, L.E., Westphal, J., Schmiedinger, I., **Kreuzburg, M.**, Bahlo, R., Koebisch, F., Böttcher, M.E. 2017. Sulfur isotope biogeochemistry of soils from an episodically flooded coastal wetland, southern Baltic Sea. 11th Baltic Sea Science Congress 2017 (BSSC 2017). Rostock, Germany, 12.06.2017 - 16.06.2017 (Poster)

Fernández Fernández, L.E., Westphal, J., Schmiedinger, I., **Kreuzburg, M.**, Bahlo, R., Koebisch, F., Böttcher, M.E. 2017. Sulfur isotope biogeochemistry of soils from an episodically flooded coastal wetland, southern Baltic Sea. European Geosciences Union General Assembly 2017 (EGU 2017). Vienna, Austria, 23.04.2017 - 29.04.2017 (Poster).

**Kreuzburg, M.**, Scholten, J., Hsu, F., Schlüter, M., Rapaglia, J., Schubert, M. 2017, 11th Baltic Sea Science Conference (BSSC). Submarine Groundwater discharge to the Eckernförde Bay, Baltic Sea: Towards a quantitative assessment (Talk).

**Kreuzburg, M.**, Voss, M., Jurasinski, G., Rehder, G. 2017, 11th Baltic Sea Science Conference (BSSC), Potential relationship between runoff from a coastal peat land on methane and nitrous oxide fluxes in shallow waters of the Baltic Sea (Poster).

Scholten, J., **Kreuzburg, M.**, Petermann, E., Lopes de Paiva, M., Köhler, D., Schlüter, M., Rapaglia J., Schubert, M. 2017. Goldschmidt Conference. <sup>222</sup>Rn Surveys for the Detection of Submarine Groundwater Discharge: Why did the tracer fail in the Eckernförde Bay? (Talk).

Westphal, J., Fernández Fernández, L.E., Rach, B., Schmiedinger, I., **Kreuzburg, M.**, Koebisch, F., Böttcher, M.E.: Sulfur isotope biogeochemistry of sediments and soils from a temperate coastal-wetland transition zone, southern Baltic Sea. German Association of Stable Isotope Research, Annual Conference 2017 (GASIR 2017). Hannover, Germany, 09.10.2017 - 11.10.2017 (Poster).

**Kreuzburg, M.**, Voss, M., Jurasinski, G., Rehder, G. 2016. Potential impact of terrestrial nutrient input from a coastal peat land on the fluxes of climate relevant trace gases in shallow waters of the Baltic Sea. ECSA56\_0228, Coastal Systems in transition “from a ‘natural’ to an ‘anthropogenically-modified’ state”, reference number O5.61 (Talk).

#### Research stays abroad

From 4th of September until 10th of December 2017, Centre for Environmental & Information Technology (EIT), Ecohydrology Research Group, Mercator Fellow: **Fereidoun Rezanezhad** in the lab of Philippe Van Cappellen.

Influences of groundwater discharge and seawater recirculation on trace gas exchange from a column experiment of coastal sediments impacted by submerged peat.

#### Grant

Roland Schlich Grant, Early Career Scientist's Travel Support (ECSTS), EGU 2019

## Acknowledgement

The completion of this doctoral thesis would not have been achieved without the excellent support of my supervisors Gregor Rehder, Maren Voss from the Institute for Baltic Sea Research, the Mercator Fellow Fereidoun Rezanezhad from the Ecohydrology Research Group, University of Waterloo, Canada and Gerald Jurasinski from the Landscape Ecology, University of Rostock. Particular thanks go to Peter Feldens, who supported me fundamentally with geophysical data.

The completion of the thesis was also achieved thanks to the interdisciplinary exchange of knowledge and support among the colleagues of the Graduate Research College Baltic TRANSCOAST. I very much appreciated to be part of this project and would like to thank all members for the great and intense time we spent.

Furthermore, I thank Stefan Otto for the support of Gas Chromatographic (GC) analytics, Iris Liskow (IOW), who carried out geochemical analysis on the investigated sediments, Christian Burmeister for nutrient analysis and Marianne Vandergriendt (Ecohydrology Research Group, University of Waterloo, Canada) for the great support on aqueous sample analysis. I thank Susanne Liebner from the GFZ Helmholtz-Zentrum Potsdam for the quantification of microbial communities.

I am grateful to all the lab support of Sierra Willow Cranmer-Smith, Caroline Coccoli, Isabelle Wittstock, Florian Schneider and Charlotte Westhoven. I thank Sebastian Lorenz and Jürgen Becker (University Greifswald), for support with the BOREAS-platform, the IOW-crews of the research work boat Klaashahn, the IOW-Scientific Diver and the research vessel Elisabeth Mann Borgese.

I thank my family, who supported me in my decisions, the friends with whom I found energy, inspiration and balance during the many hours in and on the waves of the Baltic Sea, and my beloved Stefanie Rübensaal, who has always motivated and supported me during this demanding work on the doctoral thesis.

**This doctoral thesis was conducted within the framework of the Research Training Group GRK “Baltic TRANSCOAST” and was funded by the DFG (Deutsche Forschungsgemeinschaft).**

## List of abbreviations, symbols and variables

b.s.l.	below sea level
C	Carbon
Ca <sup>2+</sup>	Calcium ion
cal yr BP	Calibrated years before present
CO <sub>2</sub>	Carbon dioxide
CH <sub>4</sub>	Methane
C <sub>org</sub>	organic soil carbon
C <sub>inorg</sub>	inorganic soil carbon
CH <sub>3</sub> COOH	Acetic acid (acetate)
Cl <sup>-</sup>	Chloride
C/N-ratio	Carbon / nitrogen ratio
DIC	Dissolved inorganic carbon
DIN	Dissolved inorganic nitrogen
DOC	Dissolved organic carbon
δ <sup>13</sup> C	per mil variation of <sup>13</sup> C/ <sup>12</sup> C relative to a standard
EGNOS	European Geostationary Navigation Overlay Service
EC	Electric conductivity
ECD	Electron Capture Detector
FID	Flame Ionization Detector
GW	Artificial groundwater
H <sup>+</sup>	Hydrogen ion
H <sub>2</sub>	Hydrogen gas
HCl	Hydrochloric acid
HgCl	Mercury(I) chloride
H <sub>2</sub> O	Dihydrogenmonoxid (Water)
H <sub>2</sub> S	Hydrogen sulfide
IOW	Institute for Baltic Sea Research
LUNG-MV	Landesamt für Umwelt, Naturschutz und Geologie Mecklenburg-Vorpommern
m a.m.s.l.	Meter above mean sea level
μl	Microliter
μM	Micromolar = μmol/l
ml	Milliliter
XIV	



$\text{N}_2\text{O}$	Nitrous Oxide
$\text{NO}_3^-$	Nitrate
$\text{N}_2$	Dinitrogen
$\text{NO}_2^-$	Nitrogen dioxide
$\text{NH}_4^+$	Ammonium
nm	Nanometer
nmol	Nanomol
$\text{O}_2$	Oxygen
$\text{PO}_4^{3-}$	Phosphate
ppm	Parts per million
ppb	Parts per billion
S	Salinity
Si	Silicon
$\text{SO}_4^{2-}$	Sulfate
SGD	Submarine Groundwater Discharge
SW	Artificial seawater
Tg	Teragram
WMO	World Meteorological Organisation
$^{224}\text{Ra}$	Radium 224

## List of Figures

**Figure 1:** Overview of the study site with (a) south western Baltic Sea, (b) lower Warnow-river system and study site in the north east of Rostock and (c) on- and offshore study area with nearshore shallow water stations and the nature reserve “Heiligensee und Hütelmoor”

**Figure 2:** The photographs of the beach areas illustrate the strongly alternating dynamics along the shoreline showing (a) low water level events (0.6 m b.s.l.) (February 2017, M. Ibenthal) with outcropping peat deposits at the waterline and (b) flooding events showing high water level (+1.6 m a.m.s.l.) (February 2019, H Burchard), resulting in the erosion of peat blocks (c). The aerial view shows the coastal area in front of the lake Heiligensee (d), which is subject to strong coastal erosion and with outcropping peat deposits along the beach face (L. Tiepolt, 2014)

**Figure 3:** Schematic representation of the mini-chamber-lander system with syringes rosette on top of the lander, the incubation chamber partly installed in the sediment, and the multimeter system.

**Figure 4:** Schematic of purge and trap system (P&T) (in-house design). (A) shows a general overview of the main components and correlated valve links. (B) depicts the GC-internal pathway of the analytes ending with the detection of methane (left site), and of nitrous oxide (right site). The system was evaluated within an intercomparison study in the framework of the SCOR WG 142 (Wilson et al., 2018).

**Figure 5:** Schematic diagram of the controlled flow regime column system. The six soil columns were simultaneously and alternately exposed to advective flow with artificial seawater from the top and artificial groundwater from the bottom (pump and reservoirs not displayed). Intrusive measuring devices were installed for porewater sampling (P1/S1) and optical oxygen monitoring (P2/S2).

**Figure 6:** The distribution of bottom water CH<sub>4</sub> (a) and N<sub>2</sub>O (b) at the 25 stations in front of the coastal

peatland area. Each data plot marks a single sampling campaign on a one-day cruise between March 2016 and June 2017. In July and December CH<sub>4</sub> concentrations show a remarkable cross-slope gradient with higher CH<sub>4</sub> concentrations towards the coastline. In September CH<sub>4</sub> accumulated in deeper bottom waters, showing highest CH<sub>4</sub> concentrations of up to 161 nmol l<sup>-1</sup>.

**Figure 7:** Measurements of salinity, temperature (°C), and concentrations of dissolved oxygen (mg l<sup>-1</sup>), methane (nmol l<sup>-1</sup>) and nitrous oxide (nmol l<sup>-1</sup>) at station 33 in July 2017.

**Figure 8:** Methane concentrations in bottom water are plotted against the distance to the waterline. Along the beach face the concentrations show a strong variation with a mean value of about 100 times the atmospheric equilibrium concentrations of ~3 nmol l<sup>-1</sup>. The concentrations measured at 0 m distance to the waterline were sampled in shallow water along the beach in <60 cm of water depth.

**Figure 9:** Porewater salinity and concentrations of DIC (mmol l<sup>-1</sup>), δ<sup>13</sup>C<sub>DIC</sub> (‰) (provided by J. Westphal, 2017), CH<sub>4</sub> (nmol l<sup>-1</sup>), N<sub>2</sub>O (nmol l<sup>-1</sup>), NH<sub>4</sub><sup>+</sup> (mmol l<sup>-1</sup>), along the southwestern to northeastern transect (stations 1 to 76) along the shallow water beach area. The box in the north marks an area of outcropping peat deposits, characterized by concentration anomalies of most solutes compared to the central and southerly area.

**Figure 10:** Dissolved methane concentrations sampled in 2017 (Anne Breznikar) within the river stream of the Warnow at four stations (for locations see Figure 1b).

**Figure 11:** Distribution of bottom water methane and nitrous oxide in the Warnow-river in June 2016, revealing high concentrations of methane at the upper-most section of the Warnow-river and a

decreasing downstream gradient towards the outlet. In contrast, concentrations of nitrous oxide are increasing towards the outlet.

**Figure 12:** Geological profile along the beach with drilling locations (B3 to B9); sediment depth in meter above mean sea level (m amsl). Refer to Figure 6 for coring locations.

**Figure 13:** Top: Bathymetry and location of the study area along the southwestern Baltic Sea coast. White line parallel to the shore in southwest-northeastern direction indicates the bathymetric cross section shown underneath. The positions of sediment cores (red stars) and grab samples (white crosses) are also indicated. The black lines show the locations of the seismic profiles. The longshore bar was identified from the parametric echosounder data (INNOMAR, see Methods). Bottom: Bathymetric SW-NE transect at the upper shoreface indicating the distribution of the main geological units.

**Figure 14:** Left: Available backscatter data with grab samples for surficial ground-truthing and near-coastal peat observations. Right: Manual clustering of the backscatter data into three seafloor facies A-C. Representative grain size distributions for each facies are displayed using the PHI scale, with  $PHI = -\log_{10} d$ , where  $d$  is the grain size in mm, with A) fine sand (black), B) gravelly medium sand (grey) and (C) gravelly coarse sand (light grey). The insert in the right panel indicates the grain size distribution (PHI-scale) in Vol %.

**Figure 15:** Sediment depths (cm),  $^{14}C$  ages, photographs, lithology, grain size distribution (with  $PHI = -\log_{10} d$ , where  $d$  is the grain size in mm), organic carbon content (%),  $\delta^{13}C$  (‰), carbon/nitrogen ratios (C/N) of the 4 offshore sediment cores (C1, C3, C4, C5) retrieved from the study site.

**Figure 16:** Seismic data of profiles A, B, C, and D. Sediment cores to prove the ground-truthing are indicated. The position of core C3 was extrapolated to the nearest shot points of seismic lines C and D. The distance to line C is 25 m, and the distance to line D is 15 m. Refer to Figure 6. for location of the seismic lines.

**Figure 17:** Correlation of salinity calculated with chloride ( $Cl^-$ ) and electronic conductivity (EC) in peat-sand (P1) and sand (S1).

**Figure 18:** The fluxes of  $CO_2$  and  $CH_4$  (upper graphs) derived from concentration change rates in the headspace of all columns for peat-sand (left) and sand (right). Depth distributions of aqueous concentrations of salinity,  $O_2$ , DOC, DIC and  $SO_4^{2-}$  are presented for each column set, over the 50 days of the experiment period and under GW and SW flow regimes. The white arrows show the flow direction, the white lines indicate the advective flow rates with negative values indicating downwards SW flow and positive values showing upwards GW flow. The black dots represent the porewater sampling depths and the time of sampling. The grey bracket left of the peat-sand data indicates the position of the peat layer in the lower section (20 to 40 cm) of the core.

**Figure 19:** Correlations between  $SO_4^{2-}$  and chlorinity for peat-sand (P1) and sand column (S1)

**Figure 20:** Depth distribution of organic carbon contents ( $C_{org}$  %), total nitrogen (TN %), inorganic carbon contents ( $C_{inorg}$  %), stable isotopic signature of organic carbon ( $\delta^{13}C$  ‰) and carbon/nitrogen (C:N) ratios in the peat-sand and sand columns (mean values of all columns). The grey boxes indicate the peat sediment within the peat-sand columns, with light grey (20–30 cm) marking the transition zone (highly decomposed peat) and dark grey marking peat deposits of low decomposition.

**Figure 21:** The graphs show (a) higher methane concentrations in deeper water depths which are found in a trough-like area in the central transect and (b) a moderate relation between the the ratio of bottom water salinity and surface water salinity and  $CH_4$  concentrations ( $nmol\ l^{-1}$ ), indicating  $CH_4$  accumulation in bottom waters due to stratification events in the water column (<6m) water depth.

**Figure 22:** Local Holocene sea level curve based on Lampe (2010) with age/depth relationships obtained in this study. The  $^{14}\text{C}$ -ages cover the local sea level curve, except from C1.2, which likely reflect measurements of reworked material.

**Figure 23:** Geological profile perpendicular to the coast with drilling locations (MP2, B6, C3 - compare Figure 13 for core locations): sediment depths in m amsl. The information of sub-sedimentary peat continuation is based on ground-truthing with core C3 and the continuation of internal reflectors in the seismic profiles.

**Figure 24:** Relation between  $\delta^{13}\text{C}_{\text{DOC}}$  and salinity and the concentration of DOC and salinity for peat-sand core (P1)

**Figure 25:** Concentrations of DIC, DOC,  $\text{SO}_4^{2-}$ , salinity,  $\text{CH}_4$  and microbial abundances (repetitive measurements: a, b) of methanogens and sulfate reducers (P1) vs. sediment depth at day 50, which marks the end of the experiment.

**Figure 26:** Depth distribution of  $\text{O}_2$  and  $\text{SO}_4^{2-}$  deviating to the initial endmember concentration, presented for each column set (column P1 and S1), over 50 days of the experiment run time.

**Figure 27:** Conceptual extraction of the carbon exchange processes in the submarine, peat-containing estuary along the shoreline of our study site with (1) elevated sea-level situation. The blue arrow visualizes the flow of SW through carbon rich sediments driven by wave dynamics, with the red arrows showing the production pathway of DIC. The process likely included a high activity of sulfate reducing bacteria resulting in discharge of DIC and (2) low sea-level situation and calm surface water conditions. The discharge of  $\text{O}_2$ -depleted GW displaces methane oxidants, increases DOC release and facilitates methane production and emission into surface waters and the atmosphere.

## List of Tables

**Table 1:** Composition of artificial groundwater (GW) and artificial seawater (SW) used in the groundwater discharge experiment

**Table 2:** Calculated accumulation rates of methane and nitrous oxide within the Incubation chamber are suggested to origin from sedimentary fluxes.

**Table 3:** Determined  $^{14}\text{C}$  ages in the study area. Age intervals are given at a 95.4 % confidence level.

## Motivation

The coastline of the study area represents a threshold zone between terrestrial and marine ecosystems. As a result of environmental interactions regarding hydrological exchange, solute transport and biogeochemical processes, this zone is subject to temporal and spatial changes of highly variable scales and magnitudes. Research on emissions of climate-relevant trace gases (e.g. CH<sub>4</sub> and N<sub>2</sub>O) from shallow coastal areas, in particular from the southern Baltic Sea, is rare, although coastal zones contribute the bulk of marine trace gas production both on a global scale and in the North Sea and Baltic Sea regions. The overall objective of this thesis was to better understand the interactions between these adjacent and tidely connected systems and to assess important drivers of nearshore biogeochemical cycles and trace gas production.

During the first year of this research project, the focus lay on intensive field work, involving research in coastal offshore areas with scientific diver missions, repetitive surveys along a near coastal transect and investigations along the interface between the Baltic Sea and the coastal peatland “Heiligensee und Hütelmoor”. Specific methodological approaches were used to investigate the subterranean mixing zone of land-derived groundwater and seawater. The main goals of the surveys along the waterline and along the offshore transects in 2016 were to identify pore- and surface water anomalies of solutes and temporal patterns with respect to physicochemical parameters and solutes.

At the same time, the shallow offshore continuation of peat deposits at the southern coast of the Baltic Sea was investigated, using a combination of hydro-acoustic methods, geologic surveys and physical and geochemical characterization of surface sediments and sediment cores, which leaded to a full geophysical and geological assessment of the development of the seabed. The objectives were to determine the sedimentary surface and subsurface structure offshore the wetland area with the extensions of former terrestrial peat deposits into the Baltic Sea and to estimate the Holocene dynamics of the wetland formation and erosion. Knowing the extension and age of the peat sediments in the Baltic Sea, allowed to constrain the onset of the peatland formation and to estimate the total extent of submerged terrestrial organic matter and its rate of degradation in shallow coastal areas. These findings motivated the multi- component/interdisciplinary column experiments that were conducted, in order to improve the fundamental, process-based

understanding of the biogeochemical processes governing carbon and nutrient transformations and exchange of trace gases in shallow waters impacted by terrestrial nutrient input from the coastal peatland. In 2017, the mobilization of peat-derived DOC and biogeochemical processes that govern carbon transformations were investigated, by flow-through column experiments using natural sediments sampled at the study site. During the experiments, we imposed alternating cycles of upward flowing oxygen-depleted groundwater and downward flowing oxygen-rich brackish water. The main goal of the experimental study was to monitor the biogeochemical processes governing carbon transformations in submerged coastal peat in the mixing zone between low-salinity groundwater and recirculated brackish water. Therefore, the emissions of CH<sub>4</sub> and CO<sub>2</sub> from the cores were measured in the experiments. To the best of our knowledge, this was the first experimental study investigating DOC mobilization and mineralization processes in submerged coastal peat soil and the production of climate relevant trace gases under dynamic (bidirectional) flow conditions, that were controlled to simulate freshwater-seawater mixing in the subterranean estuary. It can be hypothesized that submerged, formerly terrestrial peat deposits in the surf zone of the study area affect biogeochemical processes by inhibiting seawater recirculation, while emitting degradable dissolved organic carbon compounds. These processes could increase microbial activity, likely result in increased marine production and release of trace gases at the study site.

## 1. Introduction

### 1.1. Climate relevant trace gases in coastal zones

Coastal zones are important for ecological, social, economical and scientific reasons, for example development of coastlines, land usage and infrastructure, archeology, sediment dynamics and biogeochemical fluxes (Boynton et al., 1980; Slomp and Van Cappellen, 2004; Small and Nicholls, 2003; Valiela, 2009; Wong et al., 2014). Given their special interface with land and atmosphere, coastal zones are among the most productive regions on earth and at the same time subject to constant natural and anthropogenic modification and destruction. The main cause for the poor ecological status of coastal areas is considered to be an excess supply of nutrients, referred to as eutrophication. Although difficult to estimate the consequences, eutrophication is a major ecological problem in coastal areas and estuaries, enhancing growth of algae and plants, which, after sedimentation of the organic residues, increases oxygen demand in bottom waters and may constrain or eliminate aerobic benthic organism due to anoxia (Rosenberg, 1985; Vallius, 2006). The formation of such anoxic bottom water layers can enhance anoxic organic matter mineralization, increasing the production of climate-relevant trace gases such as methane ( $\text{CH}_4$ ) and nitrous oxide ( $\text{N}_2\text{O}$ ), as these are strongly controlled by the oxygen ( $\text{O}_2$ ) concentration (Bange et al., 2010; Gelesh et al., 2016). Thus, on global scales the coastal regions, especially estuaries, lagoons and upwelling zones have been identified as a major contributor of marine trace gases (Bange et al., 2010; Bange, 2006; Heyer and Berger, 2000; Rhee et al., 2009; Weiss et al., 1992).

#### 1.1.1. Methane

Methane ( $\text{CH}_4$ ) is the most important greenhouse gas after water vapour and carbon dioxide ( $\text{CO}_2$ ) with a global warming potential 25 times more potent than  $\text{CO}_2$  over a 100 year time horizon (Koch et al., 2014). On a global scale, the atmospheric  $\text{CH}_4$  concentration has increased by about 257 % since 1750, contributing ~32 % of the anthropogenic radiative forcing (Stocker et al., 2013) and has nowadays reached 1845 ppb (WMO 2016). Global methane emissions from

the open ocean into the atmosphere are modest ( $0.4\text{--}1.8 \text{ Tg CH}_4 \text{ yr}^{-1}$ ) compared to the emissions from wetlands ( $117.2 \pm 49.7 \text{ Tg CH}_4 \text{ yr}^{-1}$ ), continental shelves ( $13 \text{ Tg CH}_4 \text{ yr}^{-1}$ ) and estuaries (between 1 and 7  $\text{Tg CH}_4 \text{ yr}^{-1}$ ) (Bange et al., 1994; Borges et al., 2016; Zhang et al., 2017). Together, coastal regions and estuaries generate approximately 75 % of the total marine  $\text{CH}_4$  emissions to the atmosphere (Bange et al., 1994), though this number remains highly uncertain.

The most abundant process of marine  $\text{CH}_4$  production is microbial methanogenesis (Cicerone and Oremland, 1988) (e.g.  $\text{CO}_2 + 4\text{H}_2 \rightarrow \text{CH}_4 + 2\text{H}_2\text{O}$ ), a form of anaerobic respiration, using  $\text{CO}_2$  instead of  $\text{O}_2$  as the electron acceptor. The majority of methane production worldwide, however, results from acetate degradation (e.g.  $\text{CH}_3\text{COOH} \rightarrow \text{CO}_2 + \text{CH}_4$ ) (Deppenmeier, 2002). The formation and release of  $\text{CH}_4$  into the water column in the marine environment is closely associated to the microbial reduction of sulfate ( $\text{SO}_4^{2-}$ ) to hydrogen sulfide ( $\text{H}_2\text{S}$ ), which is the dominating metabolic process of organic matter mineralization in anoxic marine sediments (Zehnder and Mitchell, 1978). Sulfate-reducing bacteria (SRB) are able to successfully outcompete methanogens during organic matter degradation (Whiticar, 2002) for available free hydrogen ( $\text{H}_2$ ) e.g.  $4\text{H}_2 + \text{SO}_4^{2-} \rightarrow \text{HS}^- + \text{OH}^- + 3\text{H}_2\text{O}$  (Sørensen et al., 1981). Additionally, methanotrophic microbes (bacteria and archaea) oxidize  $\text{CH}_4$  to  $\text{CO}_2$  as their source of carbon and energy under oxic and anoxic conditions using oxygen ( $\text{O}_2$ ) and sulfate ( $\text{SO}_4^{2-}$ ), respectively (Jørgensen et al., 2001; Schmaljohann, 1996). Thus, in marine environments high  $\text{SO}_4^{2-}$  concentrations sustain anaerobic  $\text{CH}_4$  oxidation, which provides an effective barrier preventing sedimentary  $\text{CH}_4$  from reaching the water column (Dale et al., 2008; Iversen and Blackburn, 1981; Jørgensen et al., 2001; Reeburgh and Alperin, 1988). Nevertheless, in near-coastal shallow regions, sediment-derived  $\text{CH}_4$  still represents a significant source of dissolved  $\text{CH}_4$  in the water column (Bange, 2006; Borges et al., 2016; Gelesh et al., 2016).

### 1.1.2. *Nitrous oxide*

Coastal seas and shelf areas are affected by high loads of land-derived nitrogen, most of it being of anthropogenic origin. Dissolved nitrogen can serve as a fundamental source for the production and release of marine nitrous oxide ( $\text{N}_2\text{O}$ ) (Bange et al., 2010; Hsiao et al., 2014; Seitzinger et al., 2000; Sonesten et al.,



2018). On a global scale coastal oceans and estuaries contribute between 0.5 and 2.9 Tg N yr<sup>-1</sup> of the total natural and anthropogenic N<sub>2</sub>O sources of 17.7 Tg N yr<sup>-1</sup> (IPCC, 2007). The present day concentration within the atmosphere is 328 ppb and rises at a rate of 0.25 % yr<sup>-1</sup> (Prinn et al., 1990). Nitrous oxide has an atmospheric residence time of 114 years. It is a major ozone-depleting substance and has a global warming potential nearly 300 times greater than that of carbon dioxide, making it the third most important climate-relevant gas in the atmosphere (Ehhalt et al., 2001; Forster et al., 2007; Smith, 2010). In marine ecosystems N<sub>2</sub>O is formed by microbial processes predominantly nitrification ( $\text{NH}_4^+ \rightarrow \text{N}_2\text{O} \rightarrow \text{NO}_2^- \rightarrow \text{NO}_3^-$ ) and denitrification ( $\text{NO}_3^- \rightarrow \text{N}_2\text{O} \rightarrow \text{N}_2$ ) under oxic to suboxic conditions (Bange et al., 2010; Bange, 2006) and is dependent on external parameters such as temperature, O<sub>2</sub> concentration and organic matter supply. Higher concentrations of N<sub>2</sub>O in the water relative to the atmosphere will lead to concentration compensation and thus represents a source of atmospheric nitrous oxide. Equilibrium concentrations are dependent on water temperature, salinity, ambient air pressure and the atmospheric N<sub>2</sub>O concentrations (Bange, 2006; Weiss and Price, 1980). So far N<sub>2</sub>O was measured in the northern and south-western Baltic Sea (Rönner, 1983) showing concentrations of 79 to 148 % and 91 to 312 %, respectively, compared to an atmospheric equilibrium concentration of 10 nmol l<sup>-1</sup> (Bange et al., 1998). Strong oversaturation of N<sub>2</sub>O was also detected in the Bornholm basin with values up to 31.3 nmol l<sup>-1</sup> (equivalent to 3 times equilibrium with the atmosphere) and also in the shallow estuarine waters of the Limfjord and Norsminde Fjords, Denmark, with concentrations up to 490 nmol l<sup>-1</sup> (Bange et al., 2010; Myllykangas et al., 2017).

## **1.2. Geology and physical processes in coastal regions**

The present shorelines of the Baltic Sea have been shaped during the Littorina Sea period since about 8000 cal yr BP (Lemke 1998; Björck 1995) after the last glacial maximum (LGM). During the Holocene retreat of the glaciers and the associated rise in sea level (Lampe, 2005) submarine terraces of former shorelines have developed (Kolp, 1990). With the onset of the Littorina transgression (Lampe, 2002; Reimann et al., 2011), the southern Baltic Sea level rose rapidly to about 2 m below today's sea level, about 8000 cal yr BP. At 5800 cal yr BP a stabilization of the sea

level was observed and has remained largely stable in this area since 4000 cal yr BP facilitating the formation of coastal wetlands. The age and position of basal peat deposits, as formed in former coastal wetlands, can be used to obtain information about past sea level (Feldens and Schwarzer, 2012; Gehrels and Anderson, 2014; Milliman and Emery, 1968). Ongoing isostatic movements cause a subsidence of the southern Baltic Sea coast by about 0.1–0.2 cm yr<sup>-1</sup> (Lampe, 2005; Lampe et al., 2011; Rosentau et al., 2007). The relative sea level rise of approximately 0.1–0.12 cm yr<sup>-1</sup> (Dietrich and Liebsch, 2000) increases the pressure on the local coastal wetlands caused by the eustatic sea level rise, and thus affects the presence of bedforms in shallow waters.

Ongoing coastal water dynamics such as waves and currents-induced erosion, sediment transport and accumulation have influenced the evolution of coastlines immensely and have led to coastline displacement due to land-loss or land reclamation and therefore changed spatial extensions of coastal ecosystems and habitats (Harff et al., 2009; Lehfeldt and Milbradt, 2000; Schlungbaum and Voigt, 2001). In the Baltic Sea, local sea-level rise can vary widely due to isostatic adaptation (Köster 1961). The majority of global coastlines such as the wadden sea and shallow beaches, river deltas, estuaries, cliffs but also tropical mangroves, marchland and other types of coastal wetlands consist of permeable, soft sediments and increasingly suffer from adverse processes such as erosion, flooding and submergence. The impact of submergence on coastal areas is accelerated by sea level rise and land subsidence caused by large-scale drainage for agricultural use and will therefore stress and shape coastal urban living areas and ecosystems in the future (Hooijer et al., 2012; Nieuwenhuis and Schokking, 1997). Along the Baltic Sea, about 1800 km<sup>2</sup> of coastal low-lying wetland is influenced by saltwater intrusion (Sterr, 2008). Sea level rise is further expected to result in a loss of wetland areas in inland direction, provided that accumulation of sediments is lower than erosion and the vertical growth rate is below that of sea level rise (Lampe and Janke, 2004a; Vestergaard, 1997). Although coastal wetlands account for only ~15 % of the global wetland area, their ecosystem services are estimated to account for 43.5 % of the value of all natural biomes (Davidson et al., 2019) and have long been recognized as highly endangered by sea water intrusion, erosion and submergence (Nicholls and Cazenave, 2010; Vestergaard, 1997; Wong et al., 2014).

### **1.3. Hydrological processes across the terrestrial marine interface**

The coastal systems in which subterranean land-derived freshwater measurably dilutes coastal seawater within the coastal aquifer, contain a so-called subterranean estuary as they show the most important features of surface estuaries (Moore, 1999). The land-sea interface is subject to hydrological exchange with significant impacts on mineralization processes within the subterranean estuary (Michael et al., 2005; Moore, 1999; Robinson et al., 2007; Slomp and Van Cappellen, 2004) and wetlands (Hahn et al., 2015; Neubauer, 2013). These exchange processes will be enforced by more frequently occurring storm events and sea-level rise in the future (Nicholls and Cazenave, 2010; Plag and Jules-Plag, 2013; Wang et al., 2016). In some areas of the Baltic Sea, coastline retreat has caused submergence of terrestrial, organic carbon rich peat sediments (Kreuzburg et al., 2018; Lampe et al., 2010; Sergeev et al., 2015a). Erosion and submergence are reinforced by land subsidence of peatland and can alter the hydrologic exchange processes and pathways across the land-sea interface (Hooijer et al., 2012; Nieuwenhuis and Schokking, 1997) such as seawater intrusion, surficial runoff, sub-surface mixing, and submarine groundwater discharge (SGD).

Submarine groundwater discharge, comprises all flow of water from the seabed into the coastal ocean (Burnett et al., 2003) and consists predominantly of recirculated seawater, driven through permeable sediments by wave action, density gradients and sea level dynamics (Cyberski, 2011; Moore, 2010; Robinson et al., 2007; Santos et al., 2012). Only a minor fraction of SGD is freshwater and typically amounts to about 4–10 % (Burnett et al., 2006; Li et al., 1999; Moore, 2010). This fraction is mainly controlled by groundwater recharge and the hydraulic gradients between land and sea, and is often O<sub>2</sub>-depleted and enriched in nutrients, methane (CH<sub>4</sub>) and free hydrogen (H<sub>2</sub>) (Andersen et al., 2005; Bugna et al., 1996; Slomp and Van Cappellen, 2004). Since coastal peatlands mostly exhibit low topographic relief, their hydraulic gradients and freshwater discharge into coastal areas tend to be relatively low (Barlow and Reichard, 2010). Nonetheless, even in coastal regions of low elevation, SGD can reach values of up to 200 cm d<sup>-1</sup> (Rapaglia, 2005) and can therefore deliver high fluxes of chemical compounds to the coastal environment. For instance, SGD-borne nitrogen fluxes can be of the same order of magnitude as those delivered by rivers (Knee et al., 2010; Knee and Paytan, 2012; Seitzinger and Harrison, 2008) and has been identified as a source of dissolved

carbon to nearshore marine environments (Bugna et al., 1996; Bussmann and Suess, 1998; Porubsky et al., 2013; Schlüter et al., 2004). Thus, SGD can have a considerable impact on biogeochemical processes and influence ecosystems in coastal regions (Hu et al., 2006; Leote et al., 2008; Paerl, 1997).

#### *1.3.1. Coastal interactions with peatlands*

Peatlands cover only 3 % of the earth's surface but store about 30 % of global soil organic carbon ( $C_{org}$ ) and 12 to 21 % of global soil organic nitrogen (Gorham, 1995; Limpens et al., 2008; Menon et al., 2007; Strack, 2008; Wang et al., 2016). Located along the coastal margins, peatlands can act as a major source of organic carbon and and nitrogen to coastal and shelf areas (Freeman et al., 2001; Mulholland, 2003; Wang et al., 2016). The uptake capacity of organic matter is predominantly controlled by the prevailing hydrological conditions (Roulet et al., 1992; Zauft et al., 2010). When drained, peatlands can switch from being a carbon sink to emitting greenhouse gases such as  $CO_2$  (Sirin and Laine, 2008; Strack, 2008). By contrast, flooded peatlands usually represent a source of atmospheric  $CH_4$  (Gatland et al., 2014; Hahn et al., 2015) and have repetitively been recognized as a major source for  $N_2O$  (Marushchak et al., 2011; Menon et al., 2007; Palmer et al., 2012; Repo et al., 2009). Hydrologic exchange such as saltwater intrusion between coastal peatlands and the adjacent shoreline may impact onshore ecosystems and biogeochemical processes in different magnitudes (Charman and Others, 2002; Hahn et al., 2015; Hoggart et al., 2014). Seawater-derived solutes such as chloride ( $Cl^-$ ), dissolved oxygen ( $O_2$ ) and sulfate ( $SO_4^{2-}$ ) can affect the mineralization of organic matter in the seabed (Chambers et al., 2014; Mulholland, 1981; Rezanezhad et al., 2016; Weston et al., 2011). A number of experimental approaches have identified the ionic strength of advective porewater, measured by electrical conductivity (EC), as an important impact factor for DOC concentrations and mobilization, where an increasing EC results in decreasing DOC release from organic soils and vice versa (Clark et al., 2011; Kalbitz et al., 2000; Limpens et al., 2008; Tiemeyer et al., 2017; Tipping and Hurley, 1988). Furthermore, Tiemeyer et al., (2017) reported that the production of DOC is dependent on the residence time of the porewater, showing a clear negative correlation between DOC concentrations and higher porewater velocities in the effluent of a saturated column

experiment. Positive correlations between the concentration and production of CH<sub>4</sub> and DOC were previously found, which could further be linked to a common subsurface organic carbon (buried peat) source (Aravena and Wassenaar, 1993; Liu et al., 2011). Marine organic-rich peat sediments can be found in offshore environments of adjoining peatlands (Delaune et al., 1994; Kreuzburg et al., 2018; Taffs et al., 2012), where they are constantly supplied with high amounts of SO<sub>4</sub><sup>2-</sup>. How these submerged peat deposits contribute to biogeochemical cycling, however, is not well understood.

#### 1.4. Study site

The study site is located in the northeast of Rostock-Warnemünde, northern Germany, and comprises a nearshore (within 1 km offshore) shallow coastal area with water depth mostly <6 m and an adjacent shoreline of 3 km length in front of the coastal peatland and nature reserve “Heiligensee und Hütelmoor” (Figure 1). The coastline of the study area is mainly facing west wind conditions.

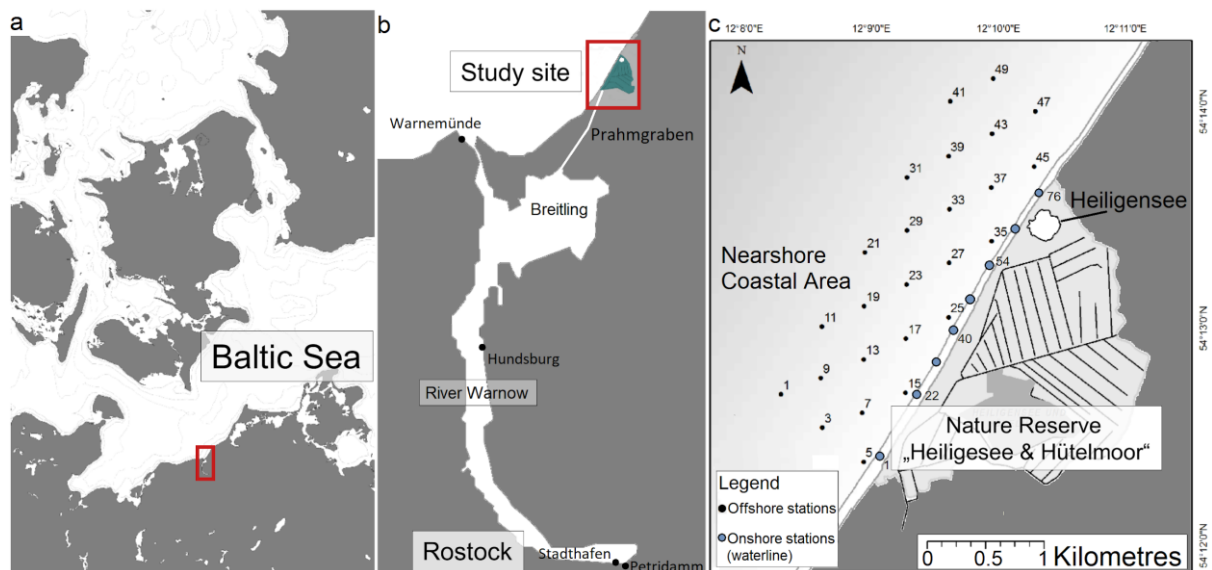


**Figure 1:** Overview of the study site with (a) south western Baltic Sea, (b) lower Warnow river system and study site in the north east of Rostock and (c) on- and offshore study area with nearshore shallow water stations and the nature reserve “Heiligensee und Hütelmoor”

##### 1.4.1. Onshore area

The peatland extends roughly 1.6 km in the north-south direction and 1.4 km in the east-west direction and is surrounded by the Rostocker Heide, a forest area with sandy soils. The peat layer consists of *Carex* and *Phragmites* with a thickness of

up to 3 m behind the dunes and thins out in landwards direction. The entire nature reserve experienced large anthropogenic disturbances. It was drained for agricultural purposes until the 1970s (Dahms, 1991; Voigtländer et al., 1996), and subsequently rewetted for restoration of the biodiversity in the 1990s (Hahn et al., 2015; Hübner and Gräff, 2013; Miegel et al., 2016). Aside from the northern area, where lake Heiligensee has been developed, the peatland still drains through an extensive channel system towards the south. The drainage with open ditches started in the 1970s, causing a severe degradation of the upper peat horizons and subsidence of the soil surface. In order to restore pristine conditions, drainage was reduced and a dam was constructed in 2010. In the last decades, the onshore area has been subject to a wide range of investigations, including gas emissions and hydrology monitoring programs as well as geologic surveys (Jurasinski et al., 2018; Koch et al., 2014; Koebsch et al., 2015; Kreuzburg et al., 2018; Lasak et al., 2010; Miegel et al., 2016; Voigtländer et al., 1996; Wen et al., 2018).

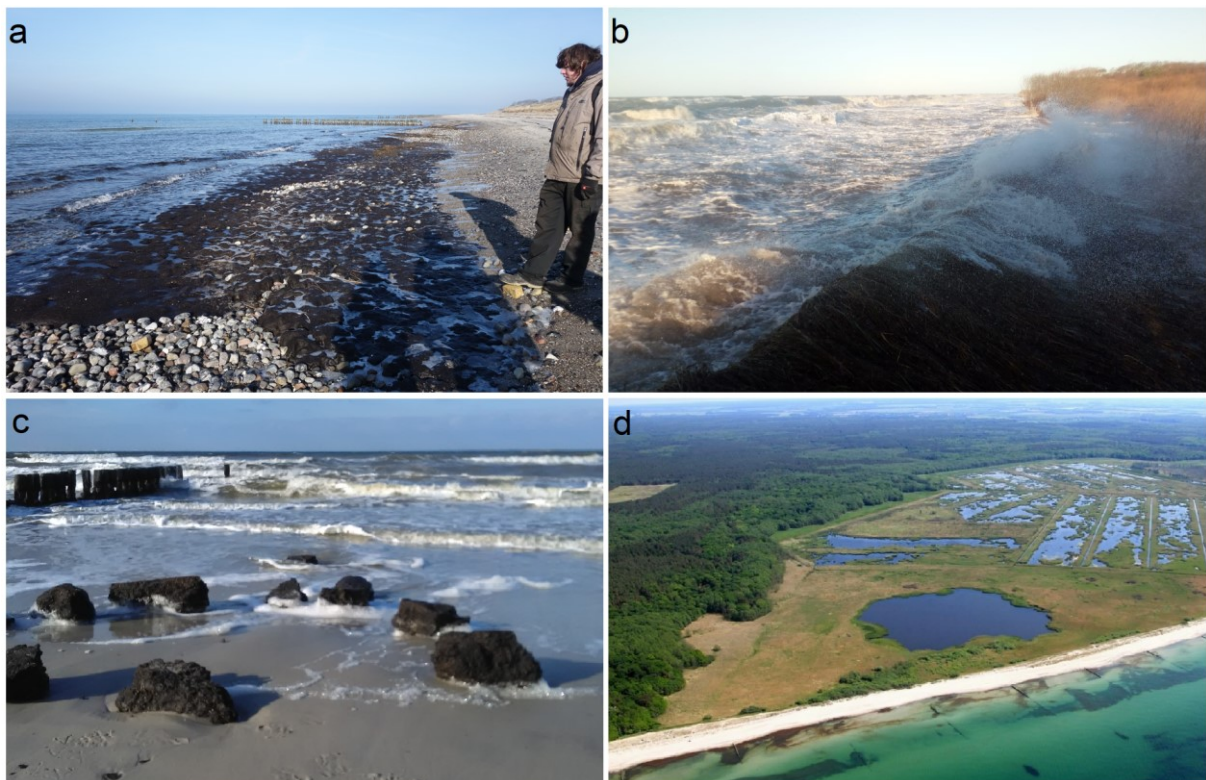


**Figure 2:** The photographs of the beach areas illustrate the strongly alternating dynamics along the shoreline showing (a) low water level events (0.6 m b.s.l.) (February, 2017, M. Ibenthal) with outcropping peat deposits at the waterline and (b) flooding events showing high water level (+1.6 m a.m.s.l.) (February, 2019, H Burchard), resulting in the erosion of peat blocks (c). The aerial view shows the coastal area in front of the lake Heiligensee (d), which is subject to strong coastal erosion and with outcropping peat deposits along the beach face (L. Tiepolt, 2014)

#### 1.4.2. *Waterline and offshore area*

The shoreline has been subject to beach nourishments, groin and dyke constructions after several wash-over events (Kolp, 1957; Voigtländer et al., 1996). Based on the observed coastal retreat rates, rough calculations of 20 to 115 cm yr<sup>-1</sup> (Rebentrost, 1973) assume a total land loss of ~3 km of this low-lying (-0.1 to +0.7 m above mean sea level) wetland since the onset of its formation (Bohne and Bohne, 2008; Voigtländer et al., 1996). To reduce coastal erosion and flooding, an artificial dune dike was built in 1903, separating and protecting the low-lying peatland from flooding of the Baltic Sea (Bohne and Bohne, 2008; Miegel et al., 2016; Voigtländer et al., 1996). Nevertheless, the area was flooded several times, most recently in 1995, which necessitated the reconstruction of the dune dike in 1996. Since 2000, the dune dike has not been rebuilt in order to achieve renaturation and the restoration of natural dynamics, resulting in estimated coastal retreat rates of 120–210 cm yr<sup>-1</sup> (General Plan Küsten und Hochwasserschutz, Mecklenburg-Vorpommern). Physical stress of coastal dynamics and retreat results in outcropping peat-layers along the beach in the northern area of the study site, whereas the central and southern area is covered by permeable heterogeneous sediments (Hübner and Gräff, 2013; Kreuzburg et al., 2018).

#### 1.4.3. *Warnow-river*

The Warnow-river enters the Baltic Sea ~6 km southwest of the coastal study site and represents the only significant supply of river water to the coastal area (Figure 1). The Warnow is subdivided into two sections. The majority of the river course with a total length of 152 km is river dominated (upper Warnow), whereas the shorter section (~13 km) of the Warnow is strongly dominated by Baltic Sea water (lower Warnow or Warnow estuary), showing increasing salinity towards the outlet (Landesamt für Umwelt, Naturschutz und Geologie Mecklenburg Vorpommern, LUNG-MV). Due to the low discharge (50–60 m<sup>3</sup>) and mixing, the estuary is strongly stratified and is characterized by a near-bottom net inflow of saline Baltic Sea water and a near-surface low saline outflow (Buer et al., 2018; Jurasinski et al., 2018; Thäns, 2012). Both the lower Warnow and minor streams such as the *Prahmgraben*, which connects the Warnow with the coastal peatland via the *Breitling* (Figure 1) (Miegel et al., 2016), are considered to be strongly eutrophic due to agricultural fertilization (LUNG–MV, 2008).

## 2. Methods

Scientific investigations in shallow water regions (0–10 m) are very difficult due to poor accessibility. In addition, they are limited by methods usually applied in marine sciences and using tools often developed for large research vessels and greater water depths. The resulting gap in knowledge was termed the „white coastal band“ (personal communication with Klaus Schwarzer, 2015). To address this issues, IOW's Klaashahn platform was used as a state-of-the-art research working boat over the past years to enhance the understanding of these shallow coastal regions.

### 2.1. Geochemical field surveys

#### 2.1.1. *Offshore water sampling*

In the offshore area, seven surveys of water sampling were carried out during which bottom- and surface water was sampled at 25 stations (Figure 1c) on one-day cruises with the research work boat Klaashahn in 2016 (March, April, June, July, September, December) and 2017 (June). Samples for analysis of CH<sub>4</sub>, N<sub>2</sub>O and nutrients were collected with a Niskin bottle in 100 ml crimp vials. All samples were filled with overflow to avoid atmospheric contamination and were immediately closed on board and preserved with saturated HgCl solution equivalent of 0.25 % of the sample volume. The vials were stored upside down at 4 °C until analysis.

##### 2.1.1.1. Water column characteristics

A cruise on the research vessel Elisabeth Mann Borgese (EMB) in 2017 enabled repetitive investigation of the water column at Station 33 (Figure 1). Salinity and temperature were recorded using a Sea-and-Sun CTD connected with Aanderaa Type 3835 for measuring the distribution of oxygen concentrations. Additionally, multilevel sampling for analysis of CH<sub>4</sub> and N<sub>2</sub>O was conducted in order to obtain information about the distribution of trace gas concentrations in the water column and its temporal variability.



### 2.1.1.2. Mini chamber lander system

At offshore stations 33, 25, and 35 (Figure 1) a Mini-Chamberlander System (Unisense®) was installed in 2017 for durations between 24 and 30 h, following the methods previously described by Thoms et al., (2018). The system is equipped with a ~27 litres incubation chamber, open at its base, enclosing and isolating a 0.09 m<sup>2</sup> area of the sediment-surface-water interface (Figure 3). Syringes of 60 ml were installed in a syringe-rosette to sample the incubated water in 2 h time intervals. Changes in physical parameters and chemistry of the incubated water were analyzed from the water samples (concentrations of CH<sub>4</sub>, N<sub>2</sub>O, Nutrients) and sensors of conductivity, temperature, oxygen. Samples from inside the incubation chamber were used to detect the accumulation or depletion of nutrients and gas concentrations and were used to calculate flux rates of CH<sub>4</sub> and N<sub>2</sub>O according to the formula 1:

$$(1) \quad F = \frac{dC}{dt} \times \frac{V}{A}$$

where F is the flux (μmol m<sup>-2</sup> d<sup>-1</sup>), dC/dt is the concentration change over time, V is the volume of water inside the incubation chamber, and A is the area enclosed by the incubation chamber. Further, oxygen and conductivity was recorded inside and outside the chamber.

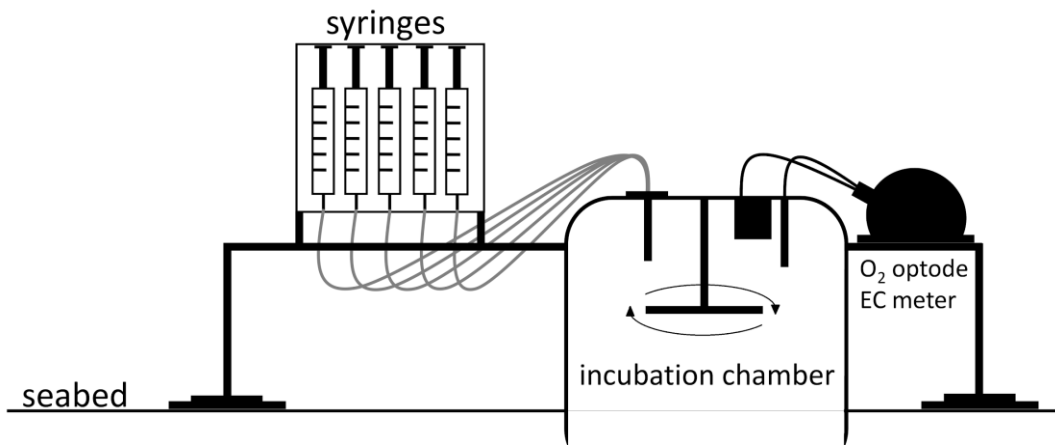


**Figure 3:** Schematic representation of the mini-chamber-lander system with syringes rosette on top of the lander, the incubation chamber partly installed in the sediment, and the multimeter system.

### 2.1.2. *Shoreline field campaigns*

The shoreline along the coastal peatland was investigated with respect to the characteristics of the surface and porewater in February 2016 and June, July and August 2017 (for onshore stations see Figure 1). Porewater samples were extracted from sediments using 1m push-point porewater lances and subsequently analyzed for oxygen, salinity, nutrients ( $\text{NH}_4^+$ ,  $\text{NO}_3^-$ , Si,  $\text{PO}_4^{3-}$ ) and trace gas concentrations ( $\text{CH}_4$ ,  $\text{N}_2\text{O}$ ).

### 2.1.3. *Investigations of the Warnow-river system*

The water masses from the Warnow-river system was first investigated in a sampling survey in June 2016. It was the aim to better estimate the impact of river water reaching the study site with the potential changes of the concentration of dissolved trace gases ( $\text{N}_2\text{O}$ ,  $\text{CH}_4$ ). The survey clearly indicated a downstream gradient with decreasing concentrations towards the outlet of the Warnow estuary and bottom water concentrations of  $1115 \text{ nmol l}^{-1}$  in the upper end of the estuary, Stadthafen (see Figure 1b). According to these high concentrations a study was planned to investigate to what extent the Warnow is a potential source of trace gases for the atmosphere, the Baltic Sea and the study site in front of the coastal peatland "Heiligensee und Hütelmoor". This study was embedded in this PhD thesis and conducted from January to June 2017 mainly by Anne Breznikar in the framework of her master thesis: "Klimarrelevante Spurengase im Warnowausstrom - Anne Breznikar, 2017".

### 2.1.4. *Analytical methods used for samples from the field campaigns*

#### 2.1.4.1. Gas Chromatography

Quantitative determinations of methane ( $\text{CH}_4$ ) and nitrous oxide ( $\text{N}_2\text{O}$ ) concentrations in seawater samples were conducted with a purge and trap system (P&T) by dynamic headspace method. An inert ultra-high purity carrier gas (Helium 99.999 % and additional preparation by purifier) purges volatile dissolved gas compounds, which is cryofocussed and injected via thermal desorption. The gases were then analyzed by a gas chromatograph (GC) (Shimadzu GC-2014), equipped with a flame ionization detector (FID) for  $\text{CH}_4$  measurements and an electron capture detector (ECD) for  $\text{N}_2\text{O}$  measurements. The Flame Ionization Detector

works at 200 °C and is based on the detection of ions formed during combustion of organic compounds in a hydrogen flame. The generation of these ions is proportional to the gas concentration in the sample. The ECD works at 345 °C and measures the flow of moving electrons by the ionized carrier gas. If the sample contains molecules with electronegative functional groups such as nitrous oxide, electrons will be captured and the current will be reduced. The reduction in electron flow is proportional to the quantity of trace gas components. The main analytical system is composed of a purge chamber (200 x 24 mm, with integrated frit, porosity 2, Erich Eydam KG, Kiel, Germany), a gas trap (stainless steel, 700 mm x 1/8", U-shaped, filled with HayeSep D, 60/80 mesh, CS Chromatographie Service GmbH, Langerwehe, Germany), a sampling loop (incorporation of gas standards) and a GC to detect CH<sub>4</sub> and N<sub>2</sub>O.

The saturation values in % (with 100 % = atmospheric equilibrium concentrations) were calculated as the ratio between the expected equilibrium concentration of the gas as a function of the mole fraction within the ambient atmosphere and the detected concentration of dissolved gas in seawater. Equilibration concentrations of N<sub>2</sub>O and CH<sub>4</sub> were calculated after (Bange, 2008) and (Wiesenburg and Guinasso, 1979), respectively.

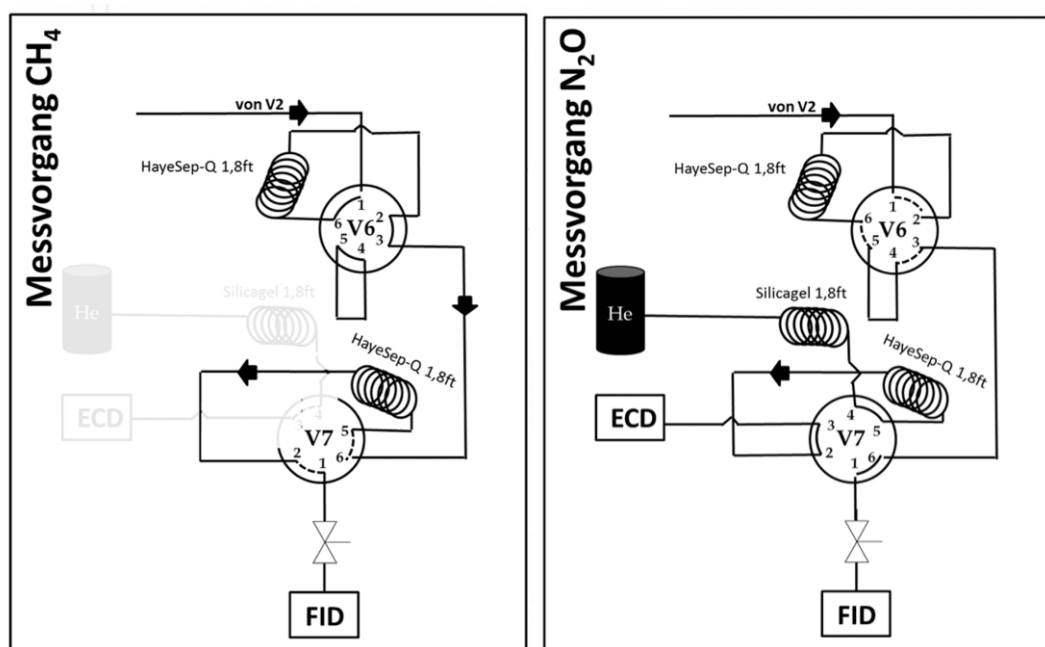


**Figure 4:** Schematic of purge and trap system (P&T) (in-house design), showing a general overview of the main components and correlated valve links and depicts the GC-internal pathway of the analytes ending with the detection of methane (left site), and of nitrous oxide (right site). The system was evaluated within an intercomparison study in the framework of the SCOR WG 142 (Wilson et al., 2018).

#### 2.1.4.2. Nutrients

Seawater samples were deep-frozen (-20 °C) until analyzation to determine nutrient concentrations and were measured colorimetrically according to Grasshoff et al., (1999) by means of a Seal Analytical QuAAtro39 automated Continuous Segment Flow Analyzer (CFSA) and allows quantitative determinations of ammonia, nitrate and nitrite, phosphate, and silicate. Each component requires a specific method: Ammonia concentrations are determined by the reaction of Berthelot, in which a blue-green colored complex is formed which is measured at 660nm. Sodium salicylate is used instead of phenol (Method No. Q-033-04 Rev. 6). Limit of quantification is 0,5  $\mu\text{mol l}^{-1}$ . The method for the automated determination of nitrate and nitrite was developed by the Royal Netherlands Institute for Sea Research (NIOZ) at which nitrate is reduced to nitrite at pH 8 in a copperized cadmium reduction coil (Method No. Q-068-05 Rev. 8 for nitrate and Q-070-05 Rev. 5 for nitrite). Total nitrite (reduced nitrate plus primarily contained nitrite) reacts under acidic conditions with sulphanilamide to form a diazo compound. Subsequent resulting Diazo compounds that then couples with N-1-naphthylethylenediamine dihydrochloride (NEDD) to form a reddish-purple azo-dye measured at 520 nm. Limit of quantification for nitrate and nitrite is 0.2  $\mu\text{mol/L}$  and 0.05 $\mu\text{mol/L}$ , respectively. The determination of phosphate is based on the colorimetric Method No. Q-048-04 Rev. 2 and is conducted by the formation of a blue phosphomolybdenum complex, caused by the reaction of phosphate, molybdate ion and antimony ion followed by the reduction of with ascorbic acid. Limit of quantification for phosphate is 0.1  $\mu\text{mol/L}$ , respectively. Soluble silicates were determined using Method No. Q-005-04 Rev. 2, which is based on the reduction of silico- molybdate complex in acid solution to molybdenum blue by ascorbic acid. Additional oxalic acid reduces interference from phosphate. The absorbance is measured at 820 nm. Limit of quantification for phosphate is 0.1  $\mu\text{mol l}^{-1}$ .

## 2.2. Geophysical surveys

*The chapters 2.2.1. to 2.2.4. are published in Kreuzburg et al., 2018. Sub-marine Continuation of Peat Deposits From a Coastal Peatland in the Southern Baltic Sea and its Holocene Development. Frontiers in Earth Science, 6(103). Available at: <https://www.frontiersin.org/articles/10.3389/feart.2018.00103/full>.*

### 2.2.1. Geophysical data

Bathymetric and backscatter intensity data were collected with a Norbit iwbms multibeam echo sounder, which was pole-mounted on the research boat Klaashahn. Data in shallow waters (1.5 to 7 meters) were recorded in June 2016 and July 2017. The Norbit iwbms uses an 80 kHz wide chirp signal centered at 400 kHz and an opening angle of 130° to 155°, set depending on water depth. Navigation data were acquired using an Applanix Surfmaster inertial navigation system utilizing the EGNOS correction. Total navigation accuracy was about 0.5 m both in the latitude and longitude direction. In addition to continuous sound velocity measurements at the multibeam transducer head, water column sound velocity was measured using an SVP probe. The preparation of bathymetric data was completed using the Hypack 2016 software. Data processing included a quality control, the automatic and manual removal of spikes, the correction of roll and pitch offsets, as well as the application of water column SVP profiles. Data were then gridded to a resolution of 0.5 m. Backscatter intensity data were processed using mbsystem (Caress and Chayes, 1995). A correction for the angular varied gain, including the multibeam residual beam pattern, was applied using mbbckangle. The backscatter data were passed through a gaussian low-pass filter to reduce speckle noise and gridded to a resolution of 0.5 m. Seismic data were acquired using an INNOMAR standard parametric echo sounder during the June 2016 survey. In total, seismic data were acquired for the area covering a distance of 30 km. The system was pole-mounted on the Klaashahn research work boat. Data were recorded at frequencies of 8, 10 and 15 kHz, of which the 15 kHz frequency is shown in this study. A low pass swell filter was applied to remove heave artefacts caused by a malfunctioning motion sensor. However, due to the rapid movements of the small work boat, the wave impact could not be entirely removed. Two-way-travel time were converted to depths using a sound velocity of 1480 m/s.

### 2.2.2. *Ground-truthing*

For seafloor ground-truthing of the backscatter data, twelve 30 cm sediment cores were taken during scientific-diver missions and 20 surface sediment grab samples were taken from a boat. Deeper vertical ground-truthing of the seismic data was achieved using 4 sediment cores (Figure 15) retrieved from maximum sediment depths of 280 cm with hand-pulling extraction tools from the BOREAS drilling platform (Lampe et al., 2009). The closed probe heads (STITZ) of 1 m and 2 m, respectively were fitted with customized PVC liners of Ø46 mm for core extraction. In total 7 sediment cores on land were taken with a percussion driller (Rammkernsonde). Open metal rods of Ø40 mm were used to sample sediment cores to a depth of -3.5 m below sea level (bsl). To assess the peat thickness in more detail, peat probings were conducted in the shallow coastal water. A Ø1 cm metal rod was pushed through the peat and stopped by the sand layer. All drilling and sampling locations were levelled with a real-time kinematic and differential GPS (Leica Viva Net-Rover).

### 2.2.3. *Grain size distribution*

Given the sandy composition of the analyzed sediments, no chemical pretreatment was performed. The grain size distribution of surface sediments (grab samples) was determined from sub-samples (~150 g) of homogenized sediments. Dry sieving was conducted with DIN standard ISO 3310-1 sieves. Fractions <0,063 mm were lost during washing and were determined by weight difference compared to the total weight after washing and drying. Fractions >2 mm were retained. Automated sieving was conducted by a computer-controlled sieving tower (AS200) and a coupled Sartorius balance. The grain size distribution of the sediment cores was determined by laser diffraction using a CILAS 1180, as not enough material for traditional sieving was available. However, grain sizes larger than 1 mm cannot be measured with this method. To allow a comparison between the grain size distributions obtained with both methods, the first mode is used as the central statistical parameter. The mode is unaffected by removing the fine (mechanical sieving) or coarse (optical grain size distribution) sediment fraction, and can be used for bimodal sediments. All grain sizes are shown using the PHI scale, with  $PHI = -\log_2 d$ , where  $d$  is the grain size in mm.

#### 2.2.4. *Geochemical sediment analysis and <sup>14</sup>C age-determination*

Organic carbon contents ( $C_{org}$ , after digestion with HCl) and stable C isotope analysis of bulk material were performed on 2 onshore- and 3 offshore sediment cores using an infrared Elemental Analyzer Multi EA 2000 CS. Oven-dried samples were ground and homogenized in an agate motor mill. Splits of 10–20 mg powdered, homogenized sample were weighed in tin ( $C_{inorg}$ ) and silver ( $C_{org}$ ) containers (Nieuwenhuize et al., 1994). Stable C isotope analysis were performed using an Isotope Ratio Mass Spectrometer (IRMS, Thermo Fisher Scientific), connected to an elemental analyzer via an open split interface. The C isotope data are reported in delta notation with  $\delta^{13}C$  (‰) =  $\{(^{13}C/^{12}C)_{sample} / (^{13}C/^{12}C)_{standard} - 1\} \times 1000$ . The used reference gas was ultra-pure CO<sub>2</sub> calibrated against international standards (IAEA-C3, IAEA-C6, NBS 22) at the Leibniz-Institute for Baltic Sea Research (IOW). Calibration for carbon quantities was done with the reagent acetanilide. The lab internal standard was peptone (Merck) with a standard deviation of <0.2 ‰. AMS <sup>14</sup>C age control of plant material, shells, wood and bulk organic carbon dating (Table 1) was done by the commercial testing laboratory Beta Analytics (<https://www.radiocarbon.com>). Calibration of <sup>14</sup>C ages was done following (Reimer et al., 2013).

### 2.3. **Column experiment study**

In this study, the mobilization of peat-derived DOC and biogeochemical processes that govern carbon transformations was investigated by flow-through column experiments using natural sediments (Figure 5). During the experiments, alternating cycles of upward flowing oxygen-depleted groundwater and downward flowing oxygen-rich brackish water was imposed. The main goal of the study was to monitor the biogeochemical processes governing carbon transformations in submerged coastal peat in the mixing zone between low-salinity groundwater and recirculated brackish water. The water level above all sediment columns was ~10 cm to simulate coastal shallow water conditions. Three of the six 40 cm long sediment cores were filled with submerged peat in the lower half and overlain with marine sand. The other three cores only contained sand. For both column types one column (P1/S1) was used to sample dissolved reactants and products of mineralization processes (e.g., SO<sub>4</sub><sup>2-</sup>, DIC, DOC), one column (P2/S2) was used for monitoring the vertical aqueous oxygen distribution, and one additional column

was used for additional control-measurements (P3/S3). The emissions of CH<sub>4</sub> and CO<sub>2</sub> were measured in all six cores. To the best of our knowledge, this is the first experimental study investigating DOC mobilization and mineralization processes in submerged coastal peat soil, in conjunction with the production of climate relevant trace gases, under dynamic (bidirectional) flow conditions mimicking freshwater-seawater mixing in the subterranean estuary (Moore, 1999). The natural sediment cores were collected in ca. 20 cm water depth off the nature reserve “Heiligensee und Hütelmoor” on the 25<sup>th</sup> of August 2017 using 60 cm long and 7.5 cm wide PVC liners. The cores (P1, P2, P3) were collected in shallow coastal waters near location 54.222139°N and 12.168361°E (Figure 12, station B4), a sample site characterized by outcropping peat layers of minor decompositional degree of H 3–4 according to von Post, (1922), covered with 10–20 cm of marine sand. Sand cores (S1, S2, S3) were collected at location 54.2108°N and 12.1582°E (Figure 12, station B8). One core of each sample site was kept as a reference to pristine geochemical parameters with that of altered conditions. In order to ensure similarity of the four replicates, cores were taken within an area of <0.25 m<sup>2</sup>. Immediately after sampling, the cores were sealed at the top and bottom with gas- and water-tight end caps and transported to the laboratory, where they were stored at 4 °C with supernatant water. On September 3<sup>rd</sup>, the cores were drained, packed with ice in a cryobox and transported to the University of Waterloo, Canada. After visual inspection the sediment sequence of the cores remained intact, but slight changes in sediment deposition cannot be excluded.

### *2.3.1. Column experiment and instrumentation*

The experimental setup included 8 columns (6 for sediment cores and 2 for water storage) made of acrylic glass matching the sediment core size. A computerized, multi-channel pump was used to control the water flow through all cores. The column system was formerly described in Rezanezhad et al., (2014) but has been specifically modified for the variable water flow regimes in this study. The columns were filled from the bottom by a custom-made lifting jack device and packed with tin-foil to prevent sub-sedimentary photosynthetic activity. Three of the columns were filled with 40 cm peat-sand cores containing ~20 cm of sand at the top. The other three columns were filled with 40 cm sand cores. The top and bottom of the



columns were closed with acrylic glass end-caps sealed tightly by O-rings inside of the end-caps. A filter membrane (Soil Measurement Systems, LLC, USA, bubbling pressure: 600 mbar) closed off the bottom of the columns with a nylon mesh (Soil Measurement Systems, LLC, USA, bubbling pressure: 32 mbar) was placed on top of the filter membrane. For each column, three steel rods connected the acrylic top and bottom end-caps and were secured with bolts. The sediment columns were connected to the water storage columns with chemically resistant polyurethane tubing. In order to completely replace the air-filled pore space with water, the initial filling was conducted from the bottom with artificially produced groundwater (see 4.2.1) at a rate of  $0.3 \text{ ml min}^{-1}$ . The total headspaces above the sediment surface were partly filled with water amounting to  $\sim 888 \text{ cm}^3$  in columns P1, P2 and P3 and  $\sim 1002 \text{ cm}^3$  in columns S1, S2 and S3, respectively. All columns contained  $\sim 478 \pm 57 \text{ cm}^3$  of air-filled headspace above the water (Figure 5).

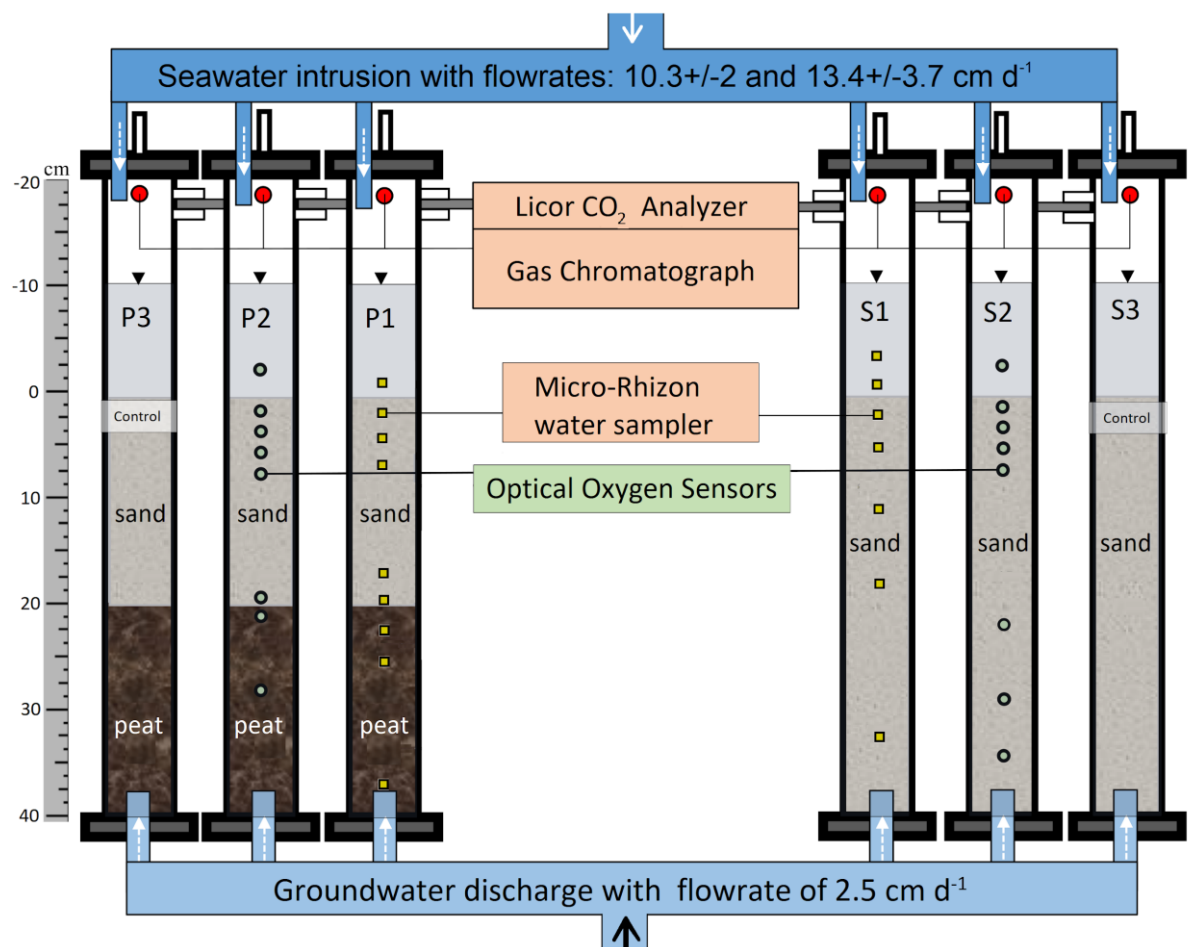


**Figure 5:** Schematic diagram of the controlled flow regime column system. The six soil columns were simultaneously and alternately exposed to advective flow with artificial seawater from the top and artificial groundwater from the bottom (pump and reservoirs not displayed). Intrusive measuring devices were installed for porewater sampling (P1/S1) and optical oxygen monitoring (P2/S2).

The storage columns were filled with artificial seawater (SW), which was continuously sparged with air, and artificial, fresh groundwater (GW), which was continuously sparged with argon to ensure oxygen-depleted conditions (details of the GW and SW compositions are given in 4.2.1). The columns were incubated at  $24 \pm 2$  °C during the entire course of the experiment. Each sediment column had 18 lateral ports (1/8" NPT compression fittings) equally spaced every 3 cm for porewater sampling. The ports were airtight and fitted with Teflon septa. In the following, all depths are referenced with respect to the sediment surface. The ports of four columns (P1, P3, S1, S3) were equipped with ceramic samplers, 5 cm in length and 0.25 cm in diameter, with a filter pore-size of 0.15  $\mu\text{m}$  (CSS5 MicroRhizon™ samplers, Ejkelamp, Netherlands, #19.21.23F) (Seeberg-Elverfeldt et al., 2005). The samplers were introduced horizontally into the sediment matrix, below the sediment surface, to extract porewater samples for porewater chemical and dissolved gas analysis (Figure 5). A vacuum pump (Soil Measurement Systems, LLC, USA, #CL-042) set at -100 mbar was used to extract porewater through the samplers. The headspace above the stable water surface in the columns was periodically closed in order to measure sediment-derived trace gas accumulation.

### 2.3.2. *Ground and seawater flow regimes*

The upwards flowing GW and downwards flowing SW were set to simulate discharge and recirculation regimes through permeable coastal sediment impacted by submerged peat. The porewater flow velocities were adapted from the column experiment conducted by Tiemeyer et al., (2017). The height of the water table within the sediment columns was imposed using a computerized, multi-channel pump connected to the water storage reservoirs. The constant ponding of the water above the sediment surfaces ensured complete water saturation in the sediments and resulted from the equilibrium between the programmed pump rate and the water outflow, whereby the water in the sediment column was continuously exchanged. The GW upwards flow was pump-controlled at rates of 2.5  $\text{cm d}^{-1}$  and the water level height was limited by the water outlet ~10 cm above the sediment surface. The SW downwards flow was controlled by the valve setting with measured rates of  $10.3 \pm 2$   $\text{cm d}^{-1}$  through peat-sand cores and  $13.4 \pm 3.7$   $\text{cm d}^{-1}$  through sand

cores. During the different flow regimes, the water was discharged on the opposite side of the inflow. Flow direction and water type was adjusted using valve settings. The level of the water table in the soil columns fluctuated between 7.5 and 10 cm above the soil surface.

Coastal aquifers can be strongly depleted in oxygen (Andersen et al., 2005; Bugna et al., 1996), while shallow water along the shoreline is usually saturated with oxygen due to constant mixing with the atmosphere. To imitate similar conditions, argon gas was used to de-oxygenate the GW and air from the laboratory was used to saturate the SW with oxygen. The artificial groundwater salinity was set at  $S \approx 1.6$ , which is slightly lower than the measured values in the field ( $S \approx 3$ ), but allowed a better differentiation of the endmember concentrations. The salinity of artificial SW is based on highest salinity measured ( $S \approx 18$ ) along the shoreline of the study site (all observations from 2017). The salinity based chloride ( $\text{Cl}^-$ ) concentrations were  $882 \pm 66 \text{ mg l}^{-1}$  (range: 806–1015) for GW and  $8666 \pm 407.1 \text{ mg l}^{-1}$  (range: 7987–9577) for SW. Chloride was used as a conservative tracer, to describe physical transport behavior and as a measure of salinity with  $S = 0.00180665 \times \text{Cl}^- \text{ mg l}^{-1}$  (Lyman, 1969). The ratio of the remaining elements in respect to chloride was set based on SGD surveys in Kiel Bay, Baltic Sea in 2015 (unpublished data). Although the salinity of the Baltic Sea is largely described, there is a lack of stoichiometric data on shallow shorelines and coastal aquifers. The detailed composition of GW and SW endmembers are given in Table 1. All six columns were fed with SW and GW, from identical water reservoirs for the 50 day-period of the experiment.

**Table 1:** Composition of artificial groundwater (GW) and artificial seawater (SW) used in the groundwater discharge experiment

Component (mmol l <sup>-1</sup> )	SO <sub>4</sub> <sup>2-</sup>	Cl <sup>-</sup>	Na <sup>+</sup>	Ca <sup>2+</sup>	Mg <sup>2+</sup>	K <sup>+</sup>	HCO <sub>3</sub> <sup>-</sup>	PO <sub>4</sub> <sup>3-</sup>	NH <sub>4</sub>	NO <sub>3</sub> <sup>-</sup>	SiO <sub>2</sub>	Salinity
SW	13.2	259	222.9	5.2	25	4.6	2.5	0.00047	0.0017	0.004	0.0085	17.8
GW	0.2	28.8	17.4	4.2	1.6	0.37	0.37	0.017	0.00021	0.007	0.065	1.6

### 2.3.3. Analytical methods

#### 2.3.3.1. Gas fluxes among the air-water interface

The gas flux,  $F_{gas}$ , from the ponding water into the air-filled headspace of each column was obtained by measuring the change in gas concentration over time in the headspace after closure from the laboratory atmosphere, according to formula 2:

$$(2) \quad F_{gas} = \frac{dC_{gas}}{dt} \times \frac{V}{S} \times \frac{P}{RT}$$

where  $dC_{gas}/dt$  describes the changing gas concentration (ppm) over time,  $V$  ( $m^3$ ) is the volume of the headspace and  $A$  ( $m^2$ ) is the exposed water surface area.  $P$  is the atmospheric pressure (Pa),  $R$  is the gas constant ( $8.314 \text{ Pa m}^3 \text{ K}^{-1} \text{ mol}^{-1}$ ),  $T$  is the absolute temperature (K). To avoid uncontrolled gas accumulation and to minimize evaporative loss from the sediments over time, the air-filled headspaces of the sediment columns were continuously flushed with water-saturated air by passing the air through a water-filled vial. In order to determine the gas emissions from the aqueous phase into the headspace, the air ventilation was stopped. Fluctuations of the headspace volumes were taken into account in every gas flux measurement. The fluxes of  $CH_4$  ( $\mu\text{mol m}^{-2} \text{ d}^{-1}$ ) were monitored 2–3 times a week from all six cores. The concentrations were determined at the beginning ( $t_0$ ) and end ( $t_N$ ) of incubation ( $24 \pm 6 \text{ h}$ ) by sampling 10 ml of headspace gas using glass syringes and were subsequently measured by Gas Chromatography (Shimadzu Gas Chromatograph (Model GC-2014) equipped with an advanced Flame Ionization Detector (FID) and an Electron Capture Detector (ECD). For standards, a three-point calibration was used with the following reference gases: Level 3 ( $CH_4$  100 ppm;  $CO_2$  900 ppm;  $N_2O$  50 ppm), Level 2 ( $CH_4$  9.8 ppm;  $CO_2$  100 ppm;  $N_2O$  10 ppm) and Level 1 ( $CH_4$  5 ppm;  $CO_2$  600 ppm;  $N_2O$  1 ppm). In total, 6 ml of gaseous sample was injected into the gas chromatograph, 5 ml of which were used for flushing the 1 ml sample loop. The porewater samples for dissolved  $CH_4$  were extracted in peat-sand columns from the sediment at depths of -1 (i.e. above the sediment), 2, 5, 8, 17, 20, 23, 26, 38 cm and from the sand column at sediment depths of -4.5, -1.5, 1.5, 10.5 19.5 and 34.5 cm. Before sampling, 0.5 ml of water was extracted for flushing and to eliminate the air-filled void in the syringe. 1 ml porewater samples were collected with 10 ml watertight, pre-treated ( $HgCl = 25 \mu\text{l}$ )

glass syringes (MICRO-Mate®) by connecting them to the MicroRhizon™ water samplers. The volume of the porewater within the syringes was determined by the weight using a high precision balance. 8 ml of helium was then added to form a headspace for gas equilibration. After 2 hours of equilibration time, by carefully shaking the syringes, which has been shown to strip at least 95 % of CH<sub>4</sub> from the solution (Dillon et al., 1999), the headspace was injected into the GC. All samples were analyzed on the same day of collection. The water-headspace CO<sub>2</sub> fluxes were sampled daily by an automated multiplexer CO<sub>2</sub> flux measurement system (LI-8100, LI-COR Biosciences, Lincoln, NE, USA) via two lateral ports (Figure 5). Air from the headspace above the water surface was then circulated through the infrared gas analyzer (IRGA) of the LI-8100 and back to the column. The rate ( $dC_{CO_2}/dt$ ) was estimated from six consecutive 180 s observation windows spanning a total time interval of 15 min. Volume (m<sup>3</sup>) is a combination of the headspace volume and the sampling loop through which the headspace gas circulates.

#### 2.3.3.2. Porewater geochemical analysis

Porewater samples (8 ml per sample depth; peat-sand n = 134, sand n = 97 in total) were extracted from cores P1 and S1 with MicroRhizon™ samplers (Cabrera, 1998; Knight et al., 1998; Seeberg-Elverfeldt et al., 2005) and were sub-sampled into separate vials. One ml of each water sample was filtered through a 0.2 µm membrane filter (Thermo Scientific Polysulfone filter) for analysis of Cl<sup>-</sup>, SO<sub>4</sub><sup>2-</sup>, NO<sub>3</sub><sup>-</sup>, and acetate (C<sub>2</sub>H<sub>3</sub>O<sub>2</sub><sup>-</sup>) by Ion chromatography (IC, Dionex ICS-5000 with a capillary IonPac® AS18 column). DIC and DOC concentrations were determined from 1 ml sub-samples each following non-purgeable organic carbon (NPOC) method using a total organic Carbon analyzer (Shimadzu TOC-LCPH/CPN). All samples analyzed for DOC were pretreated with HCl. One ml water samples were collected to measure pH using the Horiba B-213 Twin pH (two-point calibration at pH 4 and 7) and electrical conductivity (EC), using a WTW EC Meter (three-point calibration at 99.1, 999, 9976 µS cm<sup>-1</sup>).

For stable C isotope analysis ( $\delta^{13}C_{DOC}$ ) sample fractions equivalent to 0.2 mg carbonate were removed from the sample aliquots and injected into 12 ml flat bottom Exetainer vials (Labco #739W) and subsequently treated with ortho-phosphoric acid and potassium persulfate. The addition of phosphoric acid converts

inorganic carbonates present in the sample to CO<sub>2</sub>, which is removed by bubbling the sample with a helium gas stream for about 10 minutes (EPA SOP for DOC, 2002; IsoPrime, 2014). Samples were then sealed and microwaved. During this heating treatment, the potassium persulfate oxidizes the dissolved organic carbon in the sample to CO<sub>2</sub>, which is then sampled from the headspace vial and analyzed for its isotopic composition. Standards ranged from -12 ‰ (EIL-36 - cane sugar) to -26.5 ‰ (EIL-35 - beet sugar). Delta values obtained by dual inlet MS calibrated with IAEA carbonate standards and verified by EA-IRMS analysis normalized with IAEA-CH3 (cellulose) + IAEA-CH6 (sugar), USGS-40 and USGS-41 (L-Glutamic Acid) (Stainton et al., 1977; St-Jean, 2003). The results of the samples and all standard runs were statistically evaluated and calculated uncertainties were ≤0.2 ‰ on the d<sup>13</sup>C.

#### 2.3.3.3. Monitoring of dissolved oxygen

The sediment cores P2 and S2 were equipped with multi-fibre optode (MuFO) oxygen sensors to measure the dissolved O<sub>2</sub> concentration at regular depth intervals. The sensor ends were installed into the sediment columns, eight installed in each column, at 2, 5, 8, 14, 17, 20, 38 cm and above the sediment (-1 cm) in the peat-sand column and at 1.5, 4.5, 7.5, 10.5, 16.5, 31.5 cm and above the sediment (-4.5, -1.5 cm) in the sand column. The MuFO, a luminescence-based optode technique, uses sensors made of fibre optic cables, with each cable having one sensing tip and one imaging tip (Larsen et al., 2011). The sensor was built in-house using a sensing solution containing Pt(II) mesoTetra (pentafluorophenyl) -porphine (PtTFPP) as the luminophore (Badocco et al., 2012). The uncoated ends were placed in front of a DSLR camera and blue LED light (447.5 nm wavelength) in a similar setup as described in (Larsen et al., 2011). The emitted light was photographed every 2 hours for the duration of the experiment and, following image processing using ImageJ software (Rasband, 2015), the light intensity was related to the O<sub>2</sub> concentration through the Stern-Volmer relationship. The sensors were calibrated by obtaining the relation between light intensity and O<sub>2</sub> concentration. As the optode light intensity responses as a function of salinity, calibrations for each sensor were conducted at a range of different salinities prior to the experiment. Statistical data analysis was performed to identify significant levels among the water flow regime under changing salinities and DOC and DIC production. Moreover, the

relationship between salinity and O<sub>2</sub> as well as between SO<sub>4</sub><sup>2-</sup> concentrations and CH<sub>4</sub> and CO<sub>2</sub> fluxes were statistically analyzed. Significant differences were accepted when the p-value was smaller than significance level  $\alpha = 0.05$ . Gridding of porewater concentrations was performed using the R-package ggplot in R (R Foundation for Statistical Computing, Vienna, Austria) within RStudio.

#### 2.3.3.4. Solid phase geochemistry

At the end of the experimental period, all peat-sand and sand cores were drained overnight, extracted from the columns and sliced in 3 cm thick pieces. The sediment slices from each depth were homogenized and separate aliquots were taken for geochemical characterization. For the latter, the samples were freeze-dried and stored at room temperature. Organic carbon contents (C<sub>org</sub>) were measured after removal of carbonates with 10 % HCl. The stable isotopic composition of solid organic carbon ( $\delta^{13}\text{C}$ ) was determined on the initial and post-experimental sediment cores. The samples were ground in an agate mortar mill. Splits of 10–20 mg powdered, homogenized sample material were weighed in tin and silver containers (Nieuwenhuize et al., 1994). The isotopic composition of stable carbon isotopes ( $\delta^{13}\text{C}$ ) was analyzed at the Leibniz-Institute for Baltic Sea Research (IOW) using an Isotope Ratio Mass Spectrometer (IRMS), Thermo Fisher Scientific, connected to an elemental analyzer via an open split interface (Multi EA 2000 CS). The reference gas was ultra-pure CO<sub>2</sub> from a bottle calibrated against international standards (IAEA-C3, IAEA-C6, NBS 22). The calibration for carbon quantities was done with acetanilide reagent. The lab internal standard was peptone (Merck) with a standard deviation of <0.2 ‰. Considering the 3 cm slice thickness, the depth data was interpreted and compared with the initial and untreated cores.

#### 2.3.3.5. Quantification of methanogens and sulfate reducers

Genomic DNA was extracted from 0.2–0.3 g of duplicates of sediment and peat samples retrieved from column P2 at the end of the experiment using an EURx GeneMatrix Soil DNA Purification Kit (Roboklon, # E3570, Berlin, Germany). DNA concentrations were quantified with a Nanophotometer P360 (Implen GmbH, Munich, Germany) and Qubit 2.0 Fluorometer (Thermo Fisher Scientific, Darmstadt, Germany). Quantitative polymerase chain reaction (qPCR) for the determination of functional gene copy numbers of methanogenic archaea and

sulfate reducing bacteria was performed via SybrGreen assays on a Bio-Rad CFX instrument (Bio-Rad, Munich, Germany), similar to as described by Wen et al., (2018) and Vuillemin et al., (2018) with slight modifications. In detail, the methyl coenzyme M reductase alpha subunit (*mcrA*) as being the functional methanogenic gene was amplified with the primer combination mlas-F/mcra-R (ggT ggT gTM ggD TTC ACM CAR TA/ CgT TCA TBg CgT AgT TVg gRT AgT) with primer annealing at 60 °C. The dissimilatory sulfite reductase beta subunit (*dsrB*) as a functional gene of sulfate reducing bacteria was quantified with the primers dsrB2060-F/dsrB4-R (CAA CAT CgT YCA YAC CCA ggg/ gTg Tag CAG TTA CCg CA) with annealing at 62 °C. Different DNA template dilutions (1:10, 1:50, 1:100) were tested prior to the qPCR runs to determine optimal template concentration without inhibitions through co-extracts. The 25 µl reactions contained 12.5 µl of KAPA SYBR® FAST mastermix (Life Technologies, CA, USA), 0.25 µM concentrations of the primers, and 5 µl of DNA template. Data acquisition was done at 80 °C to avoid quantification of primer dimers. The specificity of each run was verified through melt-curve analysis and gel electrophoresis. Only runs with efficiencies between 80 and 105 % were used for further analysis. Measurements were performed in triplicates. Equimolar DNA mixtures of *Methanosarcina barkeri*, *Methanobacterium lacus* and *Methanosarcina soligelidi* SMA21 were used for plasmid standards of *mcrA* and of *Desulfovibrio vulgaris* for *dsrB*.



### 3. Results

#### 3.1. Trace gas investigation within the study site

##### 3.1.1. Offshore concentrations of $\text{CH}_4$ and $\text{N}_2\text{O}$

The record of methane concentrations in bottom waters showed mean values of  $27 \pm 29 \text{ nmol l}^{-1}$  (range: 5–162  $\text{nmol l}^{-1}$ ) and revealed a clear impact on distinct water masses along the shoreline showing varying temperatures and salinities. Additionally, the bottom water concentration of  $\text{CH}_4$  exhibits strong temporal variations ranging with mean values of  $8 \pm 3 \text{ nmol l}^{-1}$  ( $201 \pm 74 \%$ ) at the 3<sup>rd</sup> of March 2016 ( $3.2 \pm 0.2 \text{ }^\circ\text{C}$ ) to  $80 \pm 42 \text{ nmol l}^{-1}$  ( $2845 \pm 1624 \%$ ) at the 26<sup>th</sup> of September 2016 ( $15.9 \pm 0.3 \text{ }^\circ\text{C}$ ) 2016 (Figure 6). The highest  $\text{CH}_4$  concentration in bottom waters of  $162 \text{ nmol l}^{-1}$  (5994 %) was observed in September, when pronounced salinity differences across the water column were detected between bottom ( $\sim 19$ ) and surface ( $\sim 9$ ) water. This observation is supported by a correlation between the ratio of bottom and surface water salinities and the concentration of dissolved  $\text{CH}_4$  in bottom waters ( $r^2 = 0.6$ ,  $p < 0.001$ ,  $n = 24$ ). At this condition, high  $\text{CH}_4$  was observed to accumulate in the central trough area of the offshore study site at a mean water depth of  $5.4 \pm 0.5 \text{ m}$  (Figure 13). In contrast, bottom water concentrations of  $\text{CH}_4$  revealed cross-slope gradients during periods with a less stratified water column. In July, April and December a significant increase could be observed towards the shallow coast. During these surveys, the highest  $\text{CH}_4$  concentration of  $55 \text{ nmol l}^{-1}$  (1961 %) was observed at station 35 ( $\sim 50 \text{ m}$  distance to the waterline) in July (Figure 6) that coincided with a slight temperature increase and decreasing salinities at the north eastern part of the study site (Jurasinski et al., 2018), where outcropping peat deposits have been observed (Figure 13). During the same field campaigns, the spatial and temporal concentrations of nitrous oxide ( $\text{N}_2\text{O}$ ) were investigated, showing only minor fluctuations ( $96 \pm 14 \%$ ) and no significant relation to bathymetry or shoreline structures. Yet it is noticeable, that during July a spatial variation with highest  $\text{N}_2\text{O}$  concentration of  $16 \text{ nmol l}^{-1}$  (177 %) in the south-west and lowest concentration of  $4.8 \text{ nmol l}^{-1}$  (53 %) was observed in bottom water temperatures of  $18 \text{ }^\circ\text{C}$  (Figure 6).

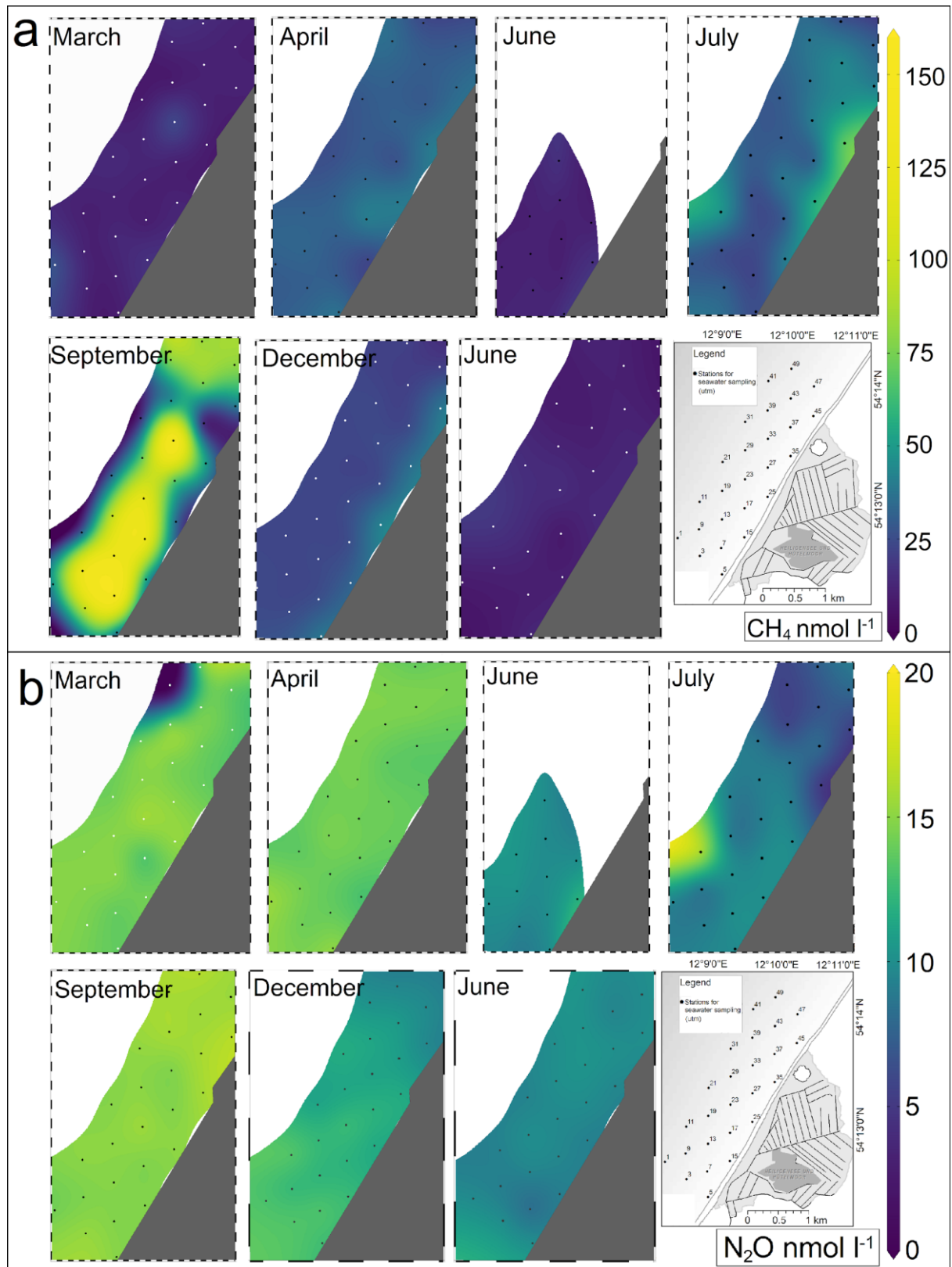


**Figure 6:** The distribution of bottom water  $\text{CH}_4$  (a) and  $\text{N}_2\text{O}$  (b) at the 25 stations in front of the coastal peatland area. Each data plot implies a single sampling campaign on a one-day cruise between March 2016 and June 2017. In July and December  $\text{CH}_4$  show a remarkable cross-slope gradient with higher  $\text{CH}_4$  concentrations towards the coastline. In September  $\text{CH}_4$  accumulated in deeper bottom waters, showing highest  $\text{CH}_4$  concentrations of up to  $161 \text{ nmol l}^{-1}$ .

Stationary water column investigations at station 33 (Figure 1) revealed the distribution and temporal variability of dissolved gases ( $\text{CH}_4$ ,  $\text{N}_2\text{O}$ ,  $\text{O}_2$ ) and physico-chemical parameters such as temperature and salinity in July 2017. Within five days the three sampling campaigns revealed strong dynamics, showing that the water masses are constantly subject to modifications and substitution (Figure 7). Whereas at 24<sup>th</sup> of July, salinity and  $\text{CH}_4$  evenly increased from 10.8 to 12.1 and from 35.4 to 56.8 (1209 to 1995 ‰), respectively, temperature and oxygen were slightly decreasing from 18.4 to 17.8 °C and from 7.5 to 7.2  $\text{mg l}^{-1}$  towards the bottom. At the 26<sup>th</sup> of July a homogenous water column revealed a lower temperature ( $\sim 16.1$  °C), constant oxygen concentrations ( $\sim 7.3$   $\text{mg l}^{-1}$ ) and water column  $\text{CH}_4$  concentrations ( $\sim 17$   $\text{nmol l}^{-1}$ ;  $\sim 505$  ‰) with slightly increased salinities (12.4), but a sudden increase of bottom water salinities (to 14.7) and bottom water  $\text{CH}_4$  (20.2  $\text{nmol l}^{-1}$ ; 631 ‰) was observed. The following sampling campaign (28<sup>th</sup> of July) revealed a significant decrease in salinity (8.7), higher oxygen ( $\sim 8.7$   $\text{mg l}^{-1}$ ), coinciding with high  $\text{CH}_4$  concentrations in surface waters (36.7 and 37.7  $\text{nmol l}^{-1}$ ; 1147 ‰), showing a strong decrease to  $\text{CH}_4$  of 6.5  $\text{nmol l}^{-1}$  (282 ‰) towards the bottom. The bottom water, however, is characterized by a sudden increase in salinity (to 14.7), which is close to values of the previous sampling campaign, two days earlier. The  $\text{N}_2\text{O}$  concentrations in the water column ranged from 9.3 to 10.5  $\text{nmol l}^{-1}$ , showing no clear pattern related to changing water masses at the investigated station and were close to saturation values ( $102 \pm 4.6$  ‰) during the same period.

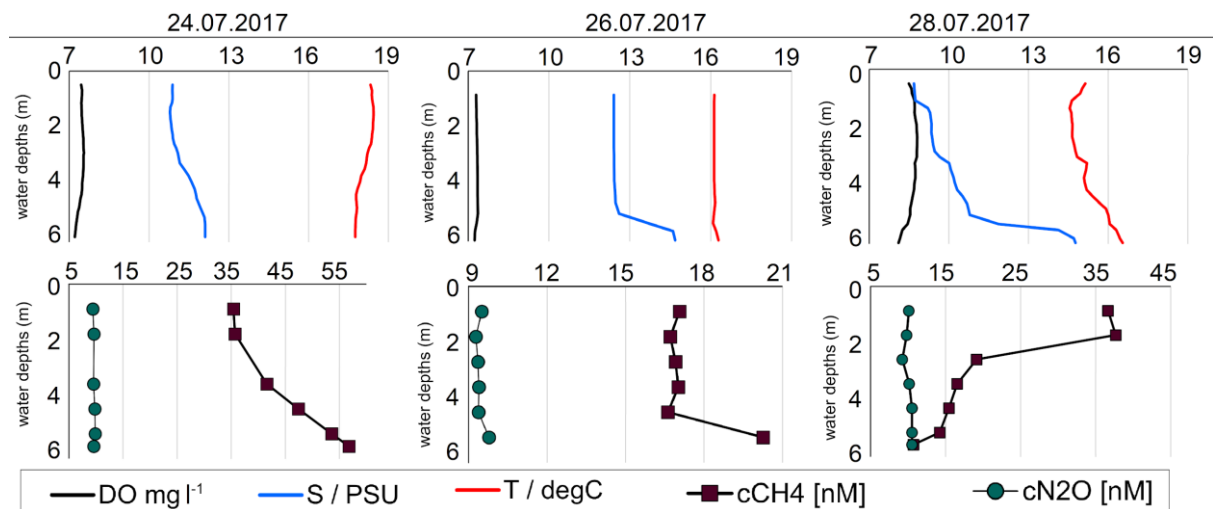


**Figure 7:** Measurements of salinity, temperature (°C), and concentrations of dissolved oxygen ( $\text{mg l}^{-1}$ ), methane ( $\text{nmol l}^{-1}$ ) and nitrous oxide ( $\text{nmol l}^{-1}$ ) at station 33 in July 2017.

### 3.1.2. Trace gas concentrations along the waterline

The shallow water along the beach was sampled for CH<sub>4</sub> concentrations during 10 one-day surveys between July and September 2017. Mean values of dissolved CH<sub>4</sub> in shallow bottom waters sampled during the offshore sampling campaigns (Figure 6) and the CH<sub>4</sub> concentrations sampled in <60 cm of water depth during surveys along the waterline (beach) are compared in Figure 8. The surveys exhibited average CH<sub>4</sub> concentrations of  $355 \pm 779$  nmol l<sup>-1</sup> (sampled CH<sub>4</sub> concentrations ranged from: 3–3358 nmol l<sup>-1</sup>). The CH<sub>4</sub> concentrations along the waterline exceeded the offshore bottom water concentrations of CH<sub>4</sub> (sampled during different seasons) by a factor of 11–17 (Figure 8).

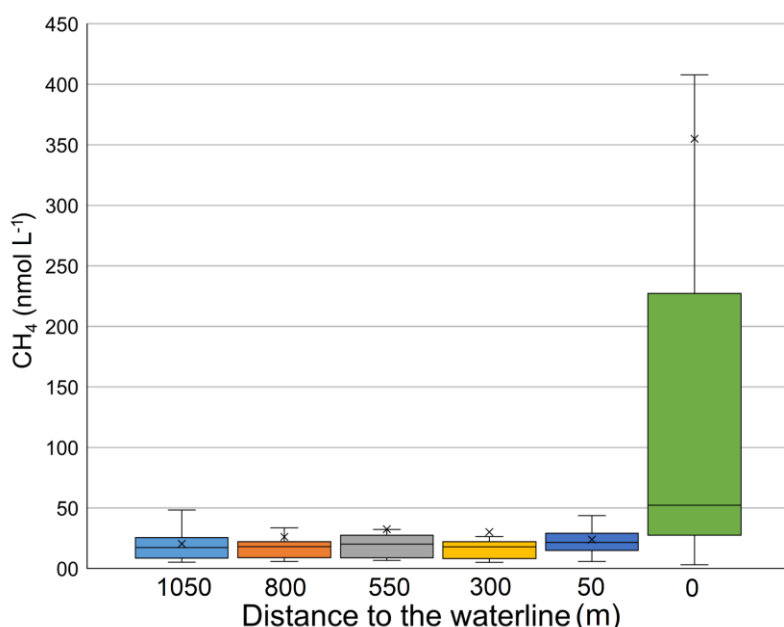


**Figure 8:** Box plots of methane concentrations in bottom water are plotted against the distance to the waterline. Along the beach face the concentrations showed a strong variation with a mean value of about 100 times the atmospheric equilibrium concentrations of  $\sim 3$  nmol l<sup>-1</sup>. The concentrations measured at the 0 distance were sampled in shallow water along the beach in <60 cm of water depth.

Measured parameters in pore- and surface water along the waterline of the study site showed strong spatial variability. Especially in the northern area, where peat sediments emerge (Figure 2a, d, 13), the porewater salinity was observed to remain significantly lower with minor fluctuations ( $8.5 \pm 1.5$ ) than in the central and southern part of the study site ( $12.7 \pm 2.8$ ) (Figure 9). The porewater in the northern area exhibited anomalies with elevated concentrations of DIC and exceptional low  $\delta^{13}\text{C}_{\text{DIC}}$  (unpublished data, provided by Julia Westphal, 2017). Furthermore, high

concentrations of  $\text{CH}_4$  ( $0.9 \text{ mmol l}^{-1}$ ), and  $\text{NH}_4^+$  have been observed (Figure 9). At the onshore stations 67 and 76 escaping gas bubbles have been observed during several sampling campaigns. High nitrous oxide concentrations of  $94 \text{ nmol l}^{-1}$  were detected at station 75 in July 2016. In contrast, significantly lower concentrations of most solutes were measured in the central and southern areas except from station 22 at which low salinities, elevated DIC,  $\text{CH}_4$  and additionally high concentrations of  $\text{N}_2\text{O}$  ( $131 \text{ nmol l}^{-1}$ ) have been detected in permeable sands in September 2016.

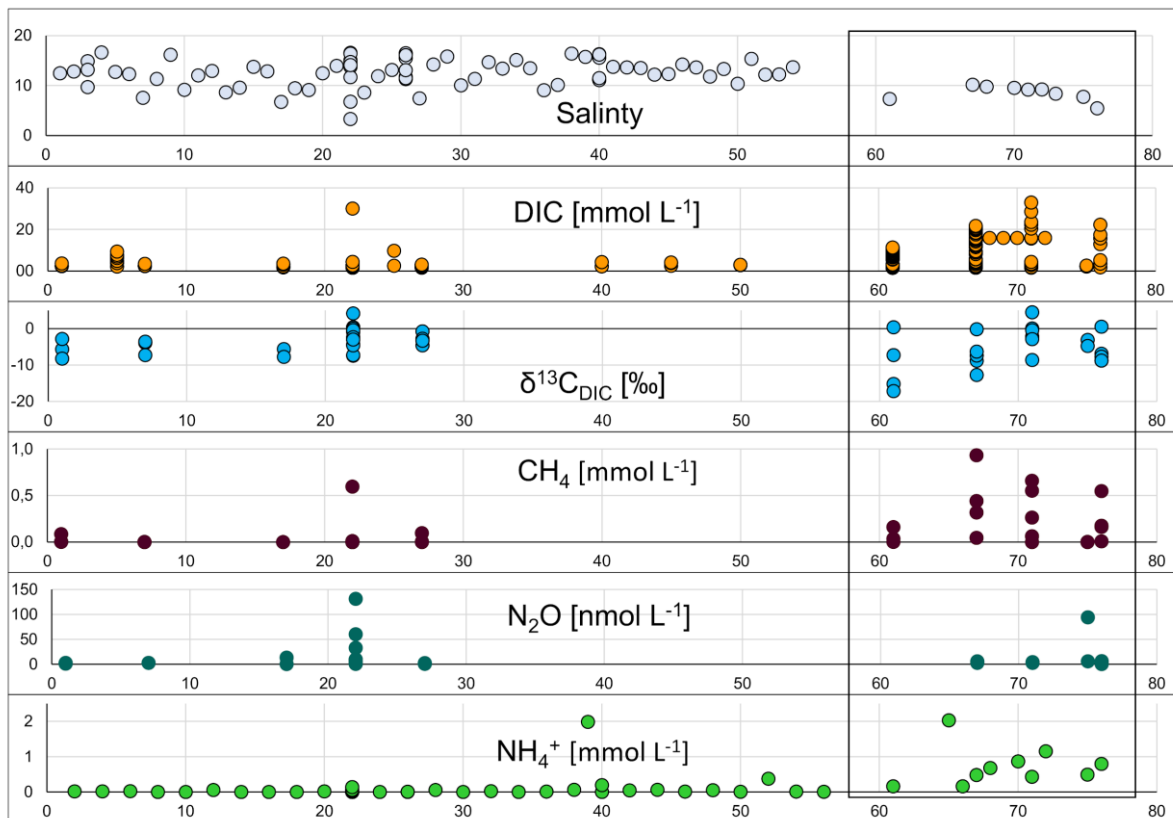


**Figure 9:** Porewater salinity and concentrations of DIC ( $\text{mmol l}^{-1}$ ),  $\delta^{13}\text{C}_{\text{DIC}}$  (‰) (provided by J. Westphal, 2017),  $\text{CH}_4$  ( $\text{nmol l}^{-1}$ ),  $\text{N}_2\text{O}$  ( $\text{nmol l}^{-1}$ ),  $\text{NH}_4^+$  ( $\text{mmol l}^{-1}$ ), along the southwestern to northeastern transect (stations 1 to 76) along the shallow water beach area. The box in the northeastern end of the transect marks an area of outcropping peat deposits, characterized by concentration anomalies of most solutes compared to the central and southerly area.

### 3.1.3. Flux measurements from chamber lander incubations

The accumulation of trace gases was investigated with in-situ incubation experiments. The results of three different incubation experiments are summarized in Table 2. No significant fluxes of  $\text{N}_2\text{O}$  were detected. In contrast, the increase of concentration increase of  $\text{CH}_4$  over time indicated fluxes with moderate ( $r^2 = 0.5$ ) to stronger ( $r^2 = 0.7$ ) correlations ( $dC/dt$ ), but in 2 out of 3 cases these correlations

were weak or not significant. Fluxes, however, were highest ( $4.5 \mu\text{mol m}^{-2} \text{d}^{-1}$ ) at offshore station 25 and about a third of the magnitude at station 35 (Figure 1c). The  $\text{CH}_4$  flux measurements during the incubation experiment at station 33 (Figure 1c) were lowest ( $0.87 \mu\text{mol m}^{-2} \text{d}^{-1}$ ) and are supported by a high correlation and significance.

**Table 2:** Calculated accumulation rates of methane and nitrous oxide within the Incubation chamber, which are suggested to origin from sedimentary fluxes.

Date	Station	n	CH <sub>4</sub> - fluxes			N <sub>2</sub> O - fluxes		
			$\mu\text{mol m}^{-2} \text{d}^{-1}$	$r^2$	p	$\mu\text{mol m}^{-2} \text{d}^{-1}$	$r^2$	p
2017/03/04	33	10	0.87	0.7	0.005	0.4	0.2	0.2
2017/07/28	25	5	4.5	0.5	0.3	0.1	0.04	0.8
2017/07/25	35	10	1.6	0.6	0.03	0.03	0.3	0.01

#### 3.1.4. Impacts of the Warnow-river on trace gas distribution

The outcome of the studies mainly conducted by Anne Breznikar concerning the export of trace gases from the Warnow-river system identified the Warnow-river as a net source for atmospheric climate relevant trace gases. The river water revealed mean surface water concentrations of  $\text{N}_2\text{O} = 21.1 \pm 10.3$  (range: 5.7–46  $\text{nmol l}^{-1}$ ;  $n = 20$ ) and  $\text{CH}_4 428 \pm 464 \text{ nmol l}^{-1}$  (range: 42–2515  $\text{nmol l}^{-1}$ ;  $n = 20$ ). Contrary to  $\text{CH}_4$ , the Warnow-river could not be confirmed as  $\text{N}_2\text{O}$  source for the Baltic Sea, showing near equilibrium concentrations at the river outlet in Warnemünde (Figure 10, 11). The same study revealed that dissolved  $\text{CH}_4$  enters the Baltic Sea with the Warnow-river discharge, albeit concentrations being subject to seasonal fluctuations (Figure 10). At the river outlet (Warnemünde)  $\text{CH}_4$  concentrations typically increases with increasing temperature, but were, however, also high in winter during the first campaign in January, which may be related to the high concentrations found near Petridamm (Figure 10).

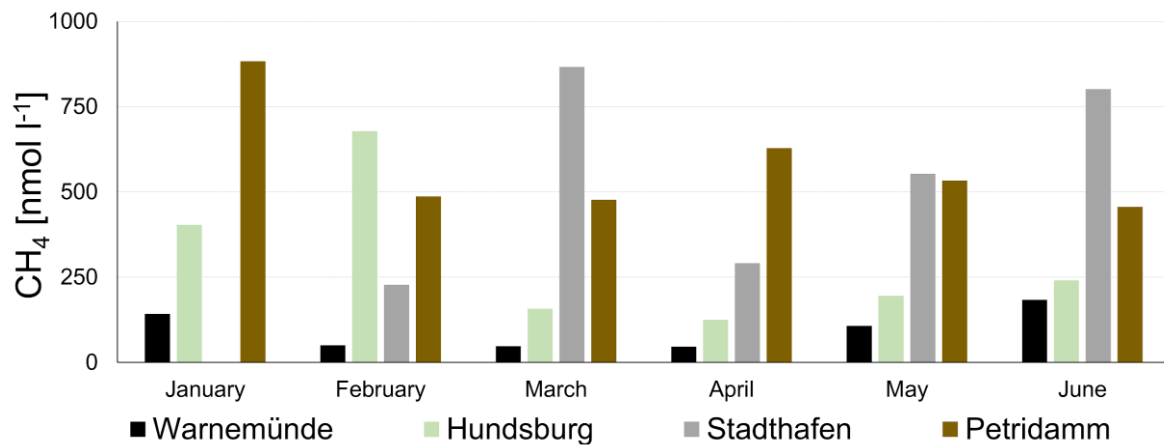


**Figure 10:** Dissolved methane concentrations sampled in 2017 (Anne Breznikar) within the river stream of the Warnow at four stations (for locations see Figure 1b, 11).

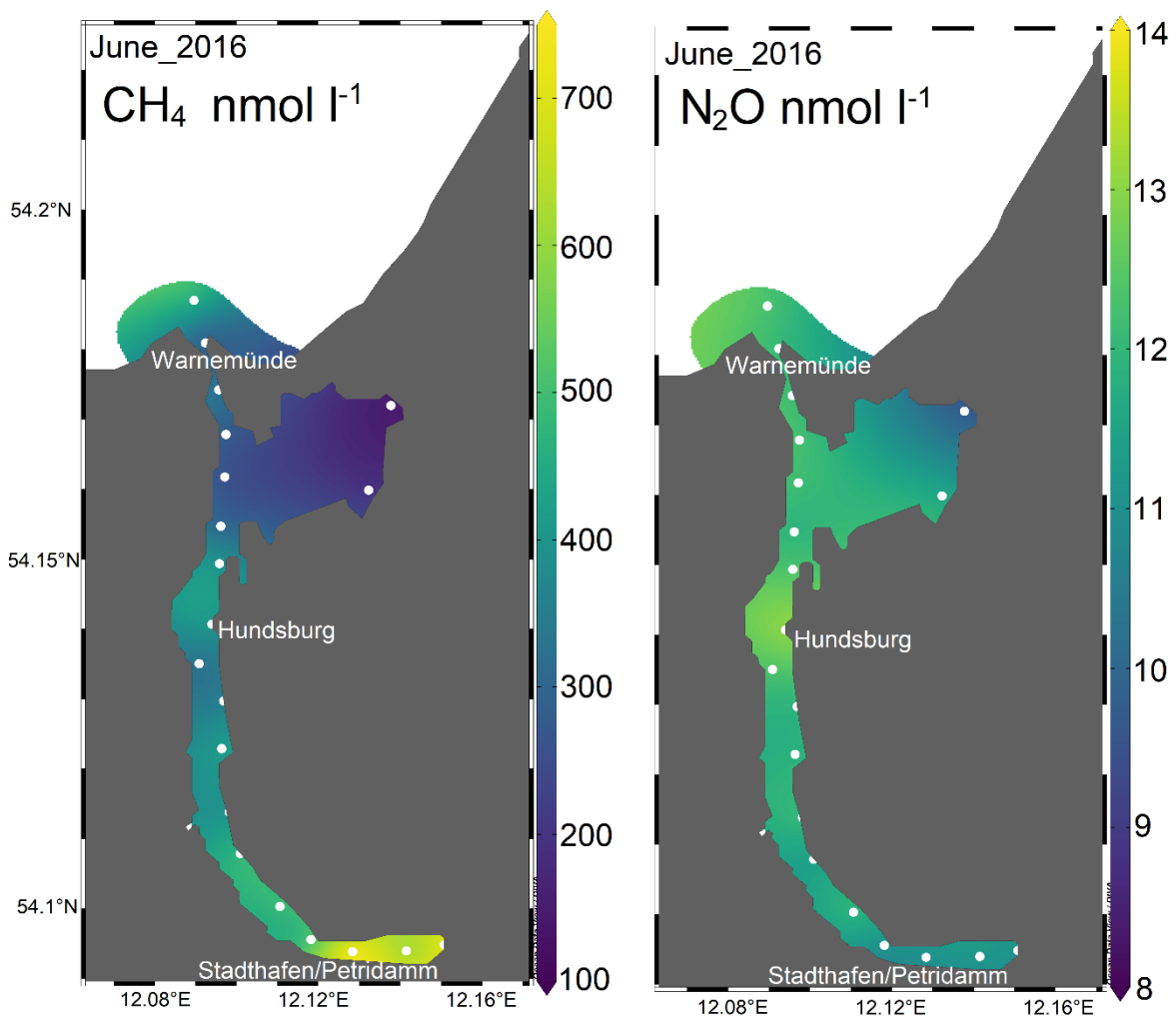


**Figure 11:** Distribution of bottom water methane and nitrous oxide in the Warnow-river in June 2016, revealing high concentrations of methane at the upper-most section of the Warnow-river and a decreasing downstream gradient towards the outlet. In contrast, concentrations of nitrous oxide are increasing towards the outlet.

### 3.2. Geological surveys

*The contents of the chapters 3.2.1. to 3.2.5. are published in Kreuzburg et al., 2018. Sub-marine Continuation of Peat Deposits From a Coastal Peatland in the Southern Baltic Sea and its Holocene Development. Frontiers in Earth Science, 6(103). Available at: <https://www.frontiersin.org/articles/10.3389/feart.2018.00103/full>.*

#### 3.2.1. Onshore

The sedimentary stratigraphy extending along the beach (Figure 12, for location see Figure 13) shows fine sand at the base, which is covered to a large extent by gyttja and peat, followed by marine medium to coarse, partly gravelly sands. The sequence overlaying the fine sand in the northeastern part of the transect is interrupted by silty to clayey sediments of up to 2.5 m thickness, from grey-blue to whitish in color. The surface of the peat layer below the top edge of the terrain descends along the transect from 0.15 m bsl (NE) in core B5 to 2.84 m bsl (SW) in core B8 with peat thickness decreasing from 1.6 m (B9) and 1.4 m (B4) to 0.1 m (B8) in the same direction. The continuation of the peat layer has been observed further inland (southeast of core B7), along the coastal areas where peat got partly eroded. Seawards, a subsidence of the peat surface between cores B3 and B5 could also be determined by additional peat explorations. Further inland behind the dune dike (MP2, Figure 13), a sediment core displayed a peat layer between -0.7 m and -3 m depths bsl underlain by a 10 cm thick layer of gyttja both continuing the stratigraphy observed at the beach (B6).

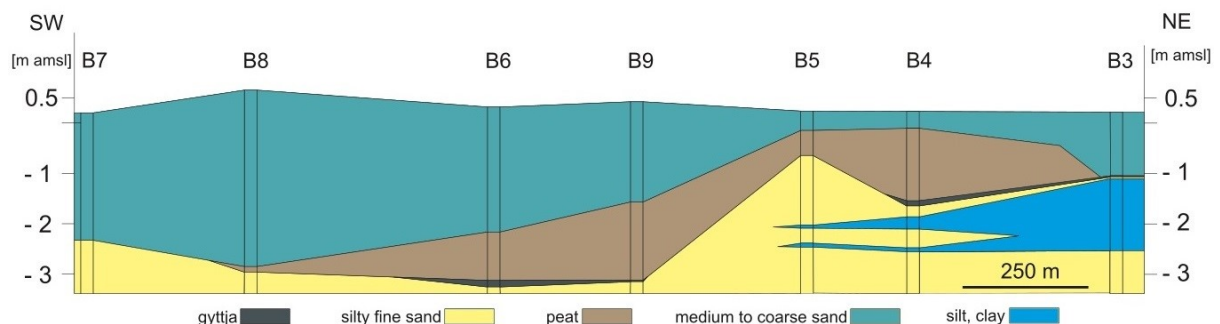


**Figure 12:** Geological profile along the beach with drilling locations (B3 to B9); sediment depth in meter above mean sea level (m amsl). Refer to Figure 13 for core locations.



### 3.2.2. *Bathymetry*

Bathymetry measurements of the seafloor in the studied shallow coastal area illustrate its heterogeneity, with a field of submarine sand ridges in the southwestern area and a flat trough-like area in the central part. This trough, which opens to the north, extends over a total length of 1.2 km in SW/NE direction. It is enclosed to the east by a coast parallel sandbar and to the southwest by sand ridges. The water depth in the broad northern part of the trough mostly exceeds ~6 m. In this area, numerous boulders and glacial till ridges, which have been observed during diver missions, are found. The northern part of the trough is crossed by several east-west to northwest-southeast oriented elevations of 450 m in length and up to 1.2 m in height. Likewise, decreasing water depths are observed towards the sea to the west and southwest of the trough. Here, a number of east-west oriented up to 320 m long sand ridges, 0.6 to 1.5 m in height and mostly 75–250 m in width with a single ridge reaching a width of 375 m, could be observed. They are oriented oblique ( $40^{\circ}$ – $60^{\circ}$ ) to the coastline in water depths of 3 to 4 m. Based on bathymetric data, that were recorded further offshore, a maximum extend of the sand ridges of about 1 km could be estimated (Figure 13). Most of the ridges incline with gentle angles ( $<0.5^{\circ}$ ) and partly show asymmetric cross sections with wider and less inclined north to northwest flanks (profile in Figure 13). In combination with seismic data, a shore-parallel longshore bar could be identified in front of the entire beach face. The height of this longshore bar is approximately 1 m and its width has been estimated to 50–100 m.

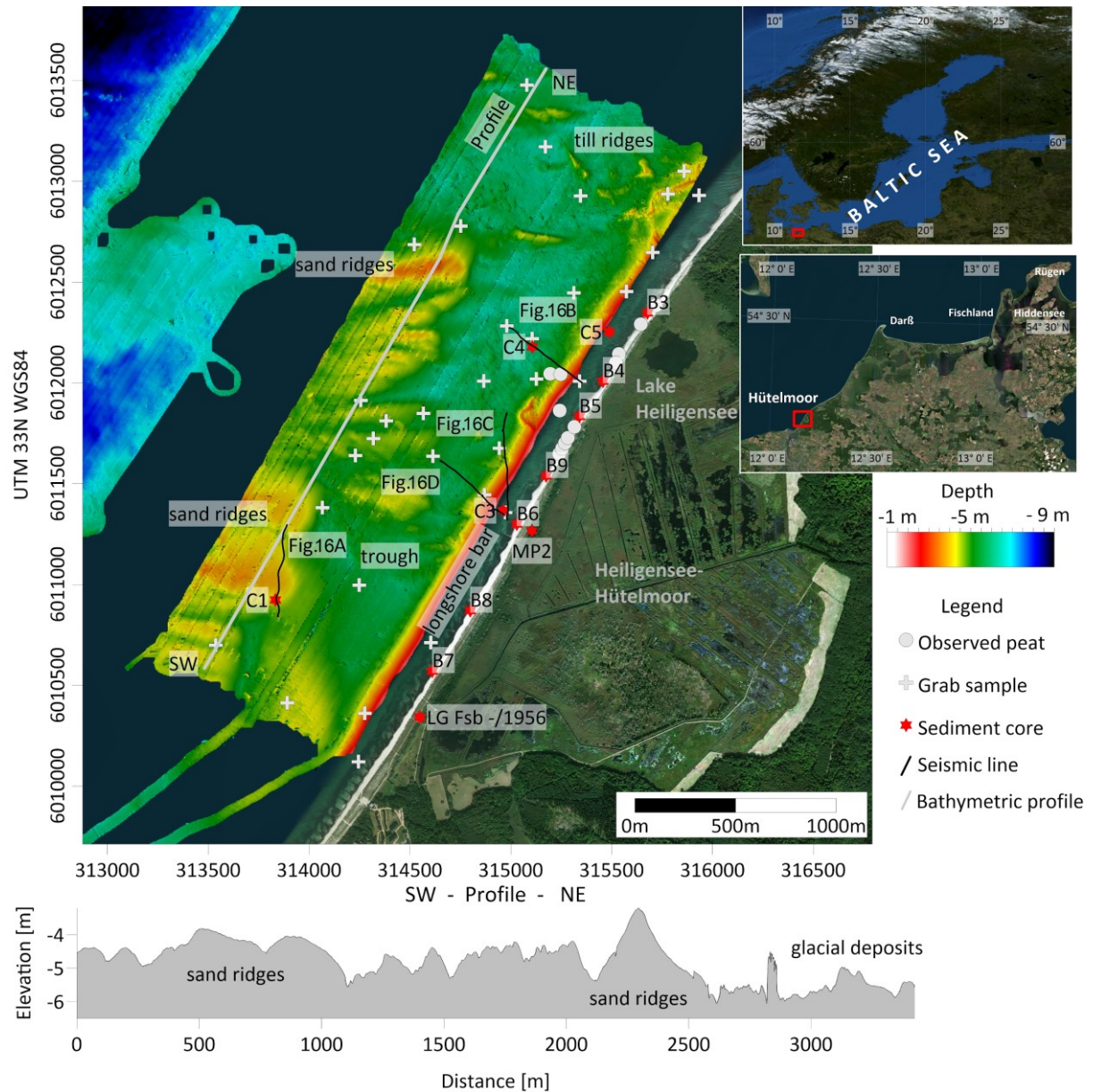


**Figure 13:** Top: Bathymetry and location of the study area along the southwestern Baltic Sea coast. White line parallel to the shore in southwest-northeastern direction indicates the bathymetric cross section shown underneath. The positions of sediment cores (red stars) and grab samples (white crosses) are also indicated. The black lines show the locations of the seismic profiles. The longshore bar was identified from the parametric echosounder data (INNOMAR, see Methods). Bottom: Bathymetric SW-NE transect at the upper shoreface indicating the distribution of the main geological features.

### 3.2.3. Seafloor composition

Three larger facies building up the investigated seabed could be distinguished by evaluating backscatter mosaics verified with gravel samples and short sediment cores (Figure 14): well sorted fine sand, medium sand with low gravel percentage, and poorly sorted coarse sand and gravel. The well sorted fine sand fraction is characterised by low backscatter intensities showing with a generally smooth and

homogeneous texture. It is mainly observed forming the sand ridges in the south and south-western part of the study area in water depths of 4 to 6 m and can be further subdivided. Although difficult to distinguish by acoustic data of the used frequency only, additionally data obtained by ground-truthing indicate a combined clay and silt content of about 5 % in the trough (Figure 14) separating the sand ridges from the beach face. This clay or silt fraction is missing in the sand ridges and, in contrast to the latter, contains a higher proportion (~5 %) of medium to coarse sand. The medium sized sand fraction with low gravel content, showing medium backscatter intensities, can be observed along the runnels in between sandridges and at the boundaries to coarser sediment deposits. Finally, poorly sorted coarse sand and gravel, with gravel content up to 50 % and numerous stones, boulders and uncovered glacial till, build up the remaining seabed and is characterized by high backscattering intensities. These deposits are predominantly observed in the north-eastern part of the study area (Figure 14).

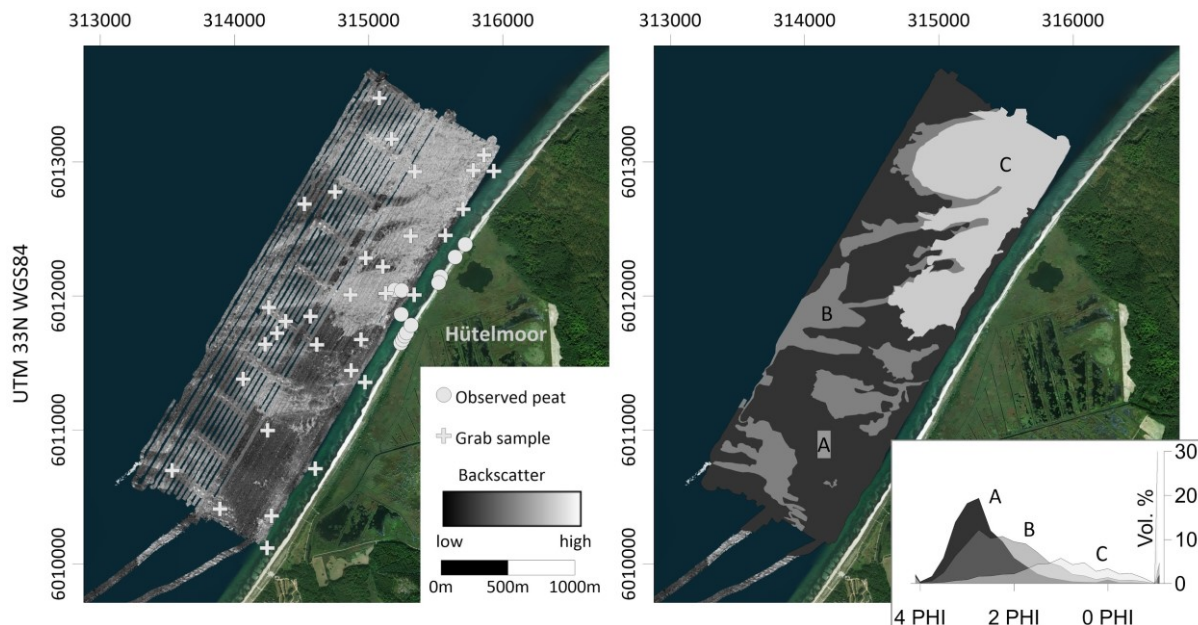


**Figure 14:** Left: Available backscatter data with grab samples for surficial ground-truthing and near-coastal peat observations. Right: Manual clustering of the backscatter data into three seafloor facies A-C. Representative grain size distributions for each facies are displayed using the PHI scale, with  $\text{PHI} = -\log_2 d$ , where  $d$  is the grain size in mm, with A) fine sand (black), B) gravelly medium sand (grey) and C) gravelly coarse sand (light grey). The insert in the right panel indicates the grain size distribution (PHI-scale) in Vol. %.

#### 3.2.4. *Sediment cores*

Seismic reflections 3 m bsl and in parallel to the sediment surface indicate the sub-sedimentary continuation of the peat layers. This interpretation was verified with sediment core C3 (Figures 15).

Sediment core C1 was retrieved in a water depth of 6.5 m (Figure 15, for location see Figure 13). The sediment sequence at the core base (280–248 cm depth) contains fine sand with scattered shell fragments, followed by decimetre-thick coarse and fine sand units, interrupted by overlying fine sand layers. A sharp boundary follows at a core depth of ca. 190 cm with two dark gyttja layers (5 and 3 cm thick, respectively) containing shell fragments that are separated by well sorted fine sand. Two radiocarbon ages ( $^{14}\text{C}$ ) from the lower organic layer were determined for shell fragments as well as organic sediments from one sample (Table 3). The marine shell fragments (*Peringia ulva*, *Macoma Baltica*) yield a significantly older age with  $8586 \pm 256$  cal yr BP as compared to the organic sediments ( $\text{C}_{\text{org}}$  5.12 %,  $\delta^{13}\text{C}$  -25.2 ‰, C/N-ratio 11.97) showing an age of  $4972 \pm 137$  cal yr BP.

The sediment core C3 (Figure 15) with a total length of 197 cm was extracted at a water depth of 1.8 m. The lowest unit (171–197 cm) consists mainly of fine sand including dark layers which yield  $\text{C}_{\text{org}}$  of 0.4 %,  $\delta^{13}\text{C}$  of -27.2 ‰ and C/N ratios of 11.6. The unit is followed by a gyttja layer ( $\text{C}_{\text{org}}$  8.1 %,  $\delta^{13}\text{C}$  -28.6 ‰, C/N-ratios 15.2) containing wooden fragments, that were dated to  $7024 \pm 73$  cal yr BP (C3.2) and a peat layer at 146–160 cm depth. Peat material from this core, showing organic carbon contents of 36.9 and 37.5 %, was dated to  $6725 \pm 87$  cal yr (C3.1), and yielded stable isotope signatures ( $\delta^{13}\text{C}$ ) of -28.9 and -27.1 ‰ and C/N ratios of 21.3 and 36.4. The sediments above the peat are separated by an erosion horizon and consist mostly of fine to medium sand with little change in grain size distribution.

The sediment core C4 with a total length of 120 cm was sampled at a water depth of 5.3 m, with the bottom part (113–120 cm) being composed of glacial till. The sediments above are separated by a sharp boundary and alternate between fine and medium sand. The surface sediments (4–12 cm) consist of dark coarse sand and coarse gravel (grain size 2–3 cm) overlayed by dark fine-sand.

The sediment core C5 was sampled in a water depth of 1 m and has a length of 117 cm. In this core the soil sediment consists of medium sized sand with poorly-rounded fine gravel. A diffuse transition is followed by two different layers of minerogenic lake sediments at 110–93 cm and 88–62 cm, separated by a well sorted fine sand layer of ~5 cm thickness. On top, the sediments become increasingly coarser with medium- to coarse-grained sands, being interrupted at 38 cm by a black layer of ~3 mm thickness having  $C_{org}$  of 1.22 %,  $\delta^{13}C$  of -24.36 ‰ and C/N of 10.66.

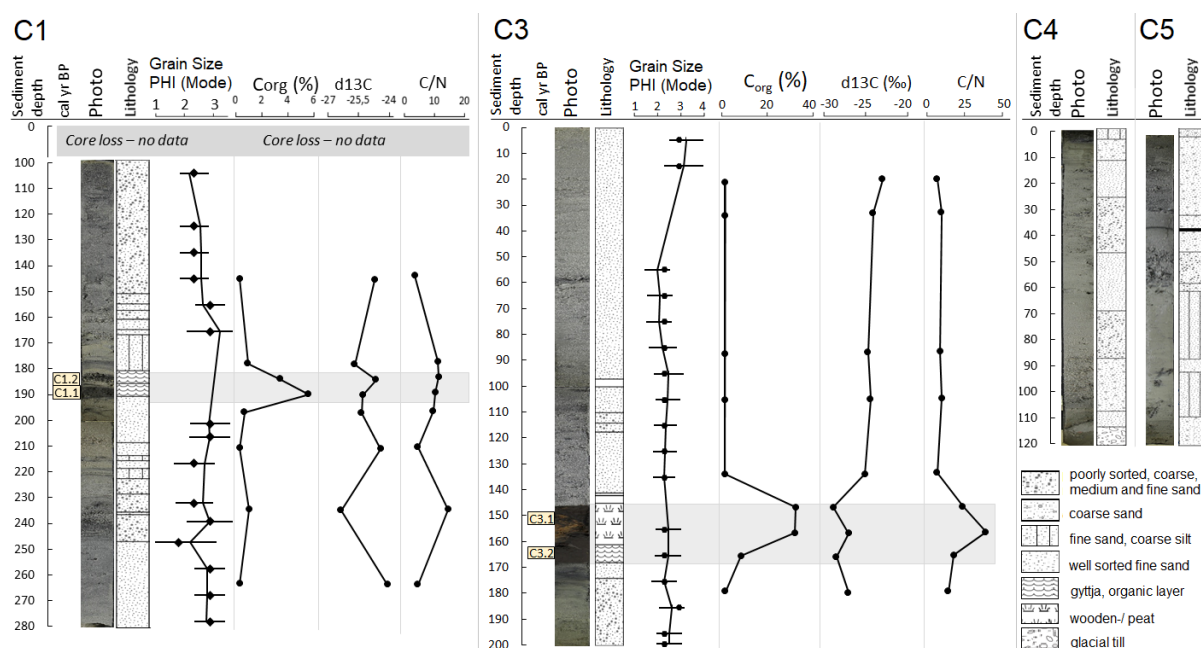


**Figure 15:** Sediment depths (cm),  $^{14}C$  ages, photographs, lithology, grain size distribution (with  $PHI = -\log_2 d$ , where  $d$  is the grain size in mm), organic carbon content (%),  $\delta^{13}C$  (‰), carbon/nitrogen ratios (C/N) of the 4 offshore sediment cores (C1, C3, C4, C5) retrieved from the study site.

**Table 3:** Determined  $^{14}C$  ages in the study area. Age intervals are given at a 95.4 % confidence level.

Core ID	Core depth (cm)	Lat (N)	Long (E)	$^{14}C$ age (yr BP)	cal yr BP	Material	C/N	$\delta^{13}C$ (‰)	$C_{org}$ (%)
C1.1	190	54.2125	12.1450	8040 +/- 30	8586 +/-256	Shell (Marine)	-	-	-
C1.2	190	54.2125	12.1450	4430 +/- 30	4972 +/-137	Gyttja	11.97	-25.2	5.12
C3.1	150	54.2168	12.1620	5900 +/- 30	6725 +/-87	Peat	36.4	-27.1	37.5
C3.2	165	54.2168	12.1620	6160 +/- 30	7024 +/-73	Wood	15.2	-28.6	8.1
B9	305	54.2185	12.1652	5950 +/- 30	6769 +/-128	Gyttja	71.46	-30.5	50.25
B6.1	300	54.2163	12.1631	3290 +/- 30	3516 +/-87	Peat	60.7	-28.08	51.06
B6.2	308	54.2163	12.1631	5150 +/- 30	5918 +/-45	Gyttja	1.46	-27.92	19.83



### 3.2.5. *Subsurface structure*

Subsurface information is inferred from seismic reflection data (Figure 16, for location see Figure 13) and ground-truthing using sediment cores of different lengths. Glacial till forms the acoustic basement for the high-frequency seismic survey and marks the base of the observed stratigraphy. It is generally dipping from North to South. In addition, the surface of the till is slightly inclined towards the offshore direction (NW) and is characterized by steep irregularities, that might indicate similar structure as compared to the outcropping till ridges in the northern area observed in the bathymetric data. The burial depth of the till surface controls the thickness of sediment on top. These irregularities are partially filled with acoustically homogeneous to transparent material (Figure 16A-D, labeled as medium sand). In areas, where these sediments protrude from the seabed, medium sand with a low gravel content was collected in grab samples (Figure 16B). Laminated sedimentary units (marked H in Figure 16A-D) are as thin as till deposits and appear in the north of the research area. The layered sediments are characterized by high amplitudes, often show internal reflectors, indicating different layers of sediments and are of Holocene age, based on dates retrieved from the sediment cores C1 and C3. In several areas the Holocene deposits display chaotic and disturbed sequences, resulting in individual reflections in the seismic data that cannot be followed throughout. The Holocene sequence contains organic sediments and peat, samples of which were extracted from the C1 and C3 sediment cores. The exact location of the peat layer, as known from the sediment cores, is difficult to detect in the seismic data. Nevertheless, thin reflections, aligned approximately parallel to the sediment surface at a depth of about 3 m bsl (Figure 16B-D), are interpreted to indicate the peat sequence observed in the cores at the same depth. The peat layer continues with reduced reflection intensities beneath the longshore sand bars, where it ends unconformably against its seaward base (Figure 16B-D). An interpretation about the peat layer continuation landwards to the core position is limited due to the shallow multiple. In the seismic data, a weakly-visible, offshore orientated lamination can be identified within the longshore sandbar, which shows a medium to low acoustic transparency, and yields a maximum observed thickness of ca. 1.5 m. In the western and south-western part of the study area, ridges composed of fine sand (Figure 16A) unconformably overlie the layer deposits. Within these sand ridges with a maximum observed thickness

of ~1 m, a very homogeneous and transparent signature with almost no internal reflections was observed. The same acoustic reflections, which are caused by fine sand, can be observed in the north in form of isolated lenses of less than 1 m thickness that occur on top of the medium sand (Figure 16B). Several of the seismic profiles acquired in the coastal zone of the central study area intersect with a shore-parallel sandbar.

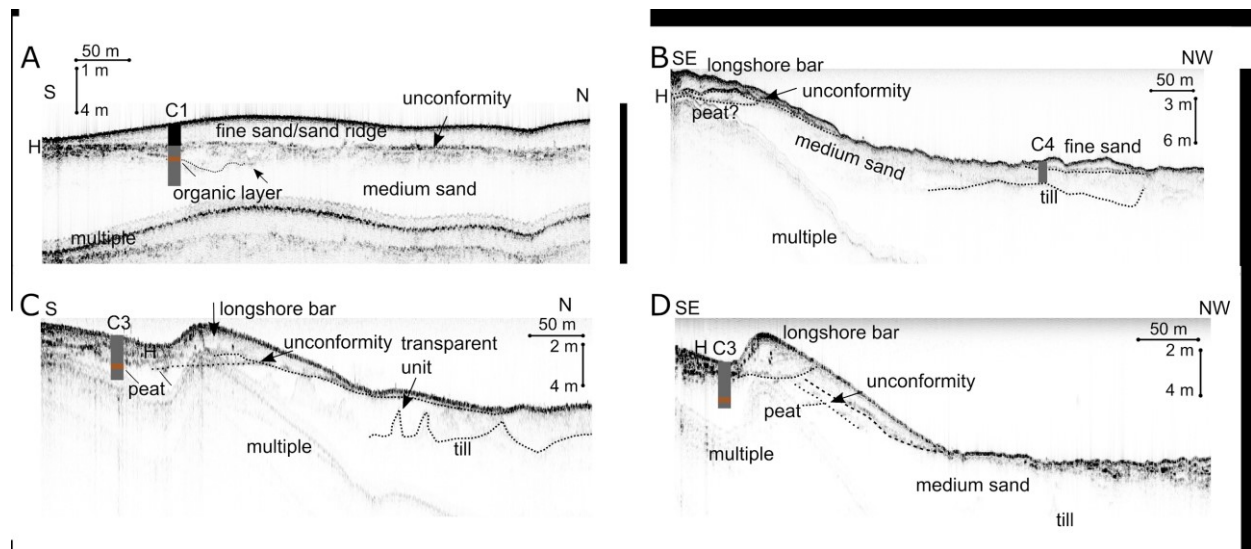


**Figure 16:** Seismic data of profiles A, B, C, and D. Sediment cores to prove the ground-truthing are indicated. The position of core C3 was extrapolated to the nearest shot points of seismic lines C and D. The distance to line C is 25 m, and the distance to line D is 15 m. Refer to Figure 13. for location of the seismic lines.

### 3.3. Column experiment

#### 3.3.1. Aqueous phase geochemistry

##### 3.3.1.1. Salinity

Good correlations between salinity either calculated with  $\text{Cl}^-$  or salinity deduced from electrical conductivity measurements were observed for both, peat-sand columns ( $r^2 = 0.79$ ,  $P < 0.001$ ,  $n = 134$ ) and sand cores ( $r^2 = 0.90$ ,  $P < 0.001$ ,  $n = 97$ ) (Figure 17). Since  $\text{Cl}^-$  is known to be unaffected by sorption processes it was chosen as the preferred measure of salinity ( $S$ ). The highest salinities ( $S > 12$ ) were measured during the three SW cycles throughout the entire peat-sand and sand columns. During the GW experiments, the salinity decreased along the column from  $\sim 9.5$  to  $\sim 6.7$ . The lowest salinity ( $S < 5$ ) was measured at the bottom of the peat-sand column during the third upward GW flow after 14 days at the end of the experiment (Figure 18, 25).

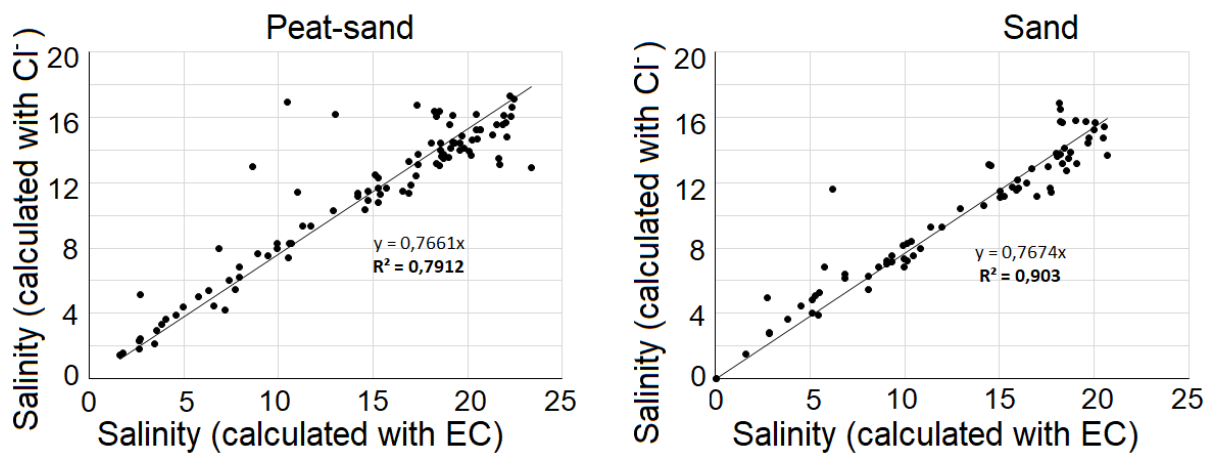


**Figure 17:** Correlation of salinity calculated with chloride ( $\text{Cl}^-$ ) and electronic conductivity (EC) in peat-sand (P1) and sand (S1).



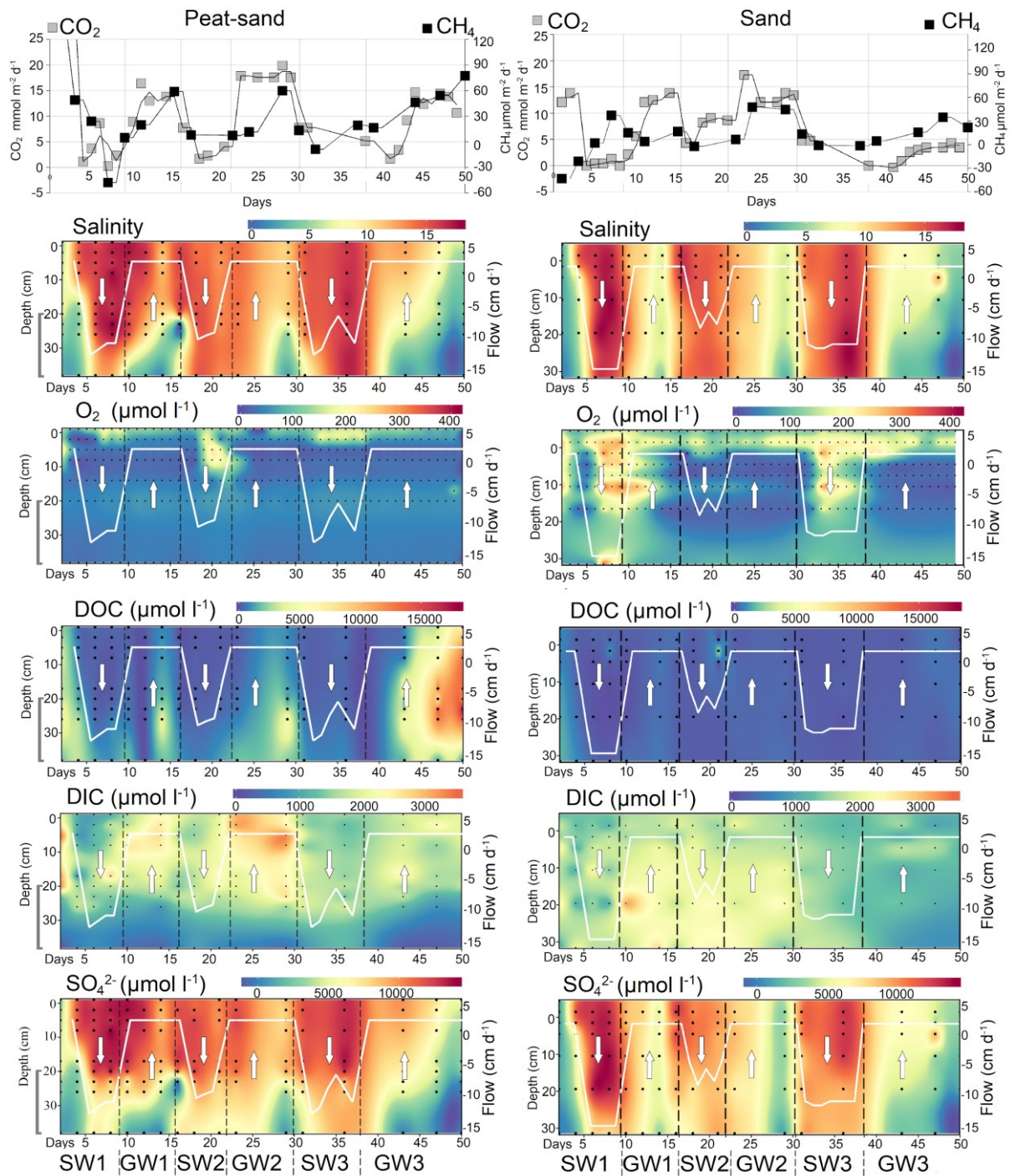


**Figure 18:** The fluxes of  $\text{CO}_2$  and  $\text{CH}_4$  (upper graphs) derived from concentration change rates in the headspace of all columns for peat-sand (left) and sand (right). Depth distributions of aqueous concentrations of salinity,  $\text{O}_2$ , DOC, DIC and  $\text{SO}_4^{2-}$  are presented for each column set, over the 50 days of the experiment period and under GW and SW flow regimes. The white arrows show the flow direction, the white lines indicate the advective flow rates with negative values indicating downwards SW flow and positive values showing upwards GW flow. The black dots represent the porewater sampling depths and the time of sampling. The grey bracket left of the peat-sand data indicates the position of the peat layer in the lower section (20 to 40 cm) of the core.

### 3.3.2. Porewater chemistry

The dissolved oxygen ( $O_2$ ) concentrations in both peat-sand (P2) and sand columns (S2), varied following the SW and GW flow regimes and were highest during SW runs in the sand columns (Figure 18). In the peat-sand column the sediments were predominately oxygen-depleted at depths  $>15$  cm. During the SW intrusions, the  $O_2$  concentrations in peat-sand columns were  $42 \pm 10.9 \mu\text{mol l}^{-1}$  in shallower sands ( $<10$  cm) and dissolved oxygen significantly decreased towards deeper peat layers. In contrast, the sand columns were entirely penetrated with oxygen. The highest  $O_2$  concentrations ( $\sim 150 \pm 10 \mu\text{mol l}^{-1}$ ) were observed in the upper part of the sand columns during SW downward flow regime. In both, peat-sand and sand columns, the concentration of dissolved  $\text{SO}_4^{2-}$  in the porewater showed a positive correlation (Figure 19) with the SW downwards flow events (peat-sand:  $r^2 = 0.85$ ; sand:  $r^2 = 0.92$ ). Thus, the SW could be generally identified as the source of  $\text{SO}_4^{2-}$ , although  $\text{SO}_4^{2-}$  concentrations showed larger scatter towards lower concentrations with increasing core depth (Figure 18, 25).

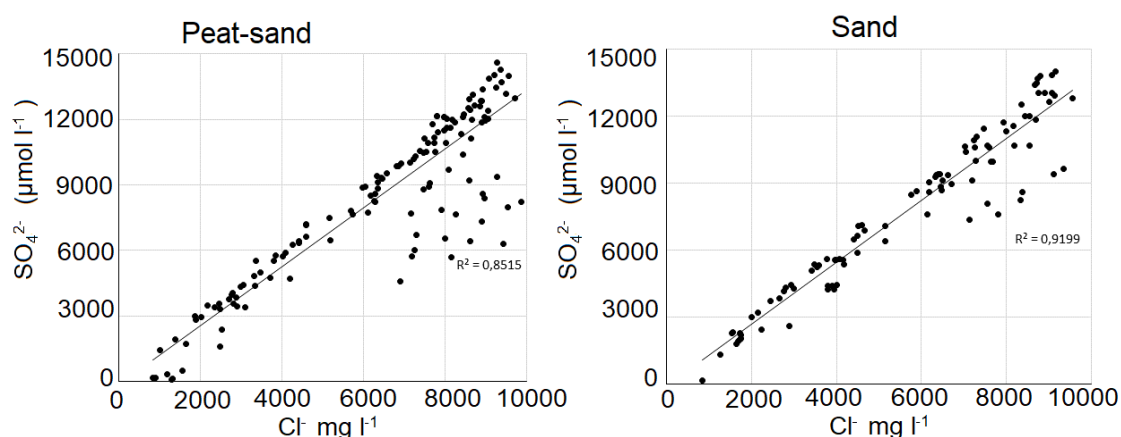


**Figure 19:** Correlations between  $\text{SO}_4^{2-}$  and chlorinity for peat-sand (P1) and sand column (S1)

During the GW upwards flow, a significant increase in concentrations of DOC ( $r^2 = 0.81$ ,  $P < 0.001$ ) correlating with decreasing salinities was detected in the peat-sand column. Furthermore, the increased production of DOC with advective groundwater upflow resulted in the ascent and finally enrichment of DOC in the sand sediment above the peat layer (Figure 18), which showed acetate concentrations of  $6 \pm 1.2 \text{ mg l}^{-1}$  (GW1),  $8.4 \pm 1.4 \text{ mg l}^{-1}$  (GW2) and  $4.6 \pm 1.3 \text{ mg l}^{-1}$  (GW3) (data not shown). With increasing salinities during SW downward flow experiments, a significant decrease of DOC concentration in the porewater was observed. After the  $O_2$

content in the surface sediments was significantly increased in the downwards flowing SW2 phase, high concentrations of DIC in the upper 10 cm sediment occurred during the following GW2 upwards flow (Figure 18). The final GW3 upwards flow event lasted for 14 days, significantly lowered the salinity and substantially increased the concentrations of DOC ( $17.9 \text{ mmol l}^{-1}$ ) within all sediments of the peat-sand core (Figure 18).

During this GW3-phase the C-isotopes of DOC ( $\delta^{13}\text{C}_{\text{DOC}}$ ) were  $26.7 \pm 4.5 \text{ ‰}$  with lowest values of  $-26.9$  to  $27.7 \text{ ‰}$  at salinities of  $S \leq 5$ . Slightly lighter  $\delta^{13}\text{C}_{\text{DOC}}$  of  $-26.7$  to  $-25.6 \text{ ‰}$  and were detected at salinities  $S > 5$ . A linear multiple regression between  $\delta^{13}\text{C}_{\text{DOC}}$ , DOC and salinity indicates a moderate adjusted determination coefficient ( $r^2 = 0.72$ ) with lighter values found with higher DOC concentration and decreasing salinities.

### 3.3.3. $\text{CO}_2$ and $\text{CH}_4$ fluxes

During GW upwards flow regimes average  $\text{CO}_2$  fluxes from the ponding water into the air-filled headspace were significantly higher in peat-sand ( $11.4 \pm 5.8 \text{ mmol m}^{-2} \text{ d}^{-1}$ ) and sand ( $6.9 \pm 5.7 \text{ mmol m}^{-2} \text{ d}^{-1}$ ) as compared to SW down flow regimes with  $4.6 \pm 3.4 \text{ mmol m}^{-2} \text{ d}^{-1}$  in peat-sand and  $3.7 \pm 3.4 \text{ mmol m}^{-2} \text{ d}^{-1}$  in sand (Figure 18). The lowest average  $\text{CO}_2$  fluxes of  $0.5 \text{ mmol m}^{-2} \text{ d}^{-1}$  were observed in the sand cores during the SW1 down flow regime. In both sediment cores, the highest fluxes occurred during GW2 ( $15.7 \pm 1.2 \text{ mmol m}^{-2} \text{ d}^{-1}$  in peat-sand and  $12.9 \pm 0.9 \text{ mmol m}^{-2} \text{ d}^{-1}$  in sand). Similar to what could be observed for  $\text{CO}_2$ , also  $\text{CH}_4$  fluxes were systematically coupled to the flow dynamics. During the SW downwards flow regimes average  $\text{CH}_4$  fluxes were  $1.5 \pm 26.6 \text{ } \mu\text{mol m}^{-2} \text{ d}^{-1}$  peat-sand and  $8 \pm 15.4 \text{ } \mu\text{mol m}^{-2} \text{ d}^{-1}$  in the sand core. Significantly higher average  $\text{CH}_4$  fluxes were recorded during GW upwards flow regimes with  $35.7 \pm 26.3 \text{ } \mu\text{mol m}^{-2} \text{ d}^{-1}$  in the peat-sand core and  $21.2 \pm 16 \text{ } \mu\text{mol m}^{-2} \text{ d}^{-1}$  in the sand core. The highest average  $\text{CH}_4$  fluxes in the sand cores were measured during GW2 ( $32.9 \pm 16.8 \text{ } \mu\text{mol m}^{-2} \text{ d}^{-1}$ ) and in the peat-sand cores during GW3 ( $48.5 \pm 25.1 \text{ } \mu\text{mol m}^{-2} \text{ d}^{-1}$ ). The longer the GW flow condition persisted, the more  $\text{CH}_4$  was emitted (from  $16.5$  to  $77.3 \text{ } \mu\text{mol m}^{-2} \text{ d}^{-1}$  within the last 14 days, GW3). During SW intrusion regimes SW1 and SW3, an observed reduction of the  $\text{CH}_4$  concentrations in the headspace indicates negative fluxes.

### 3.3.4. Abundances of methanogenic archaea and sulfate reducing bacteria

The results of the quantitative PCR in the peat-sand column, which were analyzed after drainage at the end of the experiments, reveal significantly lower abundances of methanogens (*mcrA*) and sulfate reducers (*dsrB*) in the upper 20 cm of sand sediment (*mcrA*:  $1.2 \times 10^3 \pm 1 \times 10^3$  copies/g; *dsrB*:  $1.4 \times 10^4 \pm 1.2 \times 10^4$  copies/g) compared to the lower peat section (*mcrA*:  $5.6 \times 10^5 \pm 2.1 \times 10^5$  copies/g; *dsrB*: 6.7 copies/g) (Figure 25). The highest copy numbers of *dsrB* ( $1.9 \times 10^7$  copies/g) were detected in the transition zone (see Figure 20) of highly degraded peat, whereas *mcrA* revealed highest abundances ( $1.02 \times 10^6$  copies/g) in the lowermost sample where peat got least decomposed. Generally, sulfate reducers (*dsrB*) outnumber methanogens (*mcrA*), although the abundance of *dsrB* declined towards the bottom section.

### 3.3.5. Solid phase geochemistry

Results from C, N and stable carbon isotope analysis ( $\delta^{13}\text{C}$ ) (Figure 20) revealed strong variations in elemental concentrations with depth within both, the six experimental cores (end) and the initial (init.) cores. The results of the solid phase geochemistry within the same sediment depth were summarized for peat-sand cores (P1, P2, P3) and sand cores (S1, S2, S3) and expressed in mean values. The stable isotopic composition ( $\delta^{13}\text{C}$ ) of the peat layers were in the range from -27.9 to -26.8 ‰, with a mean values of  $-27.3 \pm 0.3$  ‰ ( $n = 6$ ), and shows higher values in the upper 20 cm sand layer in the range of -25.3 to -22.6 ‰, with a mean value of  $-24.6 \pm 1.5$  ‰ ( $n = 18$ ). In peat-sand columns, the mean concentration of  $\text{C}_{\text{org}}$  in the deep peat layers (depth below 30 cm sediment depth) were  $44.2 \pm 5.3$  % ( $n = 15$ ) compared to  $15.9 \pm 20.2$  % ( $n = 9$ ) in the transition layer between the peat and sand (sediment depth of 30 – 21 cm) and  $0.04 \pm 0.02$  % in the upper sand layer (Figure 20). Total nitrogen could be detected only in the peat layers ( $\text{TN}_{\text{mean}} 1.5 \pm 0.6$  %) where it followed the distribution of  $\text{C}_{\text{org}}$  ( $r^2 = 0.85$ ,  $P = 0.007$ ). The C:N ratios were  $29.5 \pm 1.7$  in the peat layer. In contrast to the peat substrate, the concentrations of  $\text{C}_{\text{org}}$ ,  $\text{C}_{\text{inorg}}$  and TN in the sand in all the columns were very low and in some cases below detection limit. Additionally, in all the sand sediments a larger variability of the stable isotope values ( $\delta^{13}\text{C}$ ) was observed (Figure 20). The

concentration of  $C_{inorg}$  within the peat layer and the sand on top of the peat-sand core (end.) was  $6.5 \pm 5.3 \%$  and  $0.04 \pm 0.03 \%$ , respectively, and significantly different to the peat-sand core (init.).

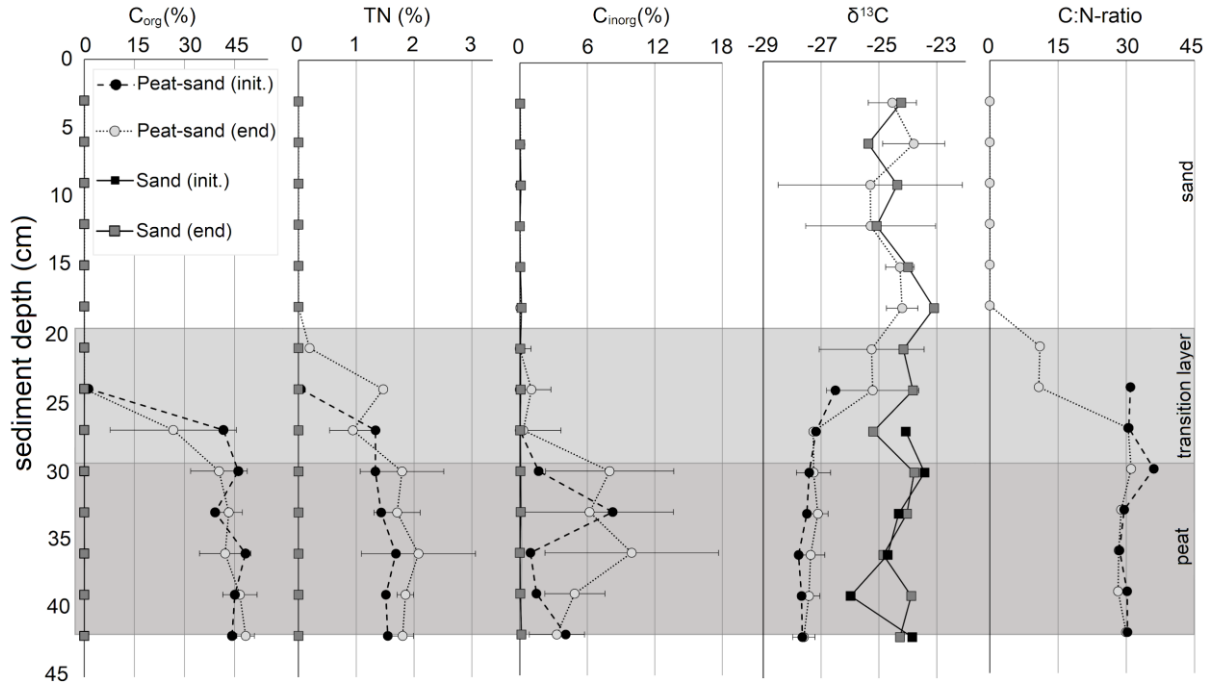


**Figure 20:** Depth distribution of organic carbon contents ( $C_{org} \%$ ), total nitrogen (TN %), inorganic carbon contents ( $C_{inorg} \%$ ), stable isotopic signature of organic carbon ( $\delta^{13}C \text{ ‰}$ ) and carbon/nitrogen (C:N) ratios in the peat-sand and sand columns (mean values of all columns). The grey boxes indicate the peat sediment within the peat-sand columns, with light grey (20–30 cm) marking the transition zone (highly decomposed peat) and dark grey marking peat deposits of low decomposition.

## 4. Discussion

### 4.1. Hydrodynamics and trace gas distribution

The overall water masses of the southern Baltic Sea are part of an earth rotation-derived north-eastern flowing current system (Elken and Matthäus, 2008), whereas the influence of the coriolis effect decreases towards nearshore coastal areas, where the current dynamics are mainly induced by wind (Krauss, 2001; Ostrowski et al., 2018). Flow velocities of up to  $30 \text{ cm s}^{-1}$  were measured near station 33 (Figure 1) in the centre of the study site (personal communication with Xaver Lange, IOW, 2019). Therefore, it can be assumed, that the water masses within the sampling transects are constantly substituted and supplied with different water masses originating from (1) Baltic Sea, Mecklenburg Bay, (2) river water of the Warnow-river and (3) groundwater discharge originating from coastal sediments (Jurasinski et al., 2018) and coastal aquifers. This three sources of different water masses impacting up on the study side area are discussed in the following sections.

#### 4.1.1. *Baltic Sea water*

Baltic Sea-water comprises the main fraction of the water masses and has therefore a major influence on the measured water chemistry in the study area in front of the Hütelmoor. For instance, Baltic Sea water is considered as the main source of sulfate ( $\text{SO}_4^{2-}$ ), an important component for anoxic mineralization processes of organic matter as well as anoxic methane oxidation (Jørgensen et al., 2001). The salinities within the Mecklenburg Bay are characterized by horizontal gradients ranging between 14 and 16 in the western opening (Fehmarn-Belt) and between 8 and 10 in the north-eastern opening (Darßer Schwelle), which results in variations of the solute concentrations. Twentyfive bottom water stations in front of the Hütelmoor were repeatedly investigated for trace gas concentrations of nitrous oxide ( $\text{N}_2\text{O}$ ) and methane ( $\text{CH}_4$ ). Although the sampling campaigns throughout the year 2016 and 2017 exhibited variable conditions of salinity, nutrient concentrations and gradients within the water column, most  $\text{N}_2\text{O}$  values recorded, were close or slightly below saturation ( $96 \pm 14 \%$ ) with varying concentrations being most likely the result of temperature caused solubility effects (Bange, 2008, 2006; Weiss and Price, 1980). In contrast,  $\text{CH}_4$  concentrations showed great spatial and seasonal

variabilities. The general seasonal pattern showed a strong increase in bottom water CH<sub>4</sub> concentrations and saturation ( $2845 \pm 1624$  %) in late summer (Figure 6). Furthermore, prevailing hydrodynamic conditions indicate a strong influence on the vertical distribution of trace gases across the water column. Although the origin of the water masses cannot be assessed due to limited data, it can be distinguished by means of salinity. Highest CH<sub>4</sub> concentrations of  $\sim 161$  nmol l<sup>-1</sup> (5994 %) were observed in bottom waters in September 2016 with increasing stratification. It can be assumed that the CH<sub>4</sub> accumulation in bottom waters increases due to limited water column mixing, which is indicated by a distinct salinity difference between bottom water ( $\sim 18$ ) and surface water ( $\sim 8$ ) (Figure 21a, b). The horizontal distribution of the CH<sub>4</sub>-enriched water body closely follows the bathymetry of the seabed (see Figures 6, 13), with CH<sub>4</sub> concentrations clearly increasing at water depth >4 m (Figure 21a). The trough-like bathymetry (Figure 13) in combination with pronounced stratification may additionally reduce the water exchange and thus increase the methane accumulation in bottom water. Additionally, there may also be peat deposits outcropping along the deep seaward flank of the coastal longshore bars, although this could not be confirmed yet. Subsequent circulation of the water column e.g. due to a small-scale local upwelling events or enhanced boundary mixing may cause CH<sub>4</sub> emissions into the atmosphere (Bange et al., 2010; Karstensen et al., 2014).

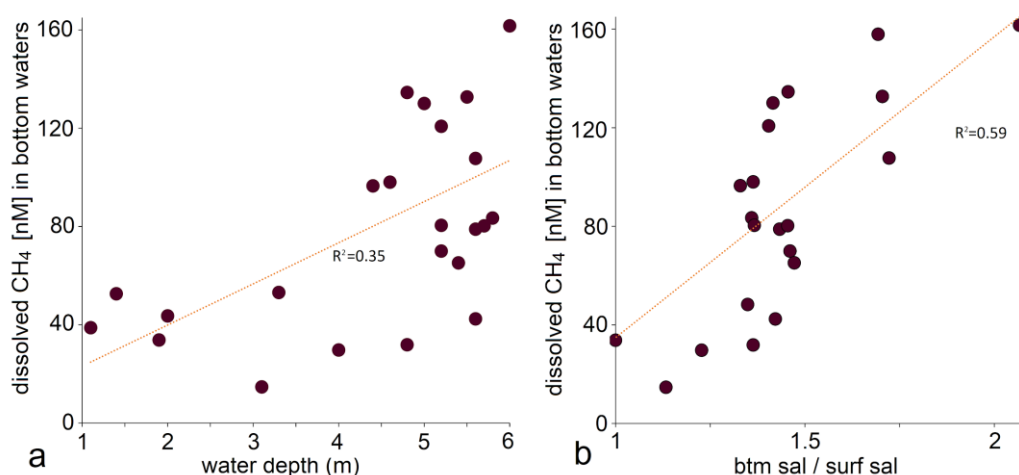


**Figure 21:** The graphs show (a) higher methane concentrations in deeper water depths which are found in a trough-like area in the central transect and (b) a moderate relation between the ratio of bottom water salinity and surface water salinity and CH<sub>4</sub> concentrations (nmol l<sup>-1</sup>), indicating CH<sub>4</sub> accumulation in bottom waters due to stratification events in <6m water depth.



#### 4.1.2. *Warnow-river water*

Variations of physico-chemical parameters in the water column were detected during CTD-profiling at the central offshore station 33 (6 m water depth, see Figures 1, 7) in July 2017. Within 5 days the properties of the water column completely changed, showing an increasing vertical salinity gradient, which indicated both the inflow of near bed saline water and low saline surface water during 24<sup>th</sup> and 28<sup>th</sup> of July (Figure 7). In contrast to almost constant N<sub>2</sub>O concentrations, the CH<sub>4</sub> concentrations varied considerably with time. In the first profile (24<sup>th</sup> of July), increasing salinities and CH<sub>4</sub> concentrations (from 35 to 55 nmol l<sup>-1</sup>) correlate negatively with temperature. While the salinity at the surface increases in the following profile (26<sup>th</sup> of July) with decreasing CH<sub>4</sub> concentration, a reversed pattern appears in the profile two days later (28<sup>th</sup> of July). This latter profile shows a significant decrease of the surface salinity, which is accompanied by an increase of CH<sub>4</sub> concentrations. The increase of CH<sub>4</sub> in the surface water likely results from the discharge of the Warnow-river plume. Modelling results have shown that, depending on the wind conditions, river water may reach the coastline of the study site (Jurasinski et al., 2018) and by this may alter the chemical composition including dissolved trace gas concentrations. Additionally, it has been reported previously (master thesis, Anne Breznikar, 2017), that the discharge of the Warnow river water can act as a source for dissolved CH<sub>4</sub> into the Baltic Sea. In surface waters of the river outlet, measured CH<sub>4</sub> concentrations yield values of  $99.4 \pm 55.4$  nmol l<sup>-1</sup> (range: 42.1–194.3 nmol l<sup>-1</sup>, n = 12) (Warnemünde, Figure 10, 11). The model simulating the estuarine circulation (established by Xaver Lange) further indicates, that the magnitude of the Warnow river outflow can increase tenfold caused by a bed-near inflow of seawater and an enhanced surface outflow of low saline water. The stratification of shallow estuarine rivers have been observed to produce bottom water hypoxia (Stanley and Nixon, 1992). A strongly stratified water column was also observed in the transects of our study site and was most pronounced during a sampling period in September 2016, during which the salinity of bottom water was twice as high as that of surface water (Figure 21b).



#### 4.1.3. Submarine groundwater discharge

The role and magnitudes of submarine groundwater discharge (SGD) in the shallow coastal area in front of the coastal peatland could not be fully confirmed yet by available approaches. As SGD consists mainly of recirculated seawater (Li et al., 1999; Moore, 2010), reliable tracers are required to determine SGD-derived fluxes of water and solutes into the shallow coastal area (Burnett et al., 2001). Assuming a two-component mixing of an inert tracer (e.g. salinity, radiogenic isotopes such as  $^{222}\text{Rn}$ ,  $^{224}\text{Ra}$ ) a two endmember components freshwater-seawater mixing model could theoretically be applied to calculate the land-derived SGD-fraction (Burnett et al., 2006; Dulaiova et al., 2005; Rapaglia et al., 2012; Schubert and Paschke, 2015), allowing relatively fast detection and quantification of SGD in the water column. However, along this coastal study site, the determination of appropriate endmember concentrations is difficult. The coastal aquifer has been observed to be constantly contaminated by seawater intrusion (confirmed by CTD divers installed within the peatland, personal communication with Julia Westphal and Miriam Ibenthal, 2017), while the seawater is continuously substituted and most likely contaminated with the signature of low-saline Warnow-river water. However, stable isotopes ( $\delta^{18}\text{O}$ ,  $\delta^2\text{H}$ ) can be applied in order to confirm a land-derived origin of submarine groundwater by comparing with the stable isotopic ratios of the meteoric water line (Rocha et al., 2015). At our study site, estimations have shown that the major fraction of submarine groundwater derives from the coastal peatland aquifer. The SGD is considered to appear at focussed as well as diffusive spots, mostly southwestern of the lake Heiligensee (Figure 1c) as well as in the central area in shallow coastal areas in front of the “Prahmgraben” (personal communication with Julia Westphal, IOW, 2018). At these locations investigated, (station 22, 61 to 76, see Figure 1c) the occurrence of SGD is indicated by lower surface sediment porewater salinities than ambient seawater (Figure 9) and by information of the applied tracer techniques (e.g. temperature) in the water column (Jurasinski et al., 2018); personal communication with Julia Westphal, 2018). Although SGD-rates were not measured, elevated discharge of solutes were detected near outcropping peat deposits and coincided with elevated concentrations of  $\text{CH}_4$  in the water column (Jurasinski et al., 2018). The dissolved  $\text{CH}_4$  in the water column is assumed to originate from the coastal seabed, which is supported by anomalies of shallow porewater compositions showing high concentrations of  $\text{CH}_4$ , DIC and  $\text{NH}_4^+$ ,

additionally arguing for suboxic or anoxic organic matter mineralization processes such as sulfate reduction, denitrification and methanogenesis (Froelich et al., 1979). Significantly lower permeabilities of the peat layers compared to marine sand sediments may further inhibit oxygen-rich seawater recirculation through the organic-rich peat layers, which reduces degradation rates. Despite the fact that it is  $^{14}\text{C}$  dated to  $6725 \pm 87$  cal yr BP it still contains high amounts of organic carbon (Table 3). Thus it can be assumed, that submerged peat deposits may contribute to the production and release of decomposable dissolved organic carbon (DOC), being subject to physico-chemical solution processes (Ardón et al., 2013; Clark and Van Der Heijden, 2011; Tiemeyer et al., 2017).

#### **4.2. Coastal development and geomorphology**

The surface and subsurface structure of the seabed in front of the coastal peatland exhibit large heterogeneities between the on- and offshore area as well as the northern and the southern areas of the study site. This could be confirmed by the combination of high-resolution hydro-acoustics, seismic surveys and sediment composition analysis, showing that well sorted fine sands predominantly form the offshore sand ridges and cover the central trough area. On the other hand, medium sands with minor gravel fraction cover the transition to the sand ridges and the northern plain area where glacial deposits are located close to the seafloor surface. Towards the south, the decreasing water depth results from increasing sedimentation of medium to fine sand, which is indicated by internal lamination of Holocene deposits (Figure 16B, C, D) in the seismic data. Sand ridges are particularly common in the North Atlantic and the North Sea (van de Meene and van Rijn, 2000; Zeiler et al., 2008), but represent a special geomorphological feature in this nearshore study area. Some of these structures can persist for several thousand years (Snedden and Dalrymple, 1999) and are formed by both tidal currents (negligible in the Baltic Sea) as well as by wind/storm generated longshore currents, while formation of the ridges requires intense storm activity (Swift et al., 1978). To our knowledge, however, no shoreface sand ridges have been reported so far in the southern Baltic Sea. The apparently rare occurrence of these features compared to other shelf regions is most likely due to the lack of sediment supply and the heterogeneous and patchy sediment composition in the Baltic Sea, causing sediment-starved conditions (Feldens et al., 2015; Schwarzer,

2010). This might explain the lower variable length-to-width ratios of ~2 to 10 (Pendleton et al., 2017) and the lower height (Nnafie et al., 2014) as compared to other nearshore ridges. The shallow bases of the sand ridges may further indicate a frequent reworking of the sand ridges by background wave action, while their orientation is in agreement with dominant SW-NE-directed longshore currents. The determined  $^{14}\text{C}$  date retrieved from the organic sediments and marine shells in core C1 (Figure 15) and seismic data provide information on the time of formation of the offshore sand ridges. The unconformity between the base of the sand ridges and the sediment material within core C1 (Figure 16A) indicates that the sand ridges were formed subsequent to the deposition of the youngest dated material below around 3582–3450 cal yr BP, a time when the Baltic Sea sea level reached its present value and remained almost stable (Figure 22). Coastal dynamics such as wave and longshore currents lead to sediment transport in a northeastern direction, accumulating along the barrier spit of the Fischland-Darß peninsula (Lampe et al., 2011). The shoreline of the study site is featured by a longshore bar (Figure 13) consisting of fine to medium sand and is the result of nearshore sedimentation processes. In the Baltic sea and other micro-tidal sandy beach systems, longshore bars with asymmetric slope angles are common, with the steeper slope typically facing the beach (Guillén and Palanques, 1993; Zhang et al., 2011). The position and stability of longshore bars is influenced by coastal dynamics such as wave energy and sea level fluctuations with rising sea level forcing an upwards movement, as a result of higher wave energy (Lippmann and Holman, 1990; Wright and Short, 1984). In response, the movement of the coastal longshore bars controls the amount of wave energy reaching the shoreline and thus affecting sediment erosion and accumulation. Additionally, the longshore bar at the study site contains mid-Holocene peat deposits (6725  $\pm$  87 cal yr BP) (C3.1, Figure 15) and thus records information about associated paleo-landscapes, pre-existing floodplains, habitat migration, sediment stability and its seasonal equilibrium morphology (Gerdes et al., 2003; Plets et al., 2007; Westley and Dix, 2006). The formation and submergence of these peat deposits reflects the decline of the coast and processing of land-based sediments. In the northern nearshore coastal area, the longshore bar is less pronounced, which is likely caused by increased coastal erosion in this area. The submarine extension and formation time of the peat deposits is discussed in the following section.

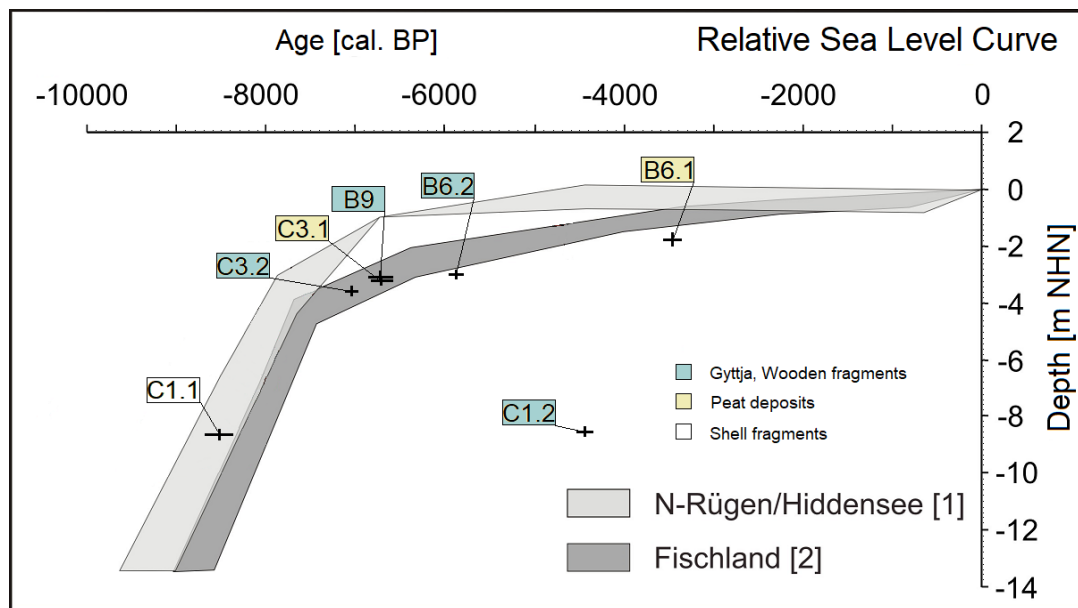


**Figure 22:** Local Holocene sea level curve based on Lampe (2010) with age/depth relationships obtained in this study. The  $^{14}\text{C}$ -ages cover the local sea level curve, except from C1.2, which likely reflect measurements of reworked material.

#### 4.2.1. Peatland formation and sea level rise

The coastal region and landscape of the southern Baltic Sea were predominantly shaped by the Weichselian glaciation around 115.000–13.000 b.p. (Niedermeyer et al., 2011), which led to sediment deposits of up to 50 m thickness. The northeast striking coastline of the study site is predominantly composed of marine sediments (medium and fine sand, gravel) but also contains former terrestrial peat deposits, exposed in the area of the coastal lake Heiligensee. These disclosed peat deposits result from coastal erosion processes in eastern direction (landwards), where the peatland and nature reserve “Heiligensee und Hütelmoor” is located. Low-lying coastal peatlands are unique features along the coastline, and were predominantly formed in the late Holocene during the sea level stagnation about 5800 cal yr BP (Lampe, 2002). The area of the present-day peatland has been formed in a former postglacial lake after the retreat of the glaciers (Kolp, 1957). The onset of the peatland formation “Heiligensee und Hütelmoor” could be determined from submerged peat detritus (basal organic/gyttja) to have been started as early as  $7024 \pm 73$  cal yr BP (sample C3.2), which is earlier than the previously estimated formation age of 5400 yr BP, (Bohne and Bohne, 2008). Overlaying peat deposits were dated to  $6725 \pm 87$  cal yr BP (C3.1) and additionally peat detritus dated at

B6.2:  $5918 \pm 45$  cal yr BP was found at the base of the peat deposits along the shoreline. Some peat deposits in the northern part of the study area were not dated, but given their base situated at 1 m bsl these can be assumed postdate the peat deposits in the central area (ca. 3 m bsl) (Figure 12). The time frame and depth of the sampled peat deposits coincide with a period of continuously decreasing sea level rise (from  $>0.1$  cm yr<sup>-1</sup> to 0.05–0.08 cm yr<sup>-1</sup>) starting around 7000 BP, thus allowing peat formation ( $\sim 0.05$ – $0.13$  cm yr<sup>-1</sup>) to keep up with the rising water table (Lampe et al., 2011, 2010; van der Linden et al., 2008). According to the data available, an earlier onset of peatland formation is not apparent, particularly since the organic-rich peat layers originating from the offshore core C1 show indications of reworked material. The geochemical signatures (C/N ratios (11.97),  $\delta^{13}\text{C}$  isotope values ( $-25.2$  ‰), observation of marine shell fragments of the bulk material) suggest organic material, typical for marine origin (Stein, 1991).

The Hütelmoor can be defined as a paludification mire, which are generally subject to continuous horizontal water permeation below the surface of the terrain (Wheeler and Proctor, 2000). The earliest formation of the peatland, however, can be traced back to local depressions in which gyttja, a lake sediment, was deposited on top of silty and clayey sediments interpreted as clastic lacustrine or fluvio-lacustrine sediments due to their high content of silt or clay and their position between basin sand and gyttja. Terrestrialization of these depressions may have further resulted in peat accumulation and peatland growth. The autochthonous formation of the sediments is confirmed by a continuous basal sediment sequence observed in the offshore core C3 (Figure 15). Thus, the bottom sand was deposited under freshwater conditions, followed by formation of gyttja during the wetlands period and finally peat sediment accumulation during the Littorina transgression.  $^{14}\text{C}$  age dating of undisturbed sediment sequences containing basal peat deposits is a powerful method and can provide useful information to investigate Holocene sea level development (Heinrich et al., 2017; Lampe et al., 2010; Lampe and Janke, 2004a, 2004b; Rößler et al., 2011). According to the local sea level curves of Fischland and Nord-Rügen (Lampe et al., 2010), the detected  $^{14}\text{C}$  ages show a slight tendency towards a lower sea level, as determined by ages in samples B6.1 and B6.2 (Table 3). This observation agrees with different rates of glacial isostatic adjustment (Lampe, 2005), with the North of Rügen experiencing uplifting, and the more southern area (Hütelmoor) subsiding along the isostatic equilibrium line.

The transition from terrestrial peat material (i.e. freshwater environment) to marine sand (i.e. saltwater environment) is indicated by a sudden change in substrate and an erosional upper boundary on top of the peat deposits in both on- and offshore peat sediments. This indicates a sudden flooding of the former peatland. The change of the environmental conditions is also supported by geochemical data derived from the organic matter with carbon/nitrogen ratios increase from 21.3 in 147 cm sediment depth and 36.4 in 157 cm sediment depth (C3, Figure 15), which are considered to be of terrestrial origin (Meyers, 1997). This is accompanied by a sudden increase of mean  $\delta^{13}\text{C}$  values from  $-27.9 \pm 0.95$  in the peat and sand deposits below the erosive boundary to  $-24.3 \pm 0.8$  in the marine sands above, suggesting a shift from a terrestrial, freshwater environment to a marine saltwater environment (Bickert, 2000). The deposition of this marine sand and the contemporaneous erosion of the underlying peat sediments can be constrained to a maximum age of  $3516 \pm 87$  cal yr BP (B6.1) under the assumption of a coherent peat system. At the same time this also provides information about the temporal onset of the coastal longshore bar. The submarine basal peat deposits as well as shallow near-coastal sediment deposition including exposed peat are subject to erosion in response to the position and stability of the longshore bar. Considering the total coastal retreat and the occurrence of former terrestrial peat deposits in the present-day offshore area, it can be assumed that the centre of the peatland has shifted from the present present-day offshore area to the current location of the Hütelmoor. This is also confirmed by peat detritus and peat of similar thickness deposited above on- and offshore basin sands in B6.2 ( $5918 \pm 45$  cal BP), B9 ( $6769 \pm 128$  cal BP) (Figure 12) and C3.2 (Figure 23) at similar depth.

#### 4.2.2. *Submerged peat deposits in marine sediments*

The retreat of the coast has transformed former terrestrial peat deposits into marine sediments. Coastal erosion and flooding of the coastal peatland can be accelerated by different factors such as sea-level rise, reduced sediment availability, coastal stress due to storm events and landside subsidence (Lampe and Janke, 2004a; Vestergaard, 1997). The geomorphology of the peat deposits in the study area developed in response to the topography of the till, resulting in shallower peat deposit of ~1 m bsl in the northern part (core B4 and B5, Figure 12). These peat deposits are found on the beach surface near lake Heiligensee ("observed peat" in

Figure 13) and are therefore exposed to the dynamics of the coastal shoreline. Minor erosion can regularly be observed after storm surges, whereas large washover events as observed in January 2019 (Figure 2 b, c) have been reported to wash-out peat blocks of several decimeter upon the beach (see also Krüger, 1995). The absence of peat layers in core C5 confirms that the offshore continuation of peat deposits is constrained to the north. However, the sediment sequences consisting of minerogenic lake sediments and fine sand contained in C5 indicate a former submarine extension of the peat layer, given the corresponding sediment sequence found below the peat deposits in core B4 (Gerdes et al., 2003). In the southern and central part of the study site the deep peat deposits are better preserved (Figure 12) and extend below the longshore bar. This is confirmed by corresponding reflections in the seismic data below its base (Figure 16B), which show similar acoustic characteristics as compared to ground-truthed reflections near core C3. In the southern area, where peat deposits could be sampled both on- and offshore (C3, B9, Figure 13), the base peat is located ~2 m lower than in the north (B4, Figure 12). The underwater peat is interpreted as the seaward continuation of the peat deposits on land (Figure 17). This assumption is supported by a comparable age of formation (Table 3), the same sediment sequences of silty fine sand, gyttja and peat (Figure 15, 12, 23) with similar depths of these layers both on onshore and offshore, and corresponding horizontal reflections in the seismic data. The reflections in the seismic data imply a seaward extension of the peat layer that was detected in C3 to the seaward dipping base of the longshore sand bar (Figure 16C-D), with no indication of peat deposits underneath the offshore sand ridges (core C1).

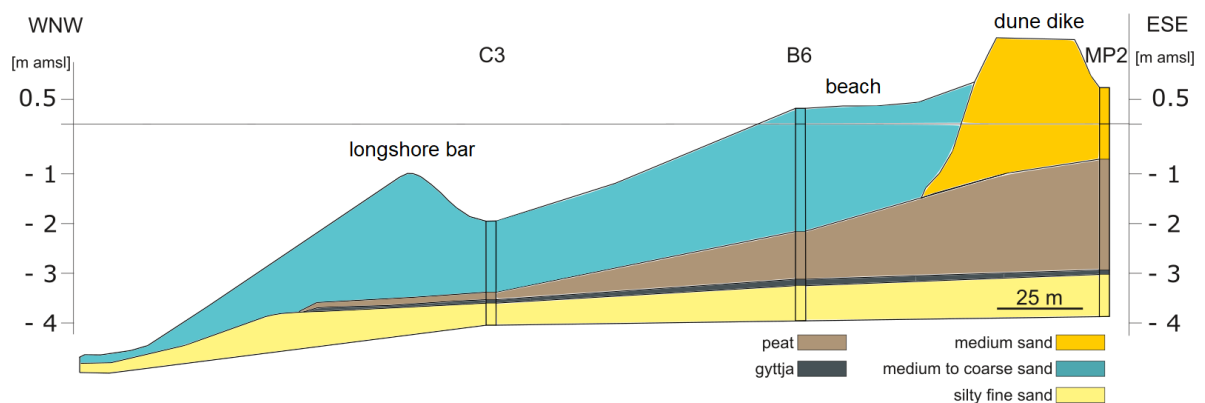


**Figure 23:** Geological profile perpendicular to the coast with drilling locations (MP2, B6, C3 - compare Figure 13 for core locations): sediment depths in m amsl. The information of sub-sedimentary peat continuation is based on ground-truthing with core C3 and the continuation of internal reflectors in the seismic profiles.

Towards the south-western periphery of the coastal peatland, the peat burial depth declines again and is completely absent in core B7 (Figure 12), but re-appears further south in sediment core LG Fsb -/1956 (Figure 13) containing peat deposits of 85 cm thickness. The hiatus in the peat deposits along the beach is most likely caused by a storm surge in 1954, which eroded the surface sand layer and caused washover and erosion of peat blocks across a length of 100 m (Kolp, 1957). The sub-sedimentary, spatial continuation of peat deposits under the coastal sandbank can be roughly defined by seismic data (Figure 16B, -C, -D). A coherent submerged area of 0.16–0.2 km<sup>2</sup> can be estimated under the assumption of a continuous deposition of peat along the coast with larger offshore extension in the central study site. This is constrained by the seaward boundary of the longshore bar and the disclosed peat deposits in the north.

#### **4.3. Experimental investigation of the interaction of submerged peat with advective groundwater and seawater flow**

##### *4.3.1. Advective flow and solute transport*

The flow-through column experiments (Figure 5) were conducted, in order to improve the understanding of carbon transformations and exchange of trace gases from the submerged peat deposits that were found along the shoreline of the coastal peatland (see chapter 2.3 and 3.3). Therefore, naturally layered peat-sand and sand sediments were alternatively supplied with oxygen-rich seawater from above and oxygen-depleted groundwater from below. Geochemical variables and fluxes in the peat-sand core were significantly distinct from the homogenous sand core. Even though it was possible to generate comparable flow regimes in the two types of sediment cores by gravity driven, valve-controlled downwards flow and pump-controlled upwards flow, the mixing of the two salinity endmembers showed clear differences. Sand cores experiments showed stronger, internal mixing compared to the peat-sand cores (Figure 18, salinity of P1 and S1). The mixing of GW and SW in the sand core extended over the entire profile, resulting in a smooth vertical salinity gradient. The formation of low saline reservoirs in the pore spaces was in most cases inhibited and such reservoirs formed only during GW3 ( $S \approx 1.6$ , Figure 18, 25). The higher density of saline SW compared to the low-saline GW



underneath may have caused density-driven convection currents as described for permeable coastal sands (Robinson et al., 2007; Santos et al., 2012). In contrast, peat soils are highly complex porous media including open and connected, dead-end and isolated pores, where flow and convergence of GW and SW is restricted to the hydrologically active pore space (Rezanezhad et al., 2016). Since biogeochemical exchange processes are related to the ionic strength of the solution, the formation of low-saline porewater reservoirs in submerged peat layers potentially enhances the concentration of DOC and formation and release of CH<sub>4</sub> if O<sub>2</sub> and SO<sub>4</sub><sup>2-</sup> are absent. In the Baltic Sea, where peat deposits and SGD are frequently observed along the coastal zones (Kotwicki et al., 2014; Kreuzburg et al., 2018; Peltonen, 2002; Schlüter et al., 2004; Sergeev et al., 2015b), these processes can have potential implications on the carbon balance and the release of methane into the water column and atmosphere.

#### 4.3.2. *Solid phase geochemistry*

The shift from a terrestrial, freshwater environment (peat) to a marine saltwater environment (sand) is recorded by a sudden change of the substrate in the peat-sand cores (P1, P2, P3). The peat layer is characterized by low C:N ratios of ~30 and light  $\delta^{13}\text{C}$  values of ~-27 ‰. The change towards heavier isotopic compositions of the organic matter closer to the sand confirms a change into marine depositional conditions (Bickert, 2000) and is also supported by lower C:N ratios of the organic matter source (Meyers, 1997). Sediment cores without peat (S1, S2, S3) and the sandy parts of the peat-sand cores have higher  $\delta^{13}\text{C}$  values of  $-24.3 \pm 1$  ‰, which is typical for a marine origin (Stein, 1991). The close proximity of marine sandy sediments with peat layers results in a high downcore gradient of organic matter of different composition and origin. Moreover, the degree of decomposition of the peat changed from less decomposed peat (H 3–4) in depths >30 cm to moderately decomposed peat (H 7–8) towards the peat-sand interface (i.e. within the transition layer), coinciding with a C<sub>org</sub> decrease of 99.9 % (Figure 20). These findings indicate that peat soil covered with permeable sediments is subject to decomposition, progressing from the sand-peat interface into deeper regions. Peat soil in >30 cm, although exposed to the coastal wave dynamics, is assumed to be less affected by marine-related leaching effects due to their high contents of organic carbon (Figure 20).

### 4.3.3. Carbon mineralization processes

#### 4.3.3.1. Mobilization and transformation of DOC

Downcore concentration profiles of DIC, DOC, salinity and sulfate in the porewaters clearly show different slopes above and below the peat layer indicating different chemical and physical processes in these substrates. Throughout the cores, salinity always steadily increases, while the other substances undergo production, consumption and conversion processes. Within the organic-rich peat soil (>30 cm), porewaters were depleted in  $\text{SO}_4^{2-}$ , which indicates sulfate reduction in the sediments above and favors  $\text{CH}_4$  production in deeper peat layers (Figure 18, 25). The generation of DOC from  $\text{C}_{\text{org}}$  appears to be primarily controlled by the ionic strength of the porewater, resulting in an inverse relation between the concentrations of  $\text{Cl}^-$  and DOC. The impact of porewater flow velocities, different flow regimes, pH, and temperature can be relevant for DOC production from organic carbon (Evans et al., 2012; Kalbitz et al., 2000; Koehler et al., 2009; Tiemeyer et al., 2017; Tipping and Hurley, 1988). In contrast to most studies, Gosch et al., (2018) observed an increase of DOC release with increasing salinities, which was explained by the specific geochemical properties of the investigated peat substrate. However, in our study, elevated concentrations of DOC and a stronger conformity of  $\delta^{13}\text{C}$  values between DOC and  $\text{C}_{\text{org}}$  were observed with salinities <5, confirming peat as the carbon source for DOC in low salinity conditions (see supplementary Figure 24). Heavier  $\delta^{13}\text{C}_{\text{DOC}}$  values were observed with increasing salinity conditions and can be the result of organic matter degradation by sulfate reduction (Anderson and Arthur, 1983; Boutton, 1991).

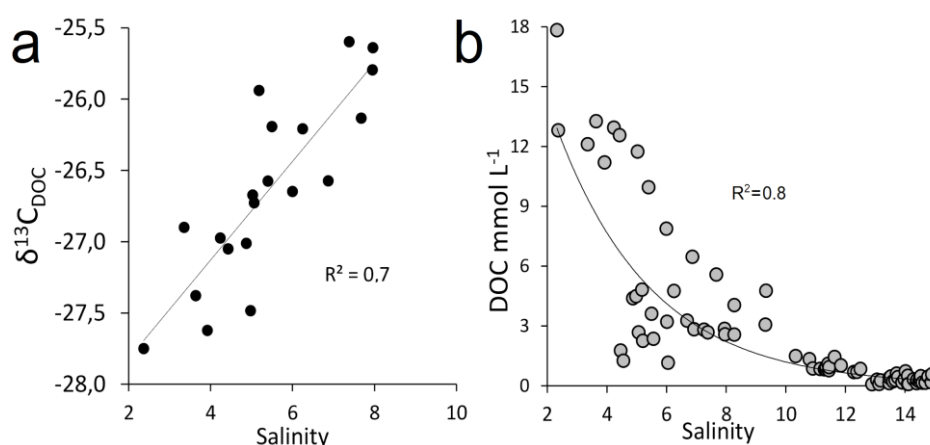


**Figure 24:** Relation between the  $\delta^{13}\text{C}_{\text{DOC}}$  and salinity and the concentration of DOC and salinity for peat-sand core (P1)

The upwards convection of DOC with advective fluxes is pronounced during GW flow regimes and is mostly pronounced during GW3, showing high concentrations ( $\text{DOC} \approx 6.5 \text{ mmol l}^{-1}$ ) even in discharging surface water (Figures 25) at day 50, which is likely caused by leaching of solid  $\text{C}_{\text{org}}$ . According to other studies (Berry et al., 1990; Gosch et al., 2018; Tiemeyer et al., 2017; Tipping and Hurley, 1988), the effects of ionic strength on DOC release are not consistent and alter with substrate and physicochemical factors (Kalbitz et al., 2000), but the mobilization of DOC from organic sediments is apparently reduced by increasing ionic strength. Sulfate reduction and oxygen respiration are responsible for the major share of DOC oxidation in marine endobenthic environments (Bender and Heggie, 1984; Henrichs and Reeburgh, 1987) and can be assumed that this is also true for the peat in our experiments. Highly decomposed peat lacks high amounts of decomposable organic matter that could be turned into DOC (Strehse et al., 2018). The peat in deeper layers shows significantly lower degrees of decomposition and has higher  $\text{C}_{\text{org}}$  contents, and thus may still contain significant amounts of decomposable DOC. The fate of this DOC in pore or surface waters containing mineralization-relevant substances (e.g. electron acceptors such as  $\text{SO}_4^{2-}$ ,  $\text{O}_2$ ) leads to the oxidation of DOC and transformation into DIC. Our results from porewaters indicate these processes, in particular at the end of the experiment, where an increase in DIC at the peat/sand interface coincides with a decrease in DOC and a deviation between  $\text{SO}_4^{2-}$  and salinity (Figure 25).

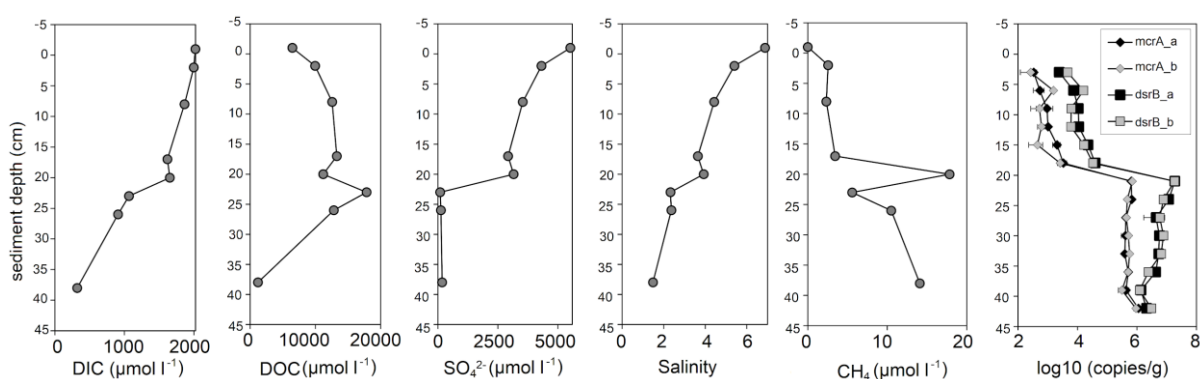


**Figure 25:** Concentrations of DIC, DOC,  $\text{SO}_4^{2-}$ , salinity,  $\text{CH}_4$  and microbial abundances (repetitive measurements: a, b) of methanogens and sulfate reducers (P1) vs. sediment depth at day 50, the end of the experiment.

Previous studies have shown that with salinities  $S > 10$ ,  $\text{SO}_4^{2-}$ -driven DOC mineralization is the preferred metabolic process, causing increased  $\text{CO}_2$  production due to DOC mineralization (Chambers et al., 2014; Weston et al., 2011). In contrast to  $\text{O}_2$ , which is depleted in the surface sediments in our experiments ( $< 10$  cm, Figures 18) there is a correlation between  $\text{Cl}^-$  and  $\text{SO}_4^{2-}$ . Without any metabolic processes, the concentration of the main electron acceptors,  $\text{O}_2$  and  $\text{SO}_4^{2-}$  in our experiment is pre-defined by the mixture of the two endmembers (SW and GW, for composition see Table 1). Under the assumption that the concentration within the GW end member is negligible, used electron acceptors ( $\Delta\text{EA}$ ) can be directly derived from the salt content:

$$(3) \quad \left( \frac{\text{EA}_{\max}}{\text{Sal}_{\max}} \text{Sal}_{\text{sample}} \right) - \text{EA}_{\text{sample}} = \Delta\text{EA}$$

This allows calculating the loss of electron acceptors by calculating the difference between this “preformed” available electron acceptors and the observed  $\text{O}_2$  and  $\text{SO}_4^{2-}$  at any point of the experiment ( $\Delta\text{O}_2$  and  $\Delta\text{SO}_4^{2-}$ , see Figure 26). The data clearly indicate the higher consumption of electron acceptors in the peat-sand cores in comparison to the sand cores, indicating sulfate-fueled oxidation driven by penetration of sulfate into the decomposable peat layer. The upward advection of DOC and DIC during the GW stages leads to the increase of both parameters in the peat-overlying sands, where further oxygen-driven DOC decomposition might be partially responsible for oxygen demand. During phases of seawater intrusion,  $\text{SO}_4^{2-}$  entering the decomposable DOC pool apparently enhances anaerobic DOC oxidation in the sediments at depth  $> 20$  cm. Full depletion of  $\text{SO}_4^{2-}$  in organic-rich sediments, in particular during GW stages where almost no new  $\text{SO}_4^{2-}$  enters the system, can facilitate methanogenesis.

Depth profiling of microbial abundances supports the suggested electron acceptor utilization along the sediment column. The abundances of sulfate reducing bacteria (*dsrB*) and methanogens (*mcrA*) increases in the peat layer in an upwards direction, indicating SRB to prefer the transition zone in which sulfate and DOC is easily available (Figure 25). Although SRB overall dominate methanogens, the copy numbers of *mcrA* are stable across the whole peat section, suggesting their abundance neither being dependent on the peat characteristics nor on the increasing abundance of the sulfate reducers in an upwards direction. Instead, this could indicate that the high availability of peat-generated dissolved DOC enables

the coexistence of both methanogenic and sulfate reducing microbial communities and that their activity is subject to the changing environmental conditions. However, it cannot be excluded that the detected overlap of both groups was at least to some extent triggered by advective fluxes in the peat-sand core.

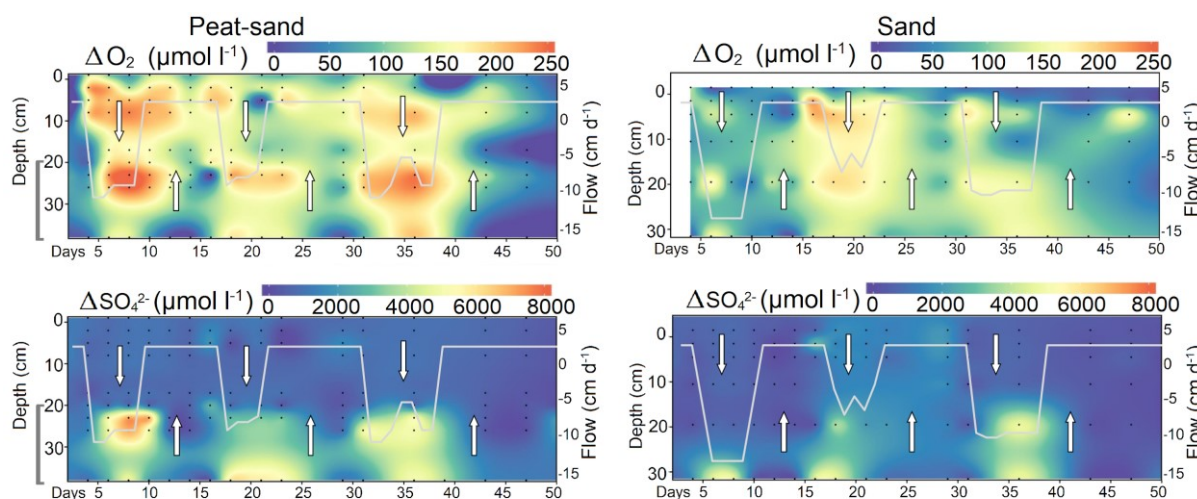


**Figure 26:** Depth distribution of  $O_2$  and  $SO_4^{2-}$  deviating to the initial endmember concentration, presented for each column set (column P1 and S1), over 50 days of the experiment period.

#### 4.3.3.2. Formation, transport and emission of gases

The upwards flowing GW decreases the porewater salinity and thus displaces required oxidants ( $SO_4^{2-}$ ) for SRB. This likely promotes anoxic DOC mineralization by methanogenesis and  $CH_4$  formation (Stadtman and Barker, 1949; Whiticar et al., 1986). It is further notable that  $CO_2$  emissions during GW1, GW2 and GW3 have reached similar and steady flux rates, which may indicate a limit of mineralization and oxidation activity controlled by the amount and composition of solutes present. Most pathways of microbial organic carbon oxidation, except for  $SO_4^{2-}$  reduction, are less active with increased  $Cl^-$  or  $HS^-$  concentrations (Chambers et al., 2011; Joye and Hollibaugh, 1995; Luo et al., 2017). However, microbial DOC oxidation by SRB and methanogens can also co-exist (Figure 25) and may depend on access and quality of the substrate (Dar et al., 2008; Holmer and Kristensen, 1994; Sela-Adler et al., 2017) and species-dependent metabolic traits (Ozuolmez et al., 2015). The emissions of  $CH_4$  have been described as the residual of  $CH_4$  production and -oxidation (e.g. aerobic and anaerobic  $CH_4$  oxidation), and can be governed by advective transport processes (Heyer and Berger, 2000). The transfer and extrapolation of  $CH_4$  emissions observed during the experiment to the field natural

situations have to be treated with caution, as the microbial and physicochemical properties of the sediment cores might have changed during sampling, transport and construction of the column set-up, and the adjusted GW and SW flow were only approximations of natural conditions at the field site. Whereas molecular diffusion is often assumed to be the main driver of air-water CH<sub>4</sub> transfer in experimental approaches (Moore and Dalva, 1993; van Winden et al., 2012), the emissions of CH<sub>4</sub> in shallow water are often dominated by ebullition (Ostrovsky, 2003) and may display large spatial and temporal variabilities (Bange, 2006; Upstill-Goddard, 2006). In the case of our experiment, the advective transport of dissolved methane, forced by alternating phases of advective in- and outflow, has a strong control on the gas flux into the water column (Figure 18). Our experimental CH<sub>4</sub> fluxes during GW discharge ( $35.7 \pm 26.3 \mu\text{mol m}^{-2} \text{d}^{-1}$  peat-sand core;  $21.2 \pm 16 \mu\text{mol m}^{-2} \text{d}^{-1}$  sand core) were in the range of the data reported by (Bange et al., (1994), where an average CH<sub>4</sub> flux of  $22\text{--}37 \mu\text{mol m}^{-2} \text{d}^{-1}$  from the continental shelves of the Baltic Sea and the North Sea, with total emissions ranging from  $0.35\text{--}0.75 \text{ Tg C yr}^{-1}$  (Bange, 2006; Upstill-Goddard, 2006), were estimated. An extrapolation of the fluxes of the small coastal area off the Hütelmoor, where peat deposits covering an area of  $1.6\text{--}2 \text{ km}^2$  have been detected (Kreuzburg et al., 2018), would result in methane fluxes of  $3.3 \times 10^{-7}\text{--}4.1 \times 10^{-7} \text{ Tg C yr}^{-1}$ . Increasing CH<sub>4</sub> fluxes were detected during GW3 (from  $16.5\text{--}77.3 \mu\text{mol m}^{-2} \text{d}^{-1}$ ). These are comparable to studies where CH<sub>4</sub> emissions of  $126\text{--}134 \mu\text{mol m}^{-2} \text{d}^{-1}$  were associated with gassy sediments containing high fractions of organic matter (Borges et al., 2016). Studies investigating SGD-related CH<sub>4</sub> fluxes report values exceeding our experimental values by a factor of 5-11, amounting  $200\text{--}400 \mu\text{mol m}^{-2} \text{d}^{-1}$  (Bussmann and Suess, 1998) and  $900 \mu\text{mol m}^{-2} \text{d}^{-1}$  (Porubsky et al., 2013). However, these results were linked to higher SGD rates and might have accumulated products of organic matter decomposition on longer time scales.

## 5. Summary & Conclusions

Offshore field studies were conducted with the working boat IOW-Klaashahn in front of the coastal peatland and nature reserve - "Heiligensee und Hütelmoor" in order to investigate the spatial and temporal distribution of trace gases such as methane ( $\text{CH}_4$ ) and nitrous oxide ( $\text{N}_2\text{O}$ ). In contrast to  $\text{N}_2\text{O}$ ,  $\text{CH}_4$  concentrations revealed spatial and temporal variations, which are interpreted mostly as the result of hydrodynamic conditions and forcing. The conditions in the water column of maximal ~6 m water depth were classified in (1) periods of less vertical mixing, showing high  $\text{CH}_4$  concentrations (up to  $161 \text{ nmol l}^{-1}$ ) in bottom waters and (2) in periods with increasing methane concentrations towards the coastline during situations of a well-mixed water column (Figure 6). The inhibited vertical mixing was clearly indicated by differences between bottom (18) and surface water (8) salinities (Figure 21a, b). Geochemical surveys and model data of the hydrodynamics have shown that, depending on wind conditions, the Warnow-river plume may pass the study area (Jurasinski et al., 2018), changing the vertical salinity distribution of the water column and influencing the measured water chemistry within the coastal study site. The continuous substitution and modification of the water body was verified by repetitive profiling at a central station (Figure 7), and is considered to be composed of (1) seawater from the Baltic Sea, (2) river water from the Warnow and (3) submarine groundwater discharge (SGD) originating from the coastal sediment and coastal aquifers. Although the water fraction contributed by shallow SGD is considered to be very low (Miegel et al., 2009), anomalies in temperature, salinity and radiogenic tracers (e.g.  $^{224}\text{Ra}$ ) are interpreted to be the result of SGD. The anomalies coincided with the coastal area of emerging peat deposits and elevated bottom  $\text{CH}_4$  concentrations ( $25.3 \pm 9.3$ ; range  $15\text{--}55 \text{ CH}_4 \text{ nmol l}^{-1}$ ), indicating potential sedimentary methane sources close to the beach (Jurasinski et al., 2018; Kreuzburg et al., 2018). Additional surveys along the coastline revealed methane concentrations of  $3.3 \text{ } \mu\text{mol l}^{-1}$  in coastal surface waters (Figure 8, 9) and  $0.9 \text{ mmol l}^{-1}$  in submarine porewater in coastal sediments, where outcropping peat deposits have been observed (Figure 13).

As peat represents a potential source of carbon-containing solutes and gases, the submarine extension of former terrestrial peat deposits was investigated using a combination of geo-acoustic surveys, onshore- and offshore sediment cores and geochemical analysis. The peat deposits were found to continue more than 90 m

(areal extent: 0.16–0.2 km<sup>2</sup>) in front of the coastline. Geochemical analysis of the submerged peat deposits revealed high organic contents (C<sub>org</sub> 37–53 %), point to terrestrial origin ( $\delta^{13}\text{C}$  -28.9 ‰), and indicate an earlier onset of the peatland formation (<sup>14</sup>C-dated to 6725 ± 87 cal yr BP) than previously estimated (~5400 cal yr BP). The <sup>14</sup>C ages of the basal peat deposits may indicate the former extension of the coastal peatland. The ongoing erosion of coastal peat-containing sediments and recirculation of sea- and groundwater through the coastal aquifer is assumed to have considerable impact on the nearshore marine carbon balance. In-situ carbon fluxes between the coastal seabed and the shallow coastal water could be quantified with an incubation chamber, but the results obtained are difficult to interpret given the uncontrolled conditions and high dynamics along the coastline. Therefore, a 50 days column experiment was designed and conducted at the ecohydrology research group, University of Waterloo, Canada in order to better understand the process-based release and transformation of peat-derived carbon. Naturally layered marine peat-sand and sand cores from the coastal area of the study site were alternately supplied with artificial oxygen-rich brackish water from above (salinity ~18) and oxygen-poor, low-saline groundwater from below (salinity ~1.6). The main results of the experimental study are summarized in Figure 27 and illustrate (1) the recirculation of seawater through organic-rich sediments of terrestrial origin (peat deposits), resulting in sulfate reduction, with DIC as the end-product and (2) the discharge of groundwater, driving the release of carbon dioxide and methane into the overlying water body. During the discharge of oxygen-depleted and low-saline groundwater through the peat layers the dissolved organic carbon (DOC) and dissolved inorganic carbon (DIC) concentrations significantly increased, which was accompanied with increasing fluxes of CH<sub>4</sub> and carbon dioxide (CO<sub>2</sub>). As sulfate reducers successfully outcompete methanogens for available free hydrogen (H<sup>+</sup>) and decomposable organic matter (Whiticar et al., 1986) a dilution-caused decrease of sulfate (SO<sub>4</sub><sup>2-</sup>) with low saline groundwater may lead to a lack of sulfate reducing-relevant electron acceptors (SO<sub>4</sub><sup>2-</sup>) in the porewater. Thus, methanogens are assumed to benefit from low-sulfate conditions, which may result in increasing CH<sub>4</sub> production, whereas the emission of carbon-related solutes is assumed to be mostly related to porewater advection. Our results provide clear evidence of bioavailable DOC produced from peat layers already submerged for considerable time spans. The results furthermore show that



substrate, transport processes, redox condition and salinity control peat degradation, organic matter mobilization, and carbon dioxide and methane release. Peat containing sediments can be hot spots of increased organic matter mineralization and may play an important role in methane production of coastal zones worldwide. Submergence of peatlands due to sea level rise, subsidence as well as rewetting of drained coastal peatlands are thus likely to reshape the near shore coastal fluxes of various environmentally important compounds in the future.

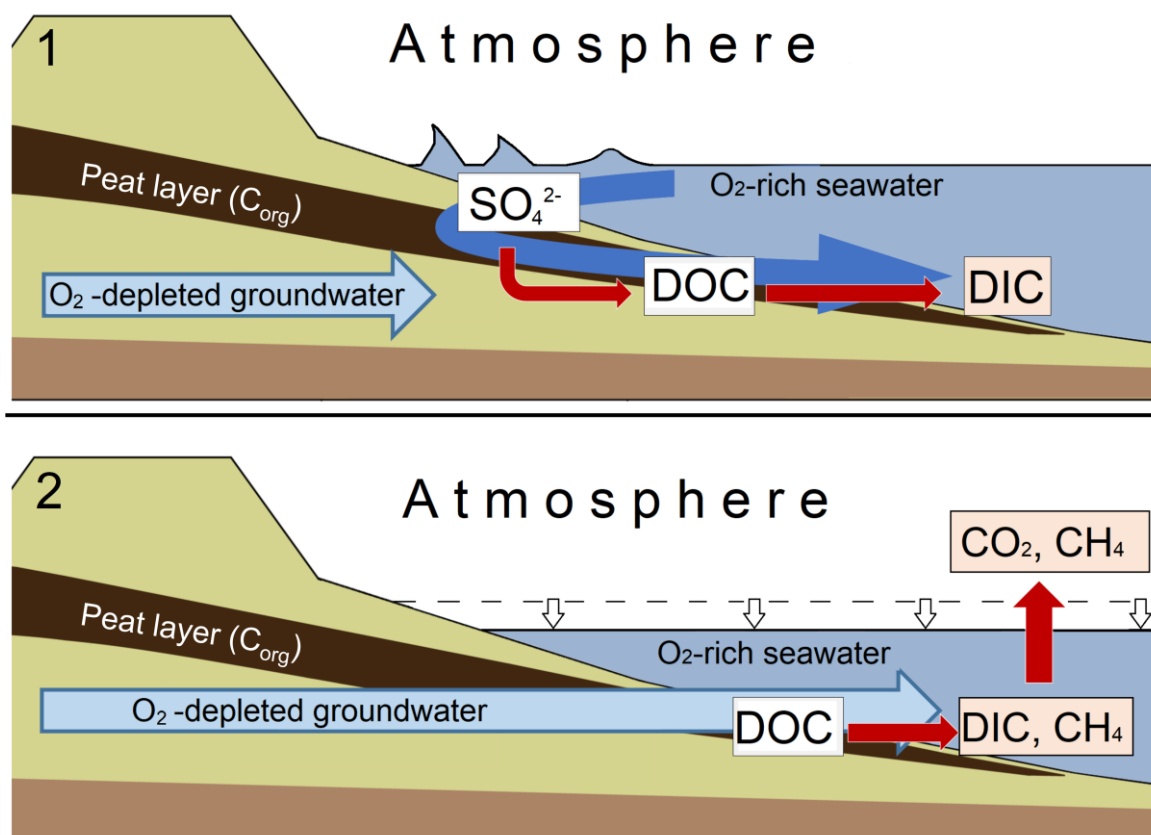


**Figure 27:** Conceptual extraction of the carbon exchange processes in the submarine, peat-containing estuary along the shoreline of our study site with (1) elevated sea-level situation. The blue arrow visualizes the flow of SW through carbon rich sediments driven by wave dynamics, with the red arrows showing the production pathway of DIC. The process likely included a high activity of sulfate reducing bacteria resulting in discharge of DIC and (2) low sea-level situation and calm surface water conditions. The discharge of O<sub>2</sub>-depleted GW displaces methane oxidants, increases DOC release and facilitates methane emission into surface waters and the atmosphere.

## 6. Outlook

Although knowledge about the dynamics of trace gases in shallow coastal regions is still associated with a high degree of uncertainty, this interdisciplinary study has demonstrated a dependence of trace gas production on sediment type with respect to the Holocene evolution of the southern Baltic Sea and coastal hydrodynamic processes. The in-situ investigations led to a deeper understanding of the distribution and formation of trace gases in shallow coastal water. However, hydrodynamic forcings, physicochemical properties and biogeochemical processes can strongly alter the carbon balance of shallow coastal regions on varying time scales not resolvable by classical field sampling schemes. Thus, this work also initiated a new approach to address the need of high temporal resolution of the relevant biogeochemical and physical data. Within the next PhD-project of subproject G2 of Baltic TRANSCOAST new state-of-the-art sensor technology will be deployed to better understand:

- (1) the conjunction, drivers and temporal dynamics of marine shallow water trace gas emissions, hydrodynamics and the influence of submerged former terrestrial organic-rich peat deposition
- (2) the temporal evolution and change in magnitudes of trace gases in response to elevated hydrological exchange processes across the land-sea boundary, focussing on the development of biogeochemical fluxes as consequence of wetland restoration.

## 7. References

- Andersen, M.S., Nyvang, V., Jakobsen, R., Postma, D., 2005. Geochemical processes and solute transport at the seawater/freshwater interface of a sandy aquifer. *Geochim. Cosmochim. Acta* 69, 3979–3994.
- Anderson, T.F., Arthur, M.A., 1983. Stable isotopes of oxygen and carbon and their application to sedimentologic and paleoenvironmental problems. *Unknown Journal*.
- Aravena, R., Wassenaar, L.I., 1993. Dissolved organic carbon and methane in a regional confined aquifer, southern Ontario, Canada: Carbon isotope evidence for associated subsurface sources. *Appl. Geochem.* 8, 483–493.
- Ardón, M., Morse, J.L., Colman, B.P., Bernhardt, E.S., 2013. Drought-induced saltwater incursion leads to increased wetland nitrogen export. *Glob. Chang. Biol.* 19, 2976–2985.
- Badocco, D., Mondin, A., Pastore, P., 2012. Determination of thermodynamic parameters from light intensity signals obtained from oxygen optical sensors. *Sens. Actuators B Chem.* 163, 165–170.
- Bange, H.W., Freing, A., Kock, A., Löscher, C., 2010. Marine Pathways to Nitrous Oxide. *Nitrous Oxide and Climate Change* 2, 36–62.
- Bange, H.W., 2008. Gaseous Nitrogen Compounds (NO, N<sub>2</sub>O, N<sub>2</sub>, NH<sub>3</sub>) in the Ocean. *Nitrogen in the Marine Environment*. <https://doi.org/10.1016/b978-0-12-372522-6.00002-5>
- Bange, H.W., 2006. Nitrous oxide and methane in European coastal waters. *Estuar. Coast. Shelf Sci.* 70, 361–374.
- Bange, H.W., Bartell, U.H., Rapsomanikis, S., Andreae, M.O., 1994. Methane in the Baltic and North Seas and a reassessment of the marine emissions of methane. *Global Biogeochem. Cycles* 8, 465–480.
- Bange, H.W., Bergmann, K., Hansen, H.P., Kock, A., Koppe, R., Malien, F., Ostrau, C., 2010. Dissolved methane during hypoxic events at the Boknis Eck Time Series Station (Eckernförde Bay, SW Baltic Sea). *Biogeosciences* 7, 1279–1284.
- Bange, H.W., Dahlke, S., Ramesh, R., Meyer-Reil, L.-A., Rapsomanikis, S., Andreae, M.O., 1998. Seasonal study of methane and nitrous oxide in the coastal waters of the southern Baltic Sea. *Estuar. Coast. Shelf Sci.* 47, 807–817.
- Barlow, P.M., Reichard, E.G., 2010. Saltwater intrusion in coastal regions of North America. *Hydrogeol. J.* 18, 247–260.
- Bender, M.L., Heggie, D.T., 1984. Fate of organic carbon reaching the deep sea floor: a status report. *Geochim. Cosmochim. Acta* 48, 977–986.
- Berry, D.F., Zelazny, L.W., Walker, H.L., 1990. Aluminum and Organic Matter Mobilization from Forest Soil Infiltrated with Acidified Calcium Sulfate Solutions. *Soil Sci. Soc. Am. J.* 54, 1757–1762.
- Bickert, T., 2000. Influence of Geochemical Processes on Stable Isotope Distribution in Marine Sediments, in: Schulz, H.D., Zabel, M. (Eds.), *Marine Geochemistry*. Springer Berlin Heidelberg, Berlin, Heidelberg, pp. 309–333.

- Bohne, B., Bohne, K., 2008. Monitoring zum Wasserhaushalt einer auf litoralem Versumpfungsmoor gewachsenen Regenmoorkalotte—Beispiel Naturschutzgebiet „Hütelmoor“ bei Rostock. Aspekte der Geoökologie. Berlin: Weißensee Verlag.
- Borges, A.V., Champenois, W., Gypens, N., Delille, B., Harlay, J., 2016. Massive marine methane emissions from near-shore shallow coastal areas. *Sci. Rep.* 6, 27908.
- Boutton, T.W., 1991. 11 - Stable Carbon Isotope Ratios of Natural Materials: II. Atmospheric, Terrestrial, Marine, and Freshwater Environments, in: Coleman, D.C., Fry, B. (Eds.), *Carbon Isotope Techniques*. Academic Press, pp. 173–185.
- Boynton, W.R., Kemp, W.M., Osborne, C.G., 1980. NUTRIENT FLUXES ACROSS THE SEDIMENT-WATER INTERFACE IN THE TURBID ZONE OF A COASTAL PLAIN ESTUARY, in: Kennedy, V.S. (Ed.), *Estuarine Perspectives*. Academic Press, pp. 93–109.
- Buer, A.-L., Gyraite, G., Wegener, P., Lange, X., Katarzyte, M., Hauk, G., Schernewski, G., 2018. Long term development of Bathing Water Quality at the German Baltic coast: spatial patterns, problems and model simulations. *Mar. Pollut. Bull.* 135, 1055–1066.
- Bugna, G.C., Chanton, J.P., Cable, J.E., Burnett, W.C., Cable, P.H., 1996. The importance of groundwater discharge to the methane budgets of nearshore and continental shelf waters of the northeastern Gulf of Mexico. *Geochim. Cosmochim. Acta* 60, 4735–4746.
- Burnett, W.C., Aggarwal, P.K., Aureli, A., Bokuniewicz, H., Cable, J.E., Charette, M.A., Kontar, E., Krupa, S., Kulkarni, K.M., Loveless, A., Moore, W.S., Oberdorfer, J.A., Oliveira, J., Ozyurt, N., Povinec, P., Privitera, A.M.G., Rajar, R., Ramessur, R.T., Scholten, J., Stieglitz, T., Taniguchi, M., Turner, J.V., 2006. Quantifying submarine groundwater discharge in the coastal zone via multiple methods. *Sci. Total Environ.* 367, 498–543.
- Burnett, W.C., Bokuniewicz, H., Huettel, M., Moore, W., Taniguchi, M., 2003. Groundwater and porewater inputs to the coastal zone. *Biogeochemistry* 66, 3–33.
- Burnett, W.C., Taniguchi, M., Oberdorfer, J., 2001. Measurement and significance of the direct discharge of groundwater into the coastal zone. *J. Sea Res.* 46, 109–116.
- Bussmann, I., Suess, E., 1998. Groundwater seepage in Eckernförder Bay (Western Baltic Sea): Effect on methane and salinity distribution of the water column. *Cont. Shelf Res.* 18, 1795–1806.
- Cabrera, R.I., 1998. Monitoring chemical properties of container growing media with small soil solution samplers. The use of trade names in this publication does not imply endorsement of the products used or criticism of similar ones not used. *Sci. Hortic.* 75, 113–119.
- Caress, D.W., Chayes, D.N., 1995. New software for processing sidescan data from sidescan-capable multibeam sonars. *Proceedings of the IEEE Oceans 95 Conference* 997–1000.
- Chambers, L.G., Davis, S.E., Troxler, T., Boyer, J.N., Downey-Wall, A., Scinto, L.J., 2014. Biogeochemical effects of simulated sea level rise on carbon loss in an Everglades mangrove peat soil. *Hydrobiologia* 726, 195–211.

- Chambers, L.G., Reddy, K.R., Osborne, T.Z., 2011. Short-Term Response of Carbon Cycling to Salinity Pulses in a Freshwater Wetland. *Soil Sci. Soc. Am. J.* 75, 2000–2007.
- Charman, D., Others, 2002. *Peatlands and environmental change*. John Wiley&Sons Ltd.
- Cicerone, R.J., Oremland, R.S., 1988. Biogeochemical aspects of atmospheric methane. *Global Biogeochem. Cycles*.
- Clark, J.M., Van Der Heijden, G.M.F., 2011. Variation in the sensitivity of DOC release between different organic soils following H<sub>2</sub>SO<sub>4</sub> and sea-salt additions. *European Journal of*.
- Clark, J.M., Van Der Heijden, G.M.F., Palmer, S.M., Chapman, P.J., Bottrell, S.H., 2011. Variation in the sensitivity of DOC release between different organic soils following H<sub>2</sub>SO<sub>4</sub> and sea-salt additions. *Eur. J. Soil Sci.* 62, 267–284.
- Cyberski, J., 2011. Climate, hydrology and hydrodynamics of the Baltic Sea. W:] *Geochemistry of Baltic Sea surface sediments (Uścinowicz, Sz. , red. )*, Warszawa 55–65.
- Dahms, P., 1991. Studie Wasserregulierung Hütelmoor. Unveröff. Studie StAUN Rostock.
- Dale, A.W., Regnier, P., Knab, N.J., Jørgensen, B.B., Van Cappellen, P., 2008. Anaerobic oxidation of methane (AOM) in marine sediments from the Skagerrak (Denmark): II. Reaction-transport modeling. *Geochim. Cosmochim. Acta* 72, 2880–2894.
- Dar, S.A., Kleerebezem, R., Stams, A.J.M., Kuenen, J.G., Muyzer, G., 2008. Competition and coexistence of sulfate-reducing bacteria, acetogens and methanogens in a lab-scale anaerobic bioreactor as affected by changing substrate to sulfate ratio. *Appl. Microbiol. Biotechnol.* 78, 1045–1055.
- Davidson, N.C., van Dam, A.A., Finlayson, C.M., McInnes, R.J., 2019. Worth of wetlands: revised global monetary values of coastal and inland wetland ecosystem services. *Mar. Freshwater Res.* <https://doi.org/10.1071/MF18391>
- Delaune, R.D., Nyman, J.A., Patrick, W.H., 1994. Peat Collapse, Ponding and Wetland Loss in a Rapidly Submerging Coastal Marsh. *J. Coast. Res.* 10, 1021–1030.
- Deppenmeier, U., 2002. The unique biochemistry of methanogenesis, in: *Progress in Nucleic Acid Research and Molecular Biology*. Academic Press, pp. 223–283.
- Dietrich, R., Liebsch, G., 2000. Zur Variabilität des Meeresspiegels an der Küste von Mecklenburg-Vorpommern. *Z. Geol. Wiss.* 28, 615–624.
- Dillon, K.S., Corbett, D.R., Chanton, J.P., Burnett, W.C., Furbish, D.J., 1999. The use of sulfur hexafluoride (SF<sub>6</sub>) as a tracer of septic tank effluent in the Florida Keys. *J. Hydrol.* 220, 129–140.
- Dulaiova, H., Peterson, R., Burnett, W.C., Lane-Smith, D., 2005. A multi-detector continuous monitor for assessment of <sup>222</sup>Rn in the coastal ocean. *J. Radioanal. Nucl. Chem.* 263, 361–363.
- Ehhalt, D., Prather, M., Dentener, F., Derwent, R., Dlugokencky, E., Others, 2001. Atmospheric chemistry and greenhouse gases. In “Climate change 2001: the scientific basis”. IPCC Working Group I, Third Assessment Report. (Eds JT Houghton, Y Ding, DJ Griggs, M Noguer, PJ van der Linden, X Dai, K Maskell, CA Johnson) pp. 239–288.

- Elken, J., Matthäus, W., 2008. Baltic Sea oceanography. Regional Climate Studies, Assessment of climate change for the Baltic Sea Basin. Annex A 1, 379–385.
- EPA SOP for DOC, 2002. EPA Standard Operating Procedure for Dissolved Organic Carbon, LG211, Revision 03, December, 2002.
- Evans, C.D., Jones, T.G., Burden, A., Ostle, N., Zieliński, P., Cooper, M.D.A., Peacock, M., Clark, J.M., Oulehle, F., Cooper, D., Freeman, C., 2012. Acidity controls on dissolved organic carbon mobility in organic soils. *Glob. Chang. Biol.* 18, 3317–3331.
- Feldens, P., Diesing, M., Schwarzer, K., Heinrich, C., Schlenz, B., 2015. Occurrence of flow parallel and flow transverse bedforms in Fehmarn Belt (SW Baltic Sea) related to the local palaeomorphology. *Geomorphology* 231, 53–62.
- Feldens, P., Schwarzer, K., 2012. The Ancyclus Lake stage of the Baltic Sea in Fehmarn Belt: Indications of a new threshold ? *Cont. Shelf Res.* 35, 43–52.
- Forster, P., Ramaswamy, V., Artaxo, P., Bernsten, T., Betts, R., Fahey, D.W., Haywood, J., Lean, J., Lowe, D.C., Myhre, G., Others, 2007. Changes in atmospheric constituents and in radiative forcing. Chapter 2, in: *Climate Change 2007. The Physical Science Basis*.
- Freeman, C., Evans, C.D., Monteith, D.T., Reynolds, B., Fenner, N., 2001. Export of organic carbon from peat soils. *Nature* 412, 785.
- Froelich, P.N., Klinkhammer, G.P., Bender, M.L., Luedtke, N.A., Heath, G.R., Cullen, D., Dauphin, P., Hammond, D., Hartman, B., Maynard, V., 1979. Early oxidation of organic matter in pelagic sediments of the eastern equatorial Atlantic: suboxic diagenesis. *Geochim. Cosmochim. Acta* 43, 1075–1090.
- Gatland, J.R., Santos, I.R., Maher, D.T., Duncan, T.M., Erler, D.V., 2014. Carbon dioxide and methane emissions from an artificially drained coastal wetland during a flood: Implications for wetland global warming potential. *Journal of Geophysical Research: Biogeosciences* 119, 1698–1716.
- Gehrels, W.R., Anderson, W.P., 2014. Reconstructing Holocene sea-level change from coastal freshwater peat: A combined empirical and model-based approach. *Mar. Geol.* 353, 140–152.
- Gelesh, L., Marshall, K., Boicourt, W., Lapham, L., 2016. Methane concentrations increase in bottom waters during summertime anoxia in the highly eutrophic estuary, Chesapeake Bay, USA. *Limnol. Oceanogr.* 61, S253–S266.
- Gerdes, G., Petzelberger, B.E.M., Scholz-Böttcher, B.M., Streif, H., 2003. The record of climatic change in the geological archives of shallow marine, coastal, and adjacent lowland areas of Northern Germany. *Quat. Sci. Rev.* 22, 101–124.
- Gorham, E., 1995. The biogeochemistry of northern peatlands and its possible responses to global warming. Biotic feedbacks in the global climate system: Will the warming feed the warming 169–187.
- Gosch, L., Janssen, M., Lennartz, B., 2018. Impact of the water salinity on the hydraulic conductivity of fen peat. *Hydrol. Process.* 32, 1214–1222.
- Grasshoff, K., Ehrhardt, M., Kremling, K., 1999. *Methods of seawater analysis*. 3rd. ref.
- Guillén, J., Palanques, A., 1993. Longshore bar and trough systems in a microtidal, storm-wave dominated coast: The Ebro Delta (Northwestern Mediterranean). *Mar. Geol.* 115, 239–252.

- Hahn, J., Köhler, S., Glatzel, S., Jurasinski, G., 2015. Methane Exchange in a Coastal Fen in the First Year after Flooding - A Systems Shift 1–25.
- Harff, J., Graf, G., Bobertz, B., 2009. Dynamics of natural and anthropogenic sedimentation (DYNAS).
- Heinrich, C., Anders, S., Schwarzer, K., 2017. Late Pleistocene and early Holocene drainage events in the eastern Fehmarn Belt and Mecklenburg Bight, SW Baltic Sea. *Boreas* 14, 75.
- Henrichs, S.M., Reeburgh, W.S., 1987. Anaerobic mineralization of marine sediment organic matter: Rates and the role of anaerobic processes in the oceanic carbon economy. *Geomicrobiol. J.* 5, 191–237.
- Heyer, J., Berger, U., 2000. Methane Emission from the Coastal Area in the Southern Baltic Sea. *Estuar. Coast. Shelf Sci.* 51, 13–30.
- Hoggart, S.P.G., Hanley, M.E., Parker, D.J., Simmonds, D.J., Bilton, D.T., Filipova-Marinova, M., Franklin, E.L., Kotsev, I., Penning-Rowsell, E.C., Rundle, S.D., Trifonova, E., Vergiev, S., White, A.C., Thompson, R.C., 2014. The consequences of doing nothing: The effects of seawater flooding on coastal zones. *Coast. Eng.* 87, 169–182.
- Holmer, M., Kristensen, E., 1994. Coexistence of sulfate reduction and methane production in an organic-rich sediment. *Marine Ecology-Progress Series* 107, 177–177.
- Hooijer, A., Page, S., Jauhiainen, J., Lee, W.A., Lu, X.X., Idris, A., Anshari, G., 2012. Subsidence and carbon loss in drained tropical peatlands. *Biogeosciences* 9, 1053–1071.
- Hsiao, S.Y., Hsu, T.C., Liu, J.W., Xie, X., Zhang, Y., Lin, J., Wang, H., Yang, J.Y.T., Hsu, S.C., Dai, M., Kao, S.J., 2014. Nitrification and its oxygen consumption along the turbid Chang Jiang River plume. *Biogeosciences* 11, 2083–2098.
- Hübner, E., Gräff, B.T., 2013. Küstenhydrologie und -topografie im Naturschutzgebiet Hütelmoor.
- Hu, C., Muller-Karger, F.E., Swarzenski, P.W., 2006. Hurricanes, submarine groundwater discharge, and Florida's red tides. *Geophys. Res. Lett.* 33, 591.
- IPCC, 2007. Climate Change 2007 - The Physical Science Basis: Working Group I Contribution to the Fourth Assessment Report of the IPCC. Cambridge University Press.
- IsoPrime, 2014. IsoPrime100 User's Guide v1.02 for Ionvantage, 2014. IsoPrime Limited, Cheadle Hulme, Cheadle, UK. 219p.
- Iversen, N., Blackburn, T.H., 1981. Seasonal rates of methane oxidation in anoxic marine sediments. *Appl. Environ. Microbiol.* 41, 1295–1300.
- Jørgensen, B.B., Weber, A., Zopfi, J., 2001. Sulfate reduction and anaerobic methane oxidation in Black Sea sediments. *Deep Sea Res. Part I* 48, 2097–2120.
- Joye, S.B., Hollibaugh, J.T., 1995. Influence of Sulfide Inhibition of Nitrification on Nitrogen Regeneration in Sediments. *Science* 270, 623–625.
- Jurasinski, G., Janssen, M., Voss, M., Böttcher, M.E., Brede, M., Burchard, H., Forster, S., Gosch, L., Gräwe, U., Gründling-Pfaff, S., Haider, F., Ibenthal, M., Karow, N.,

- Karsten, U., Kreuzburg, M., Lange, X., Leinweber, P., Massmann, G., Ptak, T., Rezanezhad, F., Rehder, G., Romoth, K., Schade, H., Schubert, H., Schulz-Vogt, H., Sokolova, I.M., Strehse, R., Unger, V., Westphal, J., Lennartz, B., 2018. Understanding the Coastal Ecocline: Assessing Sea–Land Interactions at Non-tidal, Low-Lying Coasts Through Interdisciplinary Research. *Frontiers in Marine Science* 5, 342.
- Kalbitz, K., Solinger, S., Park, J.-H., Michalzik, B., Matzner, E., 2000. CONTROLS ON THE DYNAMICS OF DISSOLVED ORGANIC MATTER IN SOILS: A REVIEW. *Soil Sci.* 165, 277.
- Karstensen, J., Liblik, T., Fischer, J., Bumke, K., Krahmann, G., 2014. Summer upwelling at the Boknis Eck time-series station (1982 to 2012) – a combined glider and wind data analysis. *Biogeosciences*. <https://doi.org/10.5194/bg-11-3603-2014>
- Knee, K.L., Paytan, A., 2012. Submarine Groundwater Discharge: A Source of Nutrients, Metals, and Pollutants to the Coastal Ocean. Elsevier Inc.
- Knee, K., Street, J.H., Grossman, E.G., Paytan, A., 2010. Nutrient inputs to the coastal ocean from submarine groundwater discharge in a groundwater-dominated system: Relation to land use (Kona coast, Hawaii, U.S.A.). *Limnol. Oceanogr.* 55, 1105–1122.
- Knight, B.P., Chaudri, A.M., McGrath, S.P., Giller, K.E., 1998. Determination of chemical availability of cadmium and zinc in soils using inert soil moisture samplers. *Environ. Pollut.* 99, 293–298.
- Koch, S., Jurasinski, G., Koebisch, F., Koch, M., Glatzel, S., 2014. Spatial variability of annual estimates of methane emissions in a *phragmites australis* (cav.) trin. ex steud. dominated restored coastal brackish fen. *Wetlands* 34, 593–602.
- Koebisch, F., Jurasinski, G., Koch, M., Hofmann, J., Glatzel, S., 2015. Controls for multi-scale temporal variation in ecosystem methane exchange during the growing season of a permanently inundated fen. *Agric. For. Meteorol.* 204, 94–105.
- Koehler, A.-K., Murphy, K., Kiely, G., Sottocornola, M., 2009. Seasonal variation of DOC concentration and annual loss of DOC from an Atlantic blanket bog in South Western Ireland. *Biogeochemistry* 95, 231–242.
- Kolp, O., 1990. The Ancylus Lake Phase of the post-glacial evolution of the Baltic Sea. *Quaestiones Geographicae* 13, 69–86.
- Kolp, O., 1957. Die nordöstliche Heide Mecklenburgs. VEB Deutscher Verlag Der Wissenschaften.
- Kotwicki, L., Grzelak, K., Czub, M., Dellwig, O., Gentz, T., Szymczycha, B., Böttcher, M.E., 2014. Submarine groundwater discharge to the Baltic coastal zone: Impacts on the meiofaunal community. *J. Mar. Syst.* 129, 118–126.
- Krauss, W., 2001. Baltic sea circulation.
- Kreuzburg, M., Ibenthal, M., Janssen, M., Rehder, G., Voss, M., Naumann, M., Feldens, P., 2018. Sub-marine Continuation of Peat Deposits From a Coastal Peatland in the Southern Baltic Sea and its Holocene Development. *Frontiers in Earth Science* 6. <https://doi.org/10.3389/feart.2018.00103>
- Krüger, K., 1995. Untersuchung zur Salzbeeinflussung überflutungsgefährdeter, forstlich genutzter Flächen im Naturschutzgebiet Hütelmoor-Heiligensee.



- Lampe, R., 2005. Lateglacial and Holocene water-level variations along the NE German Baltic Sea coast: review and new results. *Quat. Int.* 133-134, 121–136.
- Lampe, R., 2002. Holocene Evolution of the South-Western Baltic Coast: Geological, Archaeological and Palaeo-environmental Aspects: Field Meeting of INQUA Subcommission V Sea-level Changes and Coastal Evolution, Western Europe, Western Europe, September 22-27, 2002. Ernst-Moritz-Arndt-Universität.
- Lampe, R., Endtmann, E., Janke, W., Meyer, H., 2010. Relative sea-level development and isostasy along the NE German Baltic Sea coast during the past 9 ka. *E&G Quaternary Science Journal* 59, 3–20.
- Lampe, R., Janke, W., 2004a. THE HOLOCENE SEA LEVEL RISE IN THE SOUTHERN BALTIC AS REFLECTED IN COASTAL PEAT SEQUENCES 11, 19–29.
- Lampe, R., Janke, W., 2004b. The Holocene sea level rise in the Southern Baltic as reflected in coastal peat sequences. *Polish geological institute Special papers* 11, 19–30.
- Lampe, R., Lorenz, S., Janke, W., Meyer, H., Küster, M., Hübener, T., Schwarz, A., 2009. Zur Landschafts- und Gewässergeschichte der Müritz: umweltgeschichtlich orientierte Bohrungen 2004 - 2006 zur Rekonstruktion der nacheiszeitlichen Entwicklung. Geozon Science Media.
- Lampe, R., Naumann, M., Meyer, H., Janke, W., Ziekur, R., 2011. Holocene Evolution of the Southern Baltic Sea Coast and Interplay of Sea-Level Variation, Isostasy, Accommodation and Sediment Supply, in: Harff, J., Björck, S., Hoth, P. (Eds.), *The Baltic Sea Basin, Central and Eastern European Development Studies (CEEDES)*. Springer Berlin Heidelberg, pp. 233–251.
- Larsen, M., Borisov, S.M., Grunwald, B., Klimant, I., Glud, R.N., 2011. A simple and inexpensive high resolution color ratiometric planar optode imaging approach: application to oxygen and pH sensing.: A simple RGB based planar optode imaging approach. *Limnol. Oceanogr. Methods* 9, 348–360.
- Lasak, S., Hahn, J., Jurasinski, G., Köhler, S., Glatzel, S., 2010. Methanfreisetzungen im Rahmen des Auftauens eines überfluteten Küstenmoors 129–132.
- Lehfeldt, R., Milbradt, P., 2000. Longshore sediment transport modeling in 1 and 2 dimensions, in: *Advances in Hydro-Science and Engineering. Proceedings of the 4th International Conference on Hydro-Science and Engineering*, Seoul. Abstract.
- Leote, C., Ibáñez, J.S., Rocha, C., 2008. Submarine groundwater discharge as a nitrogen source to the Ria Formosa studied with seepage meters. *Biogeochemistry* 88, 185–194.
- Li, L., Barry, D.A., Stagnitti, F., Parlange, J.Y., 1999. Submarine groundwater discharge and associated chemical input to a coastal sea. *Water Resour. Res.* 35, 3253–3259.
- Limpens, J., Berendse, F., Blodau, C., Canadell, J.G., Freeman, C., Holden, J., Roulet, N., Rydin, H., Schaepman-Strub, G., 2008. Peatlands and the carbon cycle: from local processes to global implications-a synthesis. *Biogeosciences* 5, 1475–1491.
- Lippmann, T.C., Holman, R.A., 1990. The spatial and temporal variability of sand bar morphology. *J. Geophys. Res.* 95, 11575.
- Liu, D.Y., Ding, W.X., Jia, Z.J., Cai, Z.C., 2011. Relation between methanogenic archaea and methane production potential in selected natural wetland ecosystems across China. *Biogeosciences* 8, 329–338.

- Luo, M., Huang, J.-F., Zhu, W.-F., Tong, C., 2017. Impacts of increasing salinity and inundation on rates and pathways of organic carbon mineralization in tidal wetlands: a review. *Hydrobiologia* 1–19.
- Lyman, J., 1969. REDEFINITION OF SALINITY AND CHLORINITY. *Limnol. Oceanogr.* 14, 928–929.
- Marushchak, M.E., Pitkämäki, A., Koponen, H., 2011. Hot spots for nitrous oxide emissions found in different types of permafrost peatlands. *Glob. Chang. Biol.*
- Menon, S., Denman, K.L., Brasseur, G., Chidthaisong, A., Ciais, P., Cox, P.M., Dickinson, R.E., Hauglustaine, D., Heinze, C., Holland, E., Jacob, D., Lohmann, U., Ramachandran, S., Leite da Silva Dias, P., Wofsy, S.C., Zhang, X., 2007. Couplings between changes in the climate system and biogeochemistry (No. LBNL-464E). Lawrence Berkeley National Lab. (LBNL), Berkeley, CA (United States).
- Meyers, P.A., 1997. Organic geochemical proxies of paleoceanographic, paleolimnologic, and paleoclimatic processes. *Org. Geochem.* 27, 213–250.
- Michael, H. a., Mulligan, A.E., Harvey, C.F., 2005. Seasonal oscillations in water exchange between aquifers and the coastal ocean. *Nature* 436, 1145–1148.
- Miegel, K., Graeff, T., Selle, B., Salzmann, T., Franck, C., Bronstert, A., 2016. Untersuchung eines renaturierten Niedermoores an der mecklenburgischen Ostseeküste--Teil I: Systembeschreibung und hydrologische Grundcharakterisierung. *HyWa*. doi 10, 5675.
- Miegel, K., Selle, B., Gräff, T., Walther, M., Salzmann, T., Behr, L., Oswald, S., 2009. Wasserhaushalt und Salzdynamik eines küstennahen Niedermoores im Grenzbereich zwischen Binnenland und Ostsee unter sich ändernden Bedingungen 1–10.
- Milliman, J.D., Emery, K.O., 1968. Sea Levels during the Past 35,000 Years. *Science* 162, 1121–1123.
- Moore, T.R., Dalva, M., 1993. The Influence of Temperature and Water-Table Position on Carbon-Dioxide and Methane Emissions from Laboratory Columns of Peatland Soils. *J. Soil Sci.* 44, 651–664.
- Moore, W.S., 2010. The effect of submarine groundwater discharge on the ocean. *Ann. Rev. Mar. Sci.* 2, 59–88.
- Moore, W.S., 1999. The subterranean estuary: a reaction zone of ground water and sea water. *Mar. Chem.* 65, 111–125.
- Mulholland, P.J., 2003. 6 - Large-Scale Patterns in Dissolved Organic Carbon Concentration, Flux, and Sources, in: Findlay, S.E.G., Sinsabaugh, R.L. (Eds.), *Aquatic Ecosystems*. Academic Press, Burlington, pp. 139–159.
- Mulholland, P.J., 1981. Formation of particulate organic carbon in water from a southeastern swamp-stream. *Limnol. Oceanogr.* 26, 790–795.
- Myllykangas, J.-P., Jilbert, T.S., Jakobs, G., Rehder, G., Werner, J., Hietanen, S.S., Others, 2017. Effects of the 2014 major Baltic inflow on methane and nitrous oxide dynamics in the water column of the central Baltic Sea. *Earth System Dynamics*.
- Neubauer, S.C., 2013. Ecosystem Responses of a Tidal Freshwater Marsh Experiencing Saltwater Intrusion and Altered Hydrology. *Estuaries Coasts* 36, 491–507.

- Nicholls, R.J., Cazenave, A., 2010. Sea-level rise and its impact on coastal zones. *Science* 328, 1517–1520.
- Niedermeyer, R.-O., Lampe, R., Janke, W., Schwarzer, K., Duphorn, K., Kliewe, H., Werner, F., 2011. Die deutsche Ostseeküste.
- Nieuwenhuis, H.S., Schokking, F., 1997. Land subsidence in drained peat areas of the Province of Friesland, The Netherlands. *Q. J. Eng. Geol. Hydrogeol.* 30, 37–48.
- Nieuwenhuize, J., Maas, Y.E.M., Middelburg, J.J., 1994. Rapid analysis of organic carbon and nitrogen in particulate materials. *Mar. Chem.* 45, 217–224.
- Nnafie, A., de Swart, H.E., Calvete, D., Garnier, R., 2014. Effects of sea level rise on the formation and drowning of shoreface-connected sand ridges, a model study. *Cont. Shelf Res.* 80, 32–48.
- Ostrovsky, I., 2003. Methane bubbles in Lake Kinneret: Quantification and temporal and spatial heterogeneity. *Limnol. Oceanogr.* 48, 1030–1036.
- Ostrowski, R., Stella, M., Szmytkiewicz, P., Kapiński, J., Marcinkowski, T., 2018. Coastal hydrodynamics beyond the surf zone of the south Baltic Sea. *Oceanologia* 60, 264–276.
- Ozuolmez, D., Na, H., Lever, M.A., Kjeldsen, K.U., Jørgensen, B.B., Plugge, C.M., 2015. Methanogenic archaea and sulfate reducing bacteria co-cultured on acetate: teamwork or coexistence? *Front. Microbiol.* 6, 492.
- Paerl, H.W., 1997. Coastal eutrophication and harmful algal blooms: Importance of atmospheric deposition and groundwater as “new” nitrogen and other nutrient sources. *Limnol. Oceanogr.* 42, 1154–1165.
- Palmer, K., Biasi, C., Horn, M.A., 2012. Contrasting denitrifier communities relate to contrasting N<sub>2</sub>O emission patterns from acidic peat soils in arctic tundra. *ISME J.* 6, 1058–1077.
- Peltonen, K., 2002. Direct Groundwater Inflow to the Baltic Sea. Nordic Council of Ministers.
- Pendleton, E.A., Brothers, L.L., Thielert, E.R., Sweeney, E.M., 2017. Sand ridge morphology and bedform migration patterns derived from bathymetry and backscatter on the inner-continental shelf offshore of Assateague Island, USA. *Cont. Shelf Res.* 144, 80–97.
- Plag, H.-P., Jules-Plag, S., 2013. Sea-level rise and coastal ecosystems.
- Plets, R., Dix, J., Bastos, A., Best, A., 2007. Characterization of Buried inundated Peat on Seismic (Chirp) Data, Inferred from Core Information. *Archaeological Prospection* 14, 261–272.
- Porubsky, W.P., Weston, N.B., Moore, W.S., Ruppel, C., Joye, S.B., 2013. Dynamics of submarine groundwater discharge and associated fluxes of dissolved nutrients, carbon, and trace gases to the coastal zone (Okatee River estuary, South Carolina). *Geochim. Cosmochim. Acta* 131, 81–97.
- Prinn, R., Cunnold, D., Rasmussen, R., 1990. Atmospheric emissions and trends of nitrous oxide deduced from 10 years of ALE–GAGE data. *Journal of.*
- Rapaglia, J., 2005. Submarine groundwater discharge into Venice Lagoon, Italy. *Estuaries* 28, 705–713.

- Rapaglia, J., Koukoulas, S., Zaggia, L., Lichter, M., Manfé, G., Vafeidis, A.T., 2012. Quantification of submarine groundwater discharge and optimal radium sampling distribution in the Lesina Lagoon, Italy. *J. Mar. Syst.* 91, 11–19.
- Rasband, W.S., 2015. ImageJ: US National Institutes of Health. Bethesda, Maryland, USA. uRI <http://imagej.nih.gov/ij>.
- Rebentrost, G., 1973. Beschreibung von Rückgangerscheinungen der Rostocker Heide in den letzten Jahren auf der Strecke Uhlenflucht bis Stromgrabenmündung. Akademie der Wissenschaften der DDR, Institut für Meereskunde Warnemünde.
- Reeburgh, W.S., Alperin, M.J., 1988. Studies on anaerobic methane oxidation. *Scope/Unep* 66, 367–375.
- Reimann, T., Tsukamoto, S., Naumann, M., Frechen, M., 2011. The potential of using K-rich feldspars for optical dating of young coastal sediments—A test case from Darss-Zingst peninsula (southern Baltic Sea coast). *Quat. Geochronol.* 6, 207–222.
- Reimer, P.J., Bard, E., Bayliss, A., Warren Beck, J., Blackwell, P.G., Ramsey, C.B., Buck, C.E., Cheng, H., Lawrence Edwards, R., Friedrich, M., Grootes, P.M., Guilderson, T.P., Haffidason, H., Hajdas, I., Hatté, C., Heaton, T.J., Hoffmann, D.L., Hogg, A.G., Hughen, K.A., Felix Kaiser, K., Kromer, B., Manning, S.W., Niu, M., Reimer, R.W., Richards, D.A., Marian Scott, E., Southon, J.R., Staff, R.A., Turney, C.S.M., van der Plicht, J., 2013. IntCal13 and Marine13 Radiocarbon Age Calibration Curves 0–50,000 Years cal BP. *Radiocarbon* 55, 1869–1887.
- Repo, M.E., Susiluoto, S., Lind, S.E., Jokinen, S., Elsakov, V., Biasi, C., Virtanen, T., Martikainen, P.J., 2009. Large N<sub>2</sub>O emissions from cryoturbated peat soil in tundra. *Nat. Geosci.* 2, 189.
- Rezanezhad, F., Couture, R.M., Kovac, R., O’Connell, D., Van Cappellen, P., 2014. Water table fluctuations and soil biogeochemistry: An experimental approach using an automated soil column system. *J. Hydrol.* 509, 245–256.
- Rezanezhad, F., Price, J.S., Quinton, W.L., Lennartz, B., Milojevic, T., Van Cappellen, P., 2016. Structure of peat soils and implications for water storage, flow and solute transport: A review update for geochemists. *Chem. Geol.* 429, 75–84.
- Rhee, T.S., Kettle, A.J., Andreae, M.O., 2009. Methane and nitrous oxide emissions from the ocean: A reassessment using basin-wide observations in the Atlantic. *Journal of Geophysical Research*. <https://doi.org/10.1029/2008jd011662>
- Robinson, C., Li, L., Barry, D.A., 2007. Effect of tidal forcing on a subterranean estuary. *Adv. Water Resour.* 30, 851–865.
- Rocha, C., Veiga-Pires, C., Scholten, J., Knoeller, K., Gröcke, D.R., Carvalho, L., Anibal, J., Wilson, J., 2015. Assessing land–ocean connectivity via Submarine Groundwater Discharge (SGD) in the Ria Formosa Lagoon (Portugal): combining radon measurements and stable isotope hydrology. *Hydrology and Earth System Sciences Discussions*. <https://doi.org/10.5194/hessd-12-12433-2015>
- Rönner, U., 1983. Distribution, production and consumption of nitrous oxide in the Baltic Sea. *Geochim. Cosmochim. Acta* 47, 2179–2188.
- Rosenberg, R., 1985. Eutrophication—The future marine coastal nuisance? *Mar. Pollut. Bull.* 16, 227–231.
- Rosentau, R., Meyer, M., Harff, J., Dietrich, R., Richter, A., 2007. Relative sea level change in the Baltic Sea since the Littorina Transgression. *Z. Geol. Wiss.* 35, 3–16.

- Rößler, D., Moros, M., Lemke, W., 2011. The Littorina transgression in the southwestern Baltic Sea: new insights based on proxy methods and radiocarbon dating of sediment cores. *Boreas*.
- Roulet, N., Moore, T., Bubier, J., Lafleur, P., 1992. Northern fens: methane flux and climatic change. *Tellus B Chem. Phys. Meteorol.*
- Santos, I.R., Eyre, B.D., Huettel, M., 2012. The driving forces of porewater and groundwater flow in permeable coastal sediments: A review. *Estuar. Coast. Shelf Sci.* 98, 1–15.
- Schlunbaum, G., Voigt, B., 2001. Die Darß-Zingster Bodden-ein junges Gewässersystem in einer noch nicht alten Landschaft. Die Darß-Zingster Bodden. Monographie einer einzigartigen Küstenlandschaft. *Meer und Museum* 16, 5–16.
- Schlüter, M., Sauter, E.J., Andersen, C.E., Dahlgaard, H., Dando, P.R., 2004. Spatial distribution and budget for submarine groundwater discharge in Eckernförde Bay (Western Baltic Sea). *Limnol. Oceanogr.* 49, 157–167.
- Schmaljohann, R., 1996. Methane dynamics in the sediment and water column of Kiel Harbour (Baltic Sea). *Mar. Ecol. Prog. Ser.* 131, 263–273.
- Schubert, M., Paschke, A., 2015. Radon, CO<sub>2</sub> and CH<sub>4</sub> as environmental tracers in groundwater/surface water interaction studies – comparative theoretical evaluation of the gas specific water/air phase transfer kinetics. *Eur. Phys. J. Spec. Top.* 224, 709–715.
- Schwarzer, K., 2010. Aggregate resources and extraction in the Baltic Sea: an Introduction. *J. Coast. Res.* 165–172.
- Seeborg-Elverfeldt, J., Schlüter, M., Feseker, T., Kölling, M., 2005. Rhizon sampling of porewaters near the sediment-water interface of aquatic systems. *Limnol. Oceanogr. Methods* 3, 361–371.
- Seitzinger, S.P., Harrison, J.A., 2008. Land-Based Nitrogen Sources and Their Delivery to Coastal Systems.
- Seitzinger, S.P., Kroeze, C., Styles, R.V., 2000. Global distribution of N<sub>2</sub>O emissions from aquatic systems: natural emissions and anthropogenic effects. *Chemosphere - Global Change Science* 2, 267–279.
- Sela-Adler, M., Ronen, Z., Herut, B., Antler, G., Vigderovich, H., Eckert, W., Sivan, O., 2017. Co-existence of Methanogenesis and Sulfate Reduction with Common Substrates in Sulfate-Rich Estuarine Sediments. *Front. Microbiol.* 8, 766.
- Sergeev, A., Sivkov, V., Zhamoida, V., Ryabchuk, D., Bitinas, A., Mažeika, J., 2015a. Holocene organic-rich sediments within the Curonian Spit coast, the south-eastern Baltic Sea. *Baltica* 28.
- Sergeev, A., Sivkov, V., Zhamoida, V., Ryabchuk, D., Bitinas, A., Mažeika, J., 2015b. Holocene biogenic sediments of the Curonian Spit (south-eastern Baltic Sea coast). *Baltica* 28, 41–50.
- Sirin, A., Laine, J., 2008. Peatlands and greenhouse gases. *Assesment on Peatlands, Biodiversity and Climate Change* 118–138.
- Slomp, C.P., Van Cappellen, P., 2004. Nutrient inputs to the coastal ocean through submarine groundwater discharge: Controls and potential impact. *J. Hydrol.* 295, 64–86.

- Small, C., Nicholls, R.J., 2003. A Global Analysis of Human Settlement in Coastal Zones. *J. Coast. Res.* 19, 584–599.
- Smith, K.A., 2010. Nitrous Oxide and Climate Change. Earthscan.
- Snedden, J.W., Dalrymple, R.W., 1999. Modern shelf sand ridges: from historical perspective to a unified hydrodynamic and evolutionary model.
- Sonesten, L., Svendsen, L.M., Tornbjerg, H., Gustafsson, B.G., Frank-Kamenetsky, D., Haapaniemi, J., 2018. HELCOM, 2018. Sources and pathways of nutrients to the Baltic Sea.
- Sørensen, J., Christensen, D., Jørgensen, B.B., 1981. Volatile Fatty acids and hydrogen as substrates for sulfate-reducing bacteria in anaerobic marine sediment. *Appl. Environ. Microbiol.* 42, 5–11.
- Stadtman, T.C., Barker, H.A., 1949. Studies on the methane fermentation; tracer experiments on the mechanism of methane formation. *Arch. Biochem.* 21, 256–264.
- Stainton, M., Capel, M.J., Armstrong, F.A.J., 1977. Chemical analysis of fresh water.
- Stanley, D.W., Nixon, S.W., 1992. Stratification and bottom-water hypoxia in the Pamlico River estuary. *Estuaries* 15, 270–281.
- Stein, R. (Ed.), 1991. Accumulation of organic carbon in Baffin Bay and Labrador Sea sediments (ODP-Leg 105), in: *Accumulation of Organic Carbon in Marine Sediments: Results from the Deep Sea Drilling Project/Ocean Drilling Program (DSDP/ODP)*. Springer Berlin Heidelberg, Berlin, Heidelberg, pp. 40–84.
- Sterr, H., 2008. Assessment of Vulnerability and Adaptation to Sea-Level Rise for the Coastal Zone of Germany. *J. Coast. Res.* 380–393.
- St-Jean, G., 2003. Automated quantitative and isotopic ( $^{13}\text{C}$ ) analysis of dissolved inorganic carbon and dissolved organic carbon in continuous-flow using a total organic carbon analyser. *Rapid Commun. Mass Spectrom.* 17, 419–428.
- Stocker, T.F., Qin, D., Plattner, G.-K., Tignor, M., Allen, S.K., Boschung, J., Nauels, A., Xia, Y., Bex, V., Midgley, P.M., 2013. Climate Change 2013: The Physical Science Basis. Contribution of Working Group I to the Fifth Assessment Report of the Intergovernmental Panel on Climate Change 2013. There is no corresponding record for this reference.
- Strack, M., 2008. Peatlands and climate change. IPS, International Peat Society.
- Strehse, R., Bohne, H., Amha, Y., Leinweber, P., 2018. The influence of salt on dissolved organic matter from peat soils. *Org. Geochem.* 125, 270–276.
- Swift, D.J.P., Parker, G., Lanfredi, N.W., Perillo, G., Figge, K., 1978. Shoreface-connected sand ridges on American and European shelves: A comparison. *Estuarine Coastal Mar. Sci.* 7, 257–273.
- Taffs, K., Logan, B., Parr, J., Jacobsen, G., 2012. The evolution of a coastal peatland at Byron Bay, Australia: multi-proxy evidence from the microfossil record. *Bookman* 429–442.
- Thäns, M., 2012. Sommerliche Nährstoffdynamik von Stickstoff-und Phosphorverbindungen eines eutrophierten Ostseezuflusses am Beispiel des Warnowästuars. Diplomarbeit 2012. Betreuer: Brigitte Nixdorf, Maren Voss (IOW).

- Thoms, F., Burmeister, C., Dippner, J.W., Gogina, M., Janas, U., Kendzierska, H., Liskow, I., Voss, M., 2018. Impact of Macrofaunal Communities on the Coastal Filter Function in the Bay of Gdansk, Baltic Sea. *Frontiers in Marine Science* 5, 201.
- Tiemeyer, B., Pfaffner, N., Frank, S., Kaiser, K., Fiedler, S., 2017. Porewater velocity and ionic strength effects on DOC release from peat-sand mixtures: Results from laboratory and field experiments. *Geoderma* 296, 86–97.
- Tipping, E., Hurley, M.A., 1988. A model of solid-solution interactions in acid organic soils, based on the complexation properties of humic substances. *Eur. J. Soil Sci.*
- Upstill-Goddard, R.C., 2006. Air–sea gas exchange in the coastal zone. *Estuar. Coast. Shelf Sci.* 70, 388–404.
- Valiela, I., 2009. *Global Coastal Change*. John Wiley & Sons.
- Vallius, H., 2006. Permanent seafloor anoxia in coastal basins of the northwestern Gulf of Finland, Baltic Sea. *Ambio* 35, 105–108.
- van de Meene, J.W.H., van Rijn, L.C., 2000. The shoreface-connected ridges along the central Dutch coast—part 1: field observations. *Cont. Shelf Res.* 20, 2295–2323.
- van der Linden, M., Barke, J., Vickery, E., Charman, D.J., van Geel, B., 2008. Late Holocene human impact and climate change recorded in a North Swedish peat deposit. *Palaeogeogr. Palaeoclimatol. Palaeoecol.* 258, 1–27.
- van Winden, J.F., Reichart, G.-J., McNamara, N.P., Benthien, A., Damsté, J.S.S., 2012. Temperature-induced increase in methane release from peat bogs: a mesocosm experiment. *PLoS One* 7, e39614.
- Vestergaard, P., 1997. Possible impact of sea-level rise on some habitat types at the Baltic coast of Denmark. *J. Coast. Conserv.* 3, 103.
- Voigtländer, U., Schmidt, J., Scheller, W., 1996. *Pflege-und Entwicklungsplan NSG Heiligensee und Hütelmoor*.
- von Post, L., 1922. *Sveriges Geologiska Undersöknings torvinventering och några av dess hittills vunna resultat*.
- Wang, H., Richardson, C.J., Ho, M., Flanagan, N., 2016. Drained coastal peatlands: A potential nitrogen source to marine ecosystems under prolonged drought and heavy storm events—A microcosm experiment. *Sci. Total Environ.* 566–567, 621–626.
- Weiss, R.F., Price, B.A., 1980. Nitrous oxide solubility in water and seawater. *Mar. Chem.* 8, 347–359.
- Weiss, R.F., Van Woy, F.A., Salameh, P.K., Sepanski, R.J., 1992. Surface water and atmospheric carbon dioxide and nitrous oxide observations by shipboard automated gas chromatography: Results from expeditions between 1977 and 1990. Oak Ridge National Lab.
- Wen, X., Unger, V., Jurasinski, G., Koebsch, F., Horn, F., Rehder, G., Sachs, T., Zak, D., Lischeid, G., Knorr, K.-H., Böttcher, M.E., Winkel, M., Bodelier, P.L.E., Liebner, S., 2018. Predominance of methanogens over methanotrophs in rewetted fens characterized by high methane emissions. *Biogeosciences* 15, 6519–6536.
- Westley, K., Dix, J., 2006. Coastal environments and their role in prehistoric migrations. *J. Marit. Archaeol.* 1, 9–28.

- Weston, N.B., Vile, M.A., Neubauer, S.C., Velinsky, D.J., 2011. Accelerated microbial organic matter mineralization following salt-water intrusion into tidal freshwater marsh soils. *Biogeochemistry* 102, 135–151.
- Wheeler, B.D., Proctor, M.C.F., 2000. Ecological gradients, subdivisions and terminology of north-west European mires. *J. Ecol.* 88, 187–203.
- Whiticar, M.J., 2002. Diagenetic relationships of methanogenesis, nutrients, acoustic turbidity, pockmarks and freshwater seepages in Eckernförde Bay. *Mar. Geol.* 182, 29–53.
- Whiticar, M.J., Faber, E., Schoell, M., 1986. Biogenic methane formation in marine and freshwater environments: CO<sub>2</sub> reduction vs. acetate fermentation—Isotope evidence. *Geochim. Cosmochim. Acta* 50, 693–709.
- Wiesenburg, D.A., Guinasso, N.L., 1979. Equilibrium solubilities of methane, carbon monoxide, and hydrogen in water and sea water. *J. Chem. Eng. Data* 24, 356–360.
- Wilson, S.T., Bange, H.W., Arévalo-Martínez, D.L., Barnes, J., Borges, A., Brown, I., Bullister, J.L., Burgos, M., Capelle, D.W., Casso, M., Others, 2018. An intercomparison of oceanic methane and nitrous oxide measurements. *Biogeosciences*.
- Wong, P.P., Losada, I.J., Gattuso, J.-P., Hinkel, J., Khattabi, A., McInnes, K.L., Saito, Y., Sallenger, A., Others, 2014. Coastal systems and low-lying areas. *Climate change* 2104, 361–409.
- Wright, L.D., Short, A.D., 1984. Morphodynamic variability of surf zones and beaches: A synthesis. *Mar. Geol.* 56, 93–118.
- Zauft, M., Fell, H., Glaßer, F., Roszkopf, N., Zeitz, J., 2010. Carbon storage in the peatlands of Mecklenburg-Western Pomerania, north-east Germany. *Mires & Peat* 6.
- Zehnder, A.J.B., Mitchell, R., 1978. Ecology of methane formation. *Water pollution microbiology* 2, 349–376.
- Zeiler, M., Schwarzer, K., Ricklefs, K., 2008. Seabed morphology and sediment dynamics. *Die Küste* 74, 31–44.
- Zhang, B., Tian, H., Lu, C., Chen, G., Pan, S., Anderson, C., Poulter, B., 2017. Methane emissions from global wetlands: An assessment of the uncertainty associated with various wetland extent data sets. *Atmos. Environ.* 165, 310–321.
- Zhang, W., Harff, J., Schneider, R., 2011. Analysis of 50-year wind data of the southern Baltic Sea for modelling coastal morphological evolution – a case study from the Darss-Zingst Peninsula. *Oceanologia* 53, 489–518.